VORTEX MODIFICATION BY MASS INJECTION AND BY TIP GEOMETRY VARIATION

John C. Balcerak, et al

Rochester Applied Science Associates, Incorporated

Prepared for:

Army Air Mobility Research and Development Laboratory

June 1973

DISCLAIMER NOTICE

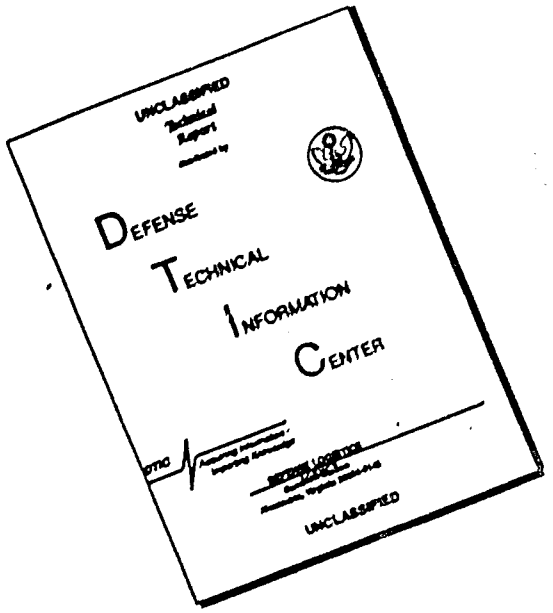

THIS DOCUMENT IS BEST QUALITY AVAILABLE. THE COPY FURNISHED TO DTIC CONTAINED A SIGNIFICANT NUMBER OF PAGES WHICH DO NOT REPRODUCE LEGIBLY.

AD

USAAMRDL TECHNICAL REPORT 73-45

VORTEX MODIFICATION BY MASS INJECTION AND BY TIP GEOMETRY VARIATION

By

John C. Balcerak
Raymond F. Feller

June 1973

EUSTIS DIRECTORATE
U. S. ARMY AIR MOBILITY RESEARCH AND DEVELOPMENT LABORATORY
FORT EUSTIS, VIRGINIA

CONTRACT DAAJ02-72-C-0097
ROCHESTER APPLIED SCIENCE ASSOCIATES, INC.
ROCHESTER, NEW YORK

DISCLAIMERS

The findings in this report are not to be construed as an official Department of the Army position unless so designated by other authorized documents.

When Government drawings, specifications, or other data are used for any purpose other than in connection with a definitely related Government procurement operation, the United States Government thereby incurs no responsibility nor any obligation whatsoever; and the fact that the Government may have formulated, furnished, or in any way supplied the said drawings, specifications, or other data is not to be regarded by implication or otherwise as in any manner licensing the holder or any other person or corporation, or conveying any rights or permission, to manufacture, use, or sell any patented invention that may in any way be related thereto.

Trade names cited in this report do not constitute an official endorsement or approval of the use of such commercial hardware or software.

DISPOSITION INSTRUCTIONS

Destroy this report when no longer needed. Do not return it to the originator.

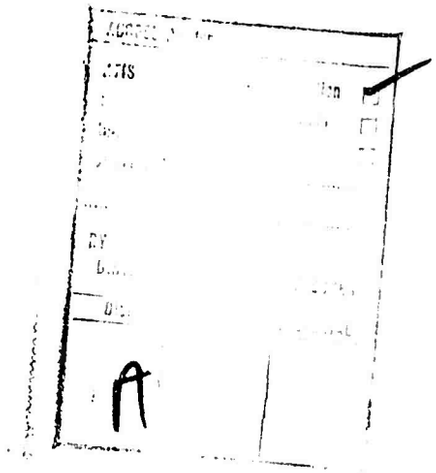

UNCLASSIFIED
Security Classification

DOCUMENT CONTROL DATA - R & D

(Security classification of title, body of abstract and indexing annotation must be entered when the overall report is classified)

1 ORIGINATING ACTIVITY (Corporate author) Rochester Applied Science Associates, Inc. 140 Allens Creek Road Rochester, New York	2a. REPORT SECURITY CLASSIFICATION UNCLASSIFIED 2b. GROUP

3 REPORT TITLE
VORTEX MODIFICATION BY MASS INJECTION AND BY TIP GEOMETRY VARIATION

4 DESCRIPTIVE NOTES (Type of report and inclusive dates)
Final Report

5 AUTHOR(S) (First name, middle initial, last name)
John C. Balcerak and Raymond F. Feller

6 REPORT DATE	7a. TOTAL NO OF PAGES	7b. NO OF REFS
June 1973	~~95~~ 96	13

8a. CONTRACT OR GRANT NO	9a. ORIGINATOR'S REPORT NUMBER(S)
DAAJ02-72-C-0097 b. PROJECT NO c. Task 1F162204AA4102 d.	USAAMRDL Technical Report 73-45 9b. OTHER REPORT NO(S) (Any other numbers that may be assigned this report) RASA REPORT 73-01

10 DISTRIBUTION STATEMENT
Approved for public release; distribution unlimited.

11 SUPPLEMENTARY NOTES	12. SPONSORING MILITARY ACTIVITY
	Eustis Directorate, U.S. Army Air Mobility Research & Development Laboratory, Ft. Eustis, Virginia

13. ABSTRACT

This report describes an experimental research program in which the outer section of a UH-1D helicopter blade was modified to incorporate a system for injecting the trailing tip vortex produced by the blade with a mass of linearly-directed air, and also an Ogee-tip section to study its effect as a passive system on vortex dissipation. The effects of mass injection were investigated at low mass flow rates, at near-sonic injection velocities, and with a two-section nozzle. The results are presented in terms of quantitative measurements of circulation strength as a function of mass flow rate and thrust, and are correlated with the results from previous research done at RASA. Also presented are flow-visualization studies which were conducted using illuminated helium bubbles, smoke, and tuft grids.

The results of this research program present additional confirming evidence that mass injection of the concentrated tip vortex is a practical approach to the elimination of the strong induced effects on a lifting surface of the circulatory flow associated with a concentrated vortex generated at the tip of a helicopter rotor blade.

DD FORM 1 NOV 1473 REPLACES DD FORM 1473, 1 JAN 63, WHICH IS OBSOLETE FOR ARMY USE.

UNCLASSIFIED
Security Classification

UNCLASSIFIED
Security Classification

14 KEY WORDS	LINK A		LINK B		LINK C	
	ROLE	WT	ROLE	WT	ROLE	WT
Mass Flow Injection						
Vortex Dissipation						
Vortex Instability						
Aerodynamics						
Acoustics						
Rotor Blades						
Tip Vortex						
Viscous Mixing						
Blade Loads						
Ogee Tip						

UNCLASSIFIED
Security Classification

ith

DEPARTMENT OF THE ARMY
U. S. ARMY AIR MOBILITY RESEARCH & DEVELOPMENT LABORATORY
EUSTIS DIRECTORATE
FORT EUSTIS, VIRGINIA 23604

This report has been reviewed by the Eustis Directorate, U.S. Army Air Mobility Research and Development Laboratory and is considered to be technically sound.

The research was performed to investigate means of dissipating or alleviating the tip vortex, including the Ogee tip and mass ejection in the vortex core. In the case of air injection, emphasis was placed on investigating a two-section nozzle and the effect of the thrust of the injected air on the reduction of the tip vortex strength. The results are encouraging and definitely suggest that the system may have practical application to the helicopter rotor.

The report is published for dissemination of the results of this investigation and for the stimulation of further research. The technical monitor for this contract was Mr. William E. Nettles, Aeromechanics, Technology Applications Division.

Task 1F162204AA4102
Contract DAAJ02-72-C-0097
USAAMRDL Technical Report 73-45
June 1973

VORTEX MODIFICATION BY MASS INJECTION AND BY TIP GEOMETRY VARIATION

Final Report

RASA REPORT 73-01

By

John C. Balcerak
Raymond F. Feller

Prepared by

Rochester Applied Science Associates, Inc.
Rochester, New York

for

EUSTIS DIRECTORATE
U. S. ARMY AIR MOBILITY RESEARCH AND DEVELOPMENT LABORATORY
FORT EUSTIS, VIRGINIA

ABSTRACT

This report describes an experimental research program in which the outer section of a UH-1D helicopter blade was modified to incorporate a system for injecting the trailing tip vortex produced by the blade with a mass of linearly directed air, and also an Ogee-tip section, to study its effect as a passive system on vortex dissipation. The effects of mass injection were investigated at low mass flow rates, at near-sonic injection velocities, and with a two-section nozzle. The results are presented in terms of quantitative measurements of circulation strength as a function of mass flow rate and thrust, and are correlated with the results from previous research done at RASA. Also presented are flow-visualization studies which were conducted using illuminated helium bubbles, smoke, and tuft grids.

The results of this research program present additional confirming evidence that mass injection of the concentrated tip vortex could eliminate the strong induced effects on a lifting surface of the circulatory flow associated with a concentrated vortex generated at the tip of a helicopter rotor blade.

FOREWORD

The work described in this report was performed by the Rochester Applied Science Associates, Inc., for the Eustis Directorate of the U. S. Army Air Mobility Research and Development Laboratory, Fort Eustis, Virginia, under Contract DAAJ02-72-C-0097, Task 1F162204AA4102. The research program was conducted under the technical cognizance of Mr. William E. Nettles of the Eustis Directorate.

Appreciation is extended by the authors to Dr. Santu T. Gangwani of RASA for his contributions in the analysis, as well as to Mr. Donald S. Gross and his staff at the University of Maryland Wind Tunnel Facility for their assistance.

TABLE OF CONTENTS

LIST OF ILLUSTRATIONS

LIST OF TABLES

LIST OF SYMBOLS

a	nondimensional ratio, v_t/Γ_0
a_j	cross-sectional exit area of injection nozzle, ft^2
c	blade chord, ft
d_j	exit diameter of injection nozzle, ft
e	base of Naperian logarithm, 2.71828
k	nondimensional ratio, Γ_c/Γ_0
L/D	ratio of lift to drag, nondimensional
$\ln$	logarithm to the base e
m_i	injected mass flow rate, lb/sec
P_m	static pressure at orifice flow meter, inches of mercury
r	radial coordinate, ft
r_c	vortex core radius at which the swirl velocity is maximum, ft
T	thrust of the jet, lb
V	free-stream velocity, ft/sec
V_i	velocity of injected mass flow, ft/sec
v	vortex swirl velocity, ft/sec
v_t	velocity at tip of blade section, ft/sec
x	downstream distance measured from blade trailing edge, ft
z	axial distance measured from a virtual origin, ft
α_R	aerodynamic angle of attack at root of blade section, deg
α_T	aerodynamic angle of attack at tip of blade section, deg

Γ	circulation strength of the trailed tip vortex, ft^2/sec
Γ_c	circulation strength of the trailed tip vortex where the swirl velocity is maximum, ft^2/sec
Γ_m	circulation strength of the trailed tip vortex with mass injection, ft^2/sec
Γ_{mc}	circulation strength of the trailed tip vortex with mass injection at which the swirl velocity is maximum, ft^2/sec
Γ_0	circulation strength of the unmodified trailed tip vortex, ft^2/sec
δ	nondimensional empirical correction factor for kinematic eddy viscosity of the jet in a free stream
ϵ_m	kinematic eddy viscosity of the injected jet, ft^2/sec
η	nondimensional parameter, $V_\infty r^2/4\nu z$
η_c	nondimensional parameter at which the swirl velocity is maximum, $V_\infty r_c^2/4\nu z$
Λ	a factor relating 'a' to the vortex Reynolds number, nondimensional
μ	advance ratio, nondimensional
ν	kinematic viscosity of the fluid, ft^2/sec
ν_t	kinematic eddy viscosity of the fluid, ft^2/sec
ψ	blade azimuthal angle, deg
Ω	blade rotational speed, rpm

I. INTRODUCTION

The concentrated vortices that are trailed off the tips of helicopter blades continue to be of great concern toward the further development of the helicopter. In recent years, research efforts to enhance the dissipation of these vortices have been expanded because of this concern. These research efforts have included investigations of both active and passive vortex-modification systems, and the positive aspects that have been demonstrated by these systems on scale models appear to have directed research toward the application of these systems to flight hardware. If these systems prove to be successful, improvement could be expected in rotor performance, blade life, acoustics and in problems associated with rotor downwash.

In regard to active vortex-modification systems, Rinehart postulated that the injection of a vortex with a mass of air would enhance the decay of the vortex (Ref. 1). On the basis of this research, tests of a vortex-injection system were conducted, and the results of these tests generally confirmed these theoretical predictions (Ref. 2). Additional tests of this system were conducted with wind-tunnel models over a wider range of scaling parameters (Refs. 3 and 4), and these data suggested that the dissipative effect that had been achieved was essentially independent of the scaling parameters.

In these investigations, however, it has been difficult to predict the requisite mass flow rates in terms of the degree of (vortex) dissipation that could be achieved, for two reasons. The first is that data in the wake has been obtained only at locations which were relatively close to the airfoil, and the variation of vortex strength as a function of time or downstream position in quantitative terms has not been established for the various models tested. Second, the measurements of vorticity in the trailed tip vortices are somewhat laborious, which restricts the amount of quantitative data that can be obtained, and the independent effects of the mass-flow rate and the velocity of injection on the circulation strength of the vortices also eluded more definitive solution. In a related aspect, it has been theorized that the dissipative process could be enhanced by injection of the vortex during its formative stage, rather than at the time that it had been almost fully developed as originally conceived. This aspect stems from desires to gain additional benefits from vortex injection in regard to the improvement of the performance characteristics of the airfoils by the relocation or the spreading of the concentrated vorticity on the airfoil itself.

In regard to helicopter applications, the important parameter in the vortex dissipation process is time. Specifically, it is the period between the instant that the vortex is trailed from one blade and the time that a following blade intersects this vortex. The blade that intersects a vortex that is trailed from a blade tip is not necessarily the one that immediately follows the latter blade. Blade-vortex intersections are related to the number of blades in the rotor system and to the flight condition. For the UH-1 series rotors, blade-vortex intersections occur in descents and turns, and some intersections occur as a blade intersects its own tip vortex when the age of the vortex is approximately 1-1/2 revolutions. On the basis of the rotor tip speed and its diameter, the time that is available before blade-vortex intersections occur is on the order of 0.1 second. In terms of distance, the trailed tip vortex would have been transported approximately 40 chord lengths "downstream" in this time period. Thus, in order for an active vortex-modification system to be effective, the dissipative action that is instituted must take effect rapidly, and hopefully generate additional dissipative action as time increases. It is postulated that additional dissipative action can be achieved by mass injection since the turbulence that is generated by mass injection would persist with time in the core of the vortex. Because of the instability that would be generated, the strength of the vortex would be continually dissipated.

Passive vortex modification systems also have potential to achieve vortex dissipation by imparting turbulence into the vortex core. Thus, for a passive vortex modification system to be effective, the formative process of the vortex must be modified to minimize the swirl velocities in the vortex core. In this process, the typical tip vortex is spread, and it is conjectured that this spreading will also minimize the induced effect of the vortex in the proximity of the lifting surface.

The research that was conducted in this program was directed toward fostering the application of vortex-modification systems to rotary-wing aircraft in several aspects. Specifically, additional data were desired to substantiate the variation of circulation strength with the mass flow rate; the effect of vortex injection at high velocities of injection, and the effects of injection with a two-stage nozzle were investigated; the effect of a passive dissipator, the Ogee-tip configuration, was investigated; and the qualitative variation of both the active and passive vortex-dissipation systems as a function of downstream position was also investigated.

II. DESCRIPTION OF MODELS AND INSTRUMENTATION

A. MODEL #1

Model #1 was the notation given to the model that was used during a previous experimental research program by RASA (Ref. 1). Three different honeycomb nozzles were installed in the model and tested. Nozzles #5 and #18 (described in Ref. 1) were tested at model tip angles of attack of 9.5 and 13.5 degrees, respectively. Nozzle #25 was fabricated for this program and tested at α_T=13.5 degrees. This nozzle had a similar cell-hole pattern as Nozzle #18, but with an additional seven cells left open to give an increased area of injection by providing a wider spanwise slot. The cross-sectional exit area of Nozzle #25 was 1.60 square inches, while the cross-sectional exit areas of Nozzles #5 and #18 were each 1.24 square inches.

B. MODEL #2

Model #2 was identical in planform and in wind tunnel installation to Model #1. This model had a measured twist of 0.14 deg/ft, and the injection nozzles were adapted in a different manner from that of Model #1. The nozzles for Model #2 were incorporated in a 2-1/4-inch wooden section which was attached to the tip of the basic blade section. The outboard section of the blade was modified to accommodate the wooden section by bonding a 3/8-inch-thick aluminum rib to the honeycomb material of the blade between the top and bottom skin aft of the D-spar. The rib was additionally secured to the blade section by button-head screws through the skin. A 1-1/4-inch-developed half-round tip cap provided the same tip configuration as that of Model #1. The entire tip assembly was secured to the blade section by bolting it through to the aluminum rib and to the solid metal leading edge. An O-ring provided the seal around the D-spar on the inside face of the 2-1/4-inch section, and a sheet rubber seal backed by a sheet aluminum cover plate provided the seal on its outside face as shown in Figure 1.

Two types of injection nozzles were tested on Model #2. A two-section nozzle configuration was tested to compare the effect of mass injection in dissipating the tip vortex from both at the three-quarter chord position and a location at the 45% chord simultaneously. A schematic diagram of the nozzle is shown in Figure 2. The injection angles were set at 3.5 and 9.5 degrees for the fore and aft nozzle sections, respectively, and the injection nozzles were constructed to give a slotted jet cross-sectional shape.

The other type of injection nozzle installed on Model #2 was a configuration to inject the air at near-sonic velocities from a position located at the three-quarter chord. Figure 3 shows a schematic diagram of the manner in which the nozzle section was constructed to house each of the three interchangeable, sonic, cross-sectional, converging-type nozzles. The high-velocity nozzles had exit diameters of 3/8, 1/2, and 5/8 inch, and were set at an injection angle of 9.5 degrees with respect to the chord plane. Each converging nozzle was constructed by filling the inside of a 1-inch-diameter aluminum tube with potting compound, sliding a sonic-shaped mandrel into the potting compound, and then removing the mandrel when the compound had hardened sufficiently, thus forming the converging-shaped nozzles. The interchangeable nozzles were held in place by screws and were butt-jointed to the nonconverging tube with an O-ring seal. The attachment of the 2-1/4-inch-wide wooden nozzle section to the main section of the model was identical to that of the two-section nozzle.

Mass flow calibrations for the 3/8-inch-, 1/2-inch-, and 5/8-inch-diameter converging nozzles are given in Appendix I. The air-supply system for the nozzle was operated at a static pressure at the orifice of 35 inches of mercury, and the corresponding mass flow rates for the nozzles were 0.06, 0.12, and 0.18 lb/sec, respectively. Because of inherent pressure losses in the system and through correlations made between the thrust and mass flow measurements, the resulting exit velocities were found to be on the order of 1000 - 1100 ft/sec.

C. OGEE MODEL

The Ogee Model was fabricated from an outboard section of a UH-1D helicopter blade and was identical in planform to Models #1 and #2 from the tunnel floor to a station located 45.9 inches up from the floor. The measured twist of this constant-chord section was the same as that of Model #2, that is, 0.14 deg/ft. The Ogee Model was installed in the wind tunnel in the same manner as Models #1 and #2, with the twist increasing the angle of attack with span, and the model was pitched about the 15.5 percent chord.

The Ogee-tip configuration was outboard of station 45.9, and resembled the shape of a typical pressure distribution over the top surface of an airfoil. The Ogee shape evolved from exploratory, small-scale, smoke-tunnel tests and wake Schlieren studies, and was designed to eliminate the separation vortex whose intense core forms and passes off the tip trailing edge (Ref. 5).

The sketch in Figure 4 shows a scaled comparison of the Ogee Model planform to that of Models #1 and #2. The span of the Ogee Model was determined on the basis that the total areas of both planforms would be equal. Construction of the Ogee-tip section outboard from station 45.9 was from wood. The outermost section of the Ogee was mortised to fit a 1/8-inch steel tenon which was bonded in the chord plane of the inner wooden section. This provision allowed for modification of the tip section outboard from station 66.05 to accommodate additional tip shapes. Planform views of the three tip shapes tested are shown in Figure 5. The unmodified Ogee tip, resembling the shape of a "finger", is elliptical in cross-sectional shape, whereas the three modified tips had more slender cross sections.

D. INSTRUMENTATION

The data readout systems at the University of Maryland Wind Tunnel were used to record the model angle of attack, tunnel conditions, and balance data. The mass flow of the injected air was computed from measurements of the pressures and temperatures across a sharp-edge orifice. The static pressure at the orifice was read out on a mercury manometer, the pressure drop across the orifice was read out on an alcohol manometer, and the temperature at the orifice was monitored by a thermocouple and read out on a potentiometer. Mass-flow calibrations for the various nozzles, in terms of the static pressure at the orifice, are given in Appendix I.

Measurements of the swirl velocity in the trailed tip vortex were made with an AEA[1] vortex meter, and the rotational speed of the meter was read out on an electronic digital counter with the signal also monitored on an oscilloscope. The University of Maryland Wind Tunnel facility provided a remotely-controlled traverse mechanism which allowed the wake to be surveyed in two-dimensions - normal to the model chord and along its span. The traverse mechanism was positioned downstream such that the vanes of the vortex meter were 6.5 chord lengths aft of the trailing edge of the models. Digital counters were used to orient the location of the vortex meter with an accuracy of ± 0.01 inch in both directions.

Three methods of flow visualization were used during the wind tunnel tests. Generated smoke was injected from a probe and released upstream of the Ogee Model to observe the flow across the tip section. Flow visualization in the proximity of the models was provided primarily by producing neutrally-buoyant helium bubbles and releasing them upstream of the model,

---

[1]Aero Engineering Associates, State College, Pennsylvania.

allowing them to flow over the tip sections. The bubbles were illuminated by a collimated beam of light, and the flow patterns were observed and photographed both with motion and still film. A tuft grid was installed onto the same frame assembly which housed the traverse mechanism, and indications of the swirl in the trailed tip vortex were observed downstream of the models at 6.5, 13, and 20 chord lengths and photographed with motion and still film.

III. DISCUSSION OF RESULTS

A. SCOPE OF TEST PROGRAM

The test program was conducted for several purposes. The first was to obtain several additional data points for the data set that was obtained in Reference 4 in order to establish the variation of the strength of the trailed vortex as a function of mass flow more clearly, particularly at low mass-flow rates. The test program was also conducted to determine the effect of mass injection at high velocities of injection, and the effect of mass injection with a two-section nozzle. The effects of a passive system, that is, an Ogee-tip configuration, were also investigated.

Vorticity surveys and balance system measurements were taken for all configurations relating to the mass-injection tests. A summary of the data pertinent to these tests, as well as the relevant data from Reference 4, is listed in Table I. Vorticity surveys for the mass-injection test conditions are shown in Appendix II. Vorticity surveys were infeasible with the (unmodified) Ogee-tip configuration because of the extensive diffusion of the concentrated vorticity that was effected by this configuration. Because of possible performance penalties that were associated with this configuration, however, several modifications were made to the outermost section of the Ogee-tip, and the effect of these modifications was investigated with regard to their performance characteristics. A summary of these data is listed in Appendix III.

Flow visualization studies using the helium-bubble technique of visualization, as well as tuft-grid studies, were also conducted for various configurations, and these data are discussed in the following sections.

B. EFFECT OF THE VELOCITY OF INJECTION

Quantitative data were obtained in this program at relatively low mass flow rates to determine the variation of the circulation strength of the injected vortices with mass flow rate more explicitly than had been obtained in the tests reported in Reference 4. For each set of conditions for the data shown in Figure 6, the area of the injection nozzle was fixed, so that the mass flow was increased by increasing the velocity of injection. Thus, at the low rates of mass flow, the velocity of injection is on the order of the free-stream velocity. The gradient of the curves for the test conditions at the lower free-stream velocities is more pronounced at the

lower mass flow rates than at the higher free-stream velocities. As the mass flow and, hence, the injection velocity are increased, the gradient of the curves for the test conditions at the higher free-stream velocities also increases sharply. These trends in the data indicate that the difference between the jet velocity and the free-stream velocity is an important parameter in the mass-injection process and that little dissipative action occurs when $V_j - V_\infty \to 0$. The data shown in Figure 6 also show that the mass flow required to dissipate a fixed amount of vorticity is dependent on the initial strength of the vortex.

In Reference 4, it was shown that a greater decrease in circulation strength could be achieved at a constant mass flow if the velocity of injection were increased (by reducing the area of the nozzle). The conditions for which this result was obtained, however, represented only approximately a 25 percent change in velocity from that of a nominal nozzle whose average exit velocity at a mass flow rate of 0.28 lb/sec was on the order of 450 fps. The question thus arose as to the effect of mass injection of a vortex at near-sonic velocities of injection. Figure 7 shows a comparison of the variation in circulation strength with mass flow between the high-velocity nozzles and those at the comparatively low exit velocities. Whereas the area of the low-velocity nozzles was fixed so that mass flow was increased by increasing the velocity of injection, the area of the high-velocity nozzles was varied to increase the mass flow while holding the velocity constant. The efficiency of the high-velocity nozzles is obvious, as noted by the sharper initial drop in circulation strength with mass flow, indicating again that the difference between the injection velocity and the free-stream velocity is a primary parameter in the injection process. Comparison of the data for the test conditions at a free-stream velocity of 150 fps shows, however, that only a fixed amount of reduction in circulation strength can be achieved at a fixed downstream location regardless of the injection velocity. The data point at a mass flow of 0.18 lb/sec for the high-velocity nozzle at V_∞=150 fps indicates that the vortex had been spread rather than dissipated further from its condition at a mass flow of 0.12 lb/sec. The vorticity distributions for these data points which show the spreading effect are shown in Appendix II. The spreading phenomenon was also observed for the low-velocity nozzles as discussed in Reference 4, that is, that there is only an optimum amount of mass flow which can be injected into a vortex to dissipate its energy. Injection of mass flow above the optimum rate will produce a further decrease in the maximum

swirl velocities in the vortex, but the vortex will spread such that the total circulation of the vortex will tend to remain relatively constant.

Figure 8 shows the vorticity distributions of injected vortices at a mass flow rate of approximately 0.20 lb/sec for relatively low velocities of injection, and at a high velocity of injection. It is seen that as the injection velocity is increased, the peak swirl velocity decreases. At the low injection velocities, the size of the vortex remains relatively constant, such that the circulation strength of the vortex was diminished. At the high injection velocity, the vortex was spread but the higher velocity of injection also effected more dissipation than the lower velocity nozzles at approximately the same mass-flow rate. The circulation strength of the vortex injected at 1045 fps was approximately one-half of that which was injected at 283 fps. Thus, although the high-velocity nozzle exhibited some inefficiency in that it spread the vortex, it was still more efficient than the low-velocity nozzles in also dissipating the vortex. The increase in the velocity of injection is also seen to shift the vortex slightly outboard, but the slight shift is too small to cause any change in the induced effect of the vortex on the performance characteristics of the airfoil.

Figure 9 shows the vorticity distributions which yield approximately the same circulation strength for two combinations of mass flow and injection velocity. For the higher injection velocity, the mass flow that was required to reduce the strength of the vortex to approximately one-third of its uninjected value is less than one-half of that which was required at the lower velocity of injection. The velocity of injection is thus seen to be a primary parameter in the injection process of vortex dissipation.

Photographs of flow visualization using the helium-bubble technique are shown in Figure 10 both with and without mass injection with the 1/2-inch-diameter high-velocity nozzle.

The downstream view shows how the typical high-velocity nozzle breaks up the solid core rotation and changes the swirling motion set up around it into a flow field which is more turbulent.

Appendix II contains the vorticity survey plots obtained from vortex meter readings made at 6.5 chord lengths downstream, and the net balance measurements for each of these test conditions of mass injection are presented in Appendix IV. As with the low-velocity injection nozzles, mass injection at high velocities does not appear to significantly affect the aerodynamic performance characteristics of the blade section.

For a full-scale helicopter, the tip speed of the blade varies in the range of approximately $650 < v_t < 950$ fps throughout the azimuth. The minimum tip speed occurs at $\psi=270°$ and the maximum at $\psi=90°$. The circulation also varies, but the minimum occurs near $\psi=90°$ and the maximum on the retreating side of the disk. The combination of these conditions tends to enhance the applicability of the vortex-injection technique to full-scale helicopters since the largest circulation strengths occur at the azimuthal locations where tip speeds are a miminum. The difference in velocity between a sonic jet and the free stream is thus near a maximum where the circulation strengths are a maximum. The application of the vortex-injection technique to full-scale hardware is also discussed further in Section IV.

C. EFFECTS OF MASS INJECTION WITH A TWO-SECTION NOZZLE

The flow-visualization studies that were conducted in the test program of Reference 4 showed that the tip vortices trailed off the lifting surfaces at approximately the three-quarter-chord position. The nozzles were designed to inject the vortices as they trailed off the lifting surfaces, that is, they were placed at the three-quarter-chord position. It was evident, however, that the vortices formed over the tip across the entire chord of the airfoil, and it was believed that possible additional beneficial effects, in regard to both vortex dissipation and performance, may be realized if the vortices were injected as they were in the process of formation. The two-section nozzle described in Section II was tested to determine these effects at a wind tunnel velocity of 150 ft/sec and a tip angle of attack of 9.5 degrees. A comparison of the variation of the circulation strength with mass flow between the two-section nozzle and that of a corresponding single-section nozzle is shown in Figure 11. The two-section nozzle is seen to be slightly more efficient in dissipating the tip vortex than the single-section nozzle at mass flow rates below approximately 0.2 lb/sec. Above this mass flow rate, the two-section nozzle spreads the vortex, whereas no spreading was effected by the single-section nozzle up to a mass flow rate of approximately 0.4 lb/sec. This phenomenon can be related to the manner in which the vortices can be injected (e.g., spanwise blowing or that normal to the chord plane wherein the vortex is not injected directly) such that vortex spreading or vortex relocation is effected, rather than vortex dissipation. The second possible benefit of the two-section nozzle, that is, in regard to possible benefits in performance, was not realized. It has been anticipated that some improvement in performance could be realized by a possible reduction in induced drag if the vortex were injected at a position farther forward on the airfoil. No improvement was realized in this respect since the dissipative effect was still found to be a function of time,

that is, the dissipative effects developed with downstream position. In the vicinity of the airfoil, the vortex formed in nearly the same manner as without injection, indicating that the vortex has not been sufficiently relocated so that the effects on performance were minimal. The performance characteristics of the two-section nozzle configuration are listed in Appendix IV.

Photographs of the flow fields with and without mass injection for the two-section nozzle configuration are shown as Figures 12 and 13. In the proximity of the airfoil, the injected mass of air eliminated the characteristic solid entrainment of bubbles near the center of the vortex, but the view depicting a greater section of the wake indicates that the flow over the airfoil was basically the same whether the vortex had been injected or not. As the wake progresses downstream, however, it is seen that the injected vortex is in the process of breaking up into a random turbulent pattern rather than continuing to tighten up into a swirling pattern as it does without mass injection.

D. EFFECTS OF A PASSIVE SYSTEM - THE OGEE-TIP - ON VORTEX DISSIPATION

In addition to the tests of the active devices to dissipate the trailed tip vortices, a passive system, the Ogee-tip configuration, was also tested to determine its effect on the modification of the trailed tip vortex. For this configuration, it was expected that wake surveys would be conducted at the same lift as that obtained with Models #1 or #2 at a wind tunnel velocity of 150 ft/sec and at a tip angle of attack of 9.5 degrees. Surveys of the wake at 6.5 chord lengths downstream were impractical, however, as the trailed vortex had become diffused to the point where little confidence could be ascribed to the vortex-meter measurements. In lieu of the detailed wake measurements, the effects of the Ogee tip were analyzed by comparison of the performance characteristics of the Ogee-tip configuration with those of the rectangular planform model. Graphical comparisons of these parameters are shown in Figures 14 through 17, and tabular presentations of the data that were obtained are listed in Appendix III.

Comparison of the lift-to-drag ratios versus angle of attack of the Ogee-tip and rectangular planform models is shown in Figure 14 for four wind tunnel velocities. Zero lift occurred at a slightly different angle of attack for each model because of the differences in twist and alignment in the wind tunnel. At low angles of attack, the lift-curve slope of the Ogee-tip model is seen to be greater than that of the rectangular planform model, and the Ogee-tip model also achieves higher lift-

to-drag ratios. At the angle of attack increases beyond the peak L/D, however, the L/D for the Ogee-tip model drops more sharply than the rectangular planform model. Figure 15 shows the typical lift and drag variations versus angle of attack for the two configurations at a wind tunnel velocity of 150 ft/sec. At the low angles of attack, the difference in the lower absolute values of the lift between the Ogee-tip and rectangular-tip configurations is offset by the difference in the absolute values of the drag, resulting in the higher lift-to-drag ratios for the Ogee-tip configurations. At the higher angles of attack, the difference in the absolute values of the lift between the two configurations tends to become broader, but the drag of the Ogee-tip configuration increases to values above that of the rectangular planform. The latter effect resulted in the much sharper drop in the L/D ratio that was shown in Figure 14. The much sharper rise in the drag for the Ogee-tip model can be attributed to the outermost section of the model, which has an elliptical airfoil that exhibits this typical characteristic in drag variation.

Figure 16 shows the variation of the center of lift versus angle of attack for the Ogee-tip and standard-tip configurations. For the standard-tip model, the center of lift is located approximately 47.4 percent of the semispan outboard of the tunnel floor. For the Ogee-tip configuration, the center of lift moves approximately 0.2 foot farther outboard or approximately 4 percent of the standard semispan. The center of lift is located approximately 40.9 percent outboard with respect to the overall semispan of the Ogee. Figure 17 shows the center of drag for the standard-tip and Ogee-tip configurations. The center of drag for the standard-tip configuration is seen to coincide with the center of lift for moderate angles of attack. The data for the Ogee-tip configuration shows a little more scatter in the same angle-of-attack range, but in general it also shows that the center of drag coincides with the center of lift. At the high angles of attack, the center of drag for the Ogee-tip configuration is seen to move farther outboard than the standard-tip configuration, which indicates that drag at the tip of the model increases much more than that on the inboard section. These data corroborate that shown in Figure 14 and indicate that a drag and torque penalty could be expected for the Ogee-tip configuration during operation at high angles of attack, which would be more severe than that for the standard-tip configuration.

Modifications in the outermost tip of the Ogee-tip configuration were also implemented, and Figure 18 shows the typical lift-to-drag variation with angle of attack for two of the three modified tips that were tested. It is seen that higher lift-to-drag ratios can be obtained as the Ogee finger is reduced in area with only slight changes in the lift-curve

slope. Balance data were not obtained for modification No. 3 of the Ogee, but on the basis of the L/D variations shown with changes in area, it would be expected that the peak L/D would fall between the unmodified Ogee and modification No. 2.

Flow-visualization studies were conducted for all outermost tip configurations using the helium-bubble technique, and Figure 19 shows the flow field in the near wake of the various tip configurations. It is seen that the unmodified Ogee tip and modifications No. 3 and 2 show no evidence of a concentrated core of rotation as that normally seen for a rectangular tip. As the outermost area of the finger is reduced, however, as in modification No. 1, it is seen that there is a stronger tendency for the flow to form a tighter swirling motion.

The quantitative and qualitative data that were obtained for the various Ogee-tip configurations indicate that variations in tip geometry can be effective in diffusing the concentrated vortex that is usually formed by rectangular-tip configurations. The various shapes of the outermost section of the Ogee also showed higher lift-curve slopes and higher peak lift-to-drag ratios than the standard-tip configuration. Above the peak L/D ratios, however, the performance characteristics of the various Ogee shapes degraded more sharply than the standard-tip shape.

E. TUFT-GRID FLOW-VISUALIZATION STUDIES

The measurements of the vorticity in the wake had to be constrained to those at 6.5 or fewer chord lengths downstream of the model because of the unsteadiness of the trailed vortices in the diffuser section of the wind tunnel. The trailed vortices were observed at positions farther downstream with the aid of tuft grids, which were placed at 6.5, 13 and 20 chord lengths downstream for various configurations. For Models #1 and #2, data that were obtained with the tuft grids were obtained at the same conditions as that for which the wake vorticity surveys were made either in the program as reported in Reference 4 or in the present program. The swirl patterns that are shown for the models that were tested in this program at 6.5 chord lengths downstream can be related to the vorticity distributions that are presented in Appendix II. For the mass-injection configurations, the tuft-grid photographs (Figures 20 through 24) can be viewed in two aspects. Firstly, the photographs show the effect of mass injection at a fixed downstream position, and they also show the effect of age at a fixed mass flow rate.

For the 6.5 chord-length position downstream of the model, the camera was positioned approximately 7 feet behind the tuft grid; for the 13 chord-length position, the camera was mounted approximately 10 feet behind the tuft grid. These positions resulted in excellent photographic resolution of the tuft grid patterns, as seen in Figures 20 through 24. For the 20 chord-length position, the camera had to be mounted on the turning vanes of the wind tunnel, approximately 30 feet from the tuft grid. This position resulted in poorer resolution of the tuft grid patterns.

Figure 20 shows a series of photographs for Model #1 at a wind tunnel velocity of 150 ft/sec and a tip angle of attack of 9.5 degrees. Figure 21 shows the series of photographs at a wind tunnel velocity of 100 ft/sec and a tip angle of attack of 13.5 degrees. The measured circulation strengths at 6.5 chord lengths downstream for these two conditions without mass injection were the same as shown in Figures 6 and 7. At V=150 ft/sec and α=9.5 degrees, little difference can be seen between the tuft-grid patterns of the noninjected vortex and that injected at 0.175 lb/sec. The vortex persisted at a mass flow of 0.280 lb/sec, but the swirl motion of the tufts appeared to have diminished slightly, particularly at 20 chord lengths downstream, where the blur pattern on the tuft grids was not as marked as it was for m_i=0 or m_i=0.175 lb/sec. At V=100 ft/sec and α=13.5 degrees, the difference in the tuft-grid patterns between the noninjected case and at m_i=0.175 lb/sec is more noticeable, in particular at 20 chord lengths downstream, where the blur pattern for m_i=0.175 lb/sec was not as marked as it was for m_i=0. At m_i=0.280 lb/sec, the swirl motion of the tufts appeared to have diminished further, and again, the difference among the tuft-grid patterns at m_i=0, 0.175 and 0.280 lb/sec is more pronounced at 20 chord lengths downstream than at 6.5 or 13.5 chord lengths downstream.

Figure 22 shows the tuft-grid patterns for V=150 ft/sec and α=13.5 degrees. For this case, the tuft-grid patterns indicate that mass injection at approximately the same mass-flow rates was not as effective as it was for an angle of attack of 9.5 degrees at V=150 ft/sec, or at an angle of attack of 13.5 degrees at V=100 ft/sec. There appears to be little difference in the tuft-grid patterns between m_i=0 and m_i=0.200 lb/sec at all downstream positions, and a slight decrease in swirl motion of the tufts at 0.280 lb/sec. The decrease in the swirl motion of the tufts is more pronounced at 20 chord lengths downstream than at 6.5 or 13.5 chord lengths downstream.

Further inspection of the tuft-grid photographs, Figures 20 through 22, shows that the vortex motion was contained in approximately an equal area for the noninjected or injected vortices. Thus, if the swirl velocities were decreased within this area, the circulation of the vortex would also be decreased.

Figures 23 and 24 show a series of tuft-grid photographs for the cases in which the velocity of injection was near sonic. The wind tunnel velocity for these cases was 150 ft/sec and the tip angles of attack were 9.5 and 13.5 degrees, as shown in Figures 23 and 24, respectively. For the lower angle of attack, Figure 23, comparison of the tuft-grid patterns of the noninjected case and one at a mass flow rate of 0.18 lb/sec shows a considerable amount of turbulent motion in the tufts for the injected vortex at 6.5 chord lengths downstream. Injection at a mass flow rate of 0.12 lb/sec does not appear to have effected this turbulent motion in the tufts. The vorticity distributions presented in Appendix II indicate that the vortex which was injected at a mass flow rate of 0.18 lb/sec had been spread, whereas that injected at a mass flow rate of 0.12 lb/sec was not. The turbulent motion in the tuft grids is evident to a lesser degree at 13 chord lengths downstream, and comparison of the tuft-grid patterns shows a decreasing degree of swirl motion in the tufts with increasing mass flow. At 20 chord lengths downstream of the model, that is, in approximately 0.23 second, no evidence of a vortex could be detected on the tuft grid.

For the higher tip angle of attack, Figure 24, at a mass flow rate of 0.18 lb/sec, the swirl motion is much more distinctive on the tufts than that at the lower tip angle of attack at the same mass flow rate. At 6.5 chord lengths downstream, the turbulent motion of the tufts is noticeably less pronounced than at the lower angle of attack (Figure 23). There is also less evidence of this turbulent motion at 13 chord lengths downstream. At 20 chord lengths downstream with mass injection, the tufts show a rather weak swirl pattern, as evidenced by the lack of the typical blur which is evident without mass injection.

The tuft-grid studies qualitatively corroborate the quantitative measurements of the vorticity in the trailed vortices, as in most cases it has been observed that the degree of swirl motion of the tufts was less as mass injection was applied. The tuft-grid studies also showed that this decrease in swirl velocity could be effected without spreading the vortex, which indicates that the circulation strength of the vortex was decreased by mass injection. The vortex motion without mass injection was shown to be persistent up to 20 chord lengths downstream. Although no quantitative measurements of the swirl velocities

as a function of downstream position could be obtained from the studies, no swirl motion was observed on the tuft grids at 20 chord lengths for one mass-flow condition, where it had been observed farther upstream. From this observation and that shown for other mass-flow conditions, it can be concluded that the effects of mass injection propagate downstream. Conversely, the tuft-grid studies showed no evidence of the reformation of the vorticity as far as 20 chord lengths downstream of the models.

Figures 25 and 26 show the tuft grid patterns for the Ogee-tip configuration for a wind tunnel velocity of 150 ft/sec, and at root angles of attack of 8, 10 and 12 degrees at 6.5 and 13 chord lengths downstream, respectively. The resolution of the photographs at 20 chord lengths downstream was not sufficient to show the noted effects of the Ogee tip. At a root angle of attack of 8 degrees, there is practically no evidence of swirl motion in the tuft grids at 6.5 chord lengths downstream, while at 13 chord lengths downstream, only slight evidence of swirl motion can be seen. As the root angle of attack is increased to 10 degrees, turbulent motion begins to appear in the tufts. At 13 chord lengths downstream, only slight evidence of swirl motion appears on the tuft grid that would be indicative of a concentrated vortex. At 12 degrees angle of attack, the turbulent motion in the tufts becomes more pronounced and spreads over a wider tuft area. Indications of swirl motion are more distinguishable 13 chord lengths downstream of the model than at 6.5 chord lengths downstream.

Qualitatively, the tuft-grid data for the Ogee-tip configuration support the quantitative balance measurements and the helium-bubble flow studies. Attempts to obtain vorticity distributions in the wake of the Ogee tip at 6.5 chord lengths downstream were unsuccessful, and the reason for this factor can be attributed to the lack of swirl motion as depicted in the photographs. Visual observation of the tufts at 20 chord lengths downstream showed no evidence of a concentrated vortex. On this basis, it can be concluded that the Ogee-tip configuration is efficient in diffusing the concentrated vortex that would normally be trailed off a conventional rotor-blade tip.

IV. ANALYSES OF RESULTS WITH APPLICATION TO FLIGHT HARDWARE

Since all of the tests that have been conducted to date have used only models, the injection requirements for a full-scale flight vehicle have not been determined experimentally. In order to extrapolate the model results to full-scale requirements, a means of scaling the results must be developed and verified. One manner of accomplishing this is to extrapolate experimental data obtained with scale models to full-scale values. This extrapolation has been done in Figure 27, which presents the correlation of the modified circulation in the wake as a function of the thrust of the jet injecting the vortex. As can be seen from the data presented in Figure 27, above a certain value of the jet thrust, very little additional dissipation is achieved for a vortex having a specific initial strength. The straight line that is drawn in Figure 27 was passed through this somewhat optimum thrust value for each vortex of different initial strength. The slope of the line is thus the pounds of thrust required to dissipate the initial strength of the vortex to approximately 40% of its initial strength at 6.5 chord lengths downstream. Thus, if the initial strength of the full-scale tip vortex is 400 ft^2/sec, this scaling parameter would predict that the jet thrust should be approximately 20 pounds to achieve the optimum dissipation at 6.5 chord lengths. Although a detailed theoretical analysis to substantiate the results of the vortex-injection technique and to scale the results to full-scale values was beyond the scope of this program, a brief, rather straightforward analysis of the diffusion of a trailing vortex by mass injection was conducted on the basis of the time-dependent decay of laminar line vortices in general.

Lamb (Ref. 6) solved the problem of the diffusion of a laminar line vortex with time. If time is replaced by z/V_∞ in Lamb's solution, where z is a distance from the trailing edge downstream, the same solution can be applied to the decay of the trailing vortex downstream. This solution is

$$\frac{\Gamma}{\Gamma_0} = 1 - e^{-\eta} \qquad (1)$$

where

$$\eta = \frac{V_\infty r^2}{4\nu z} \tag{2}$$

where Γ is circulation at any η, and Γ_0 is the circulation at $z = 0$ or η equal to infinity.

The circulation of a line vortex may be expressed as

$$\Gamma = 2\pi r v_\phi \tag{3}$$

where v_ϕ is swirl velocity. If the core radius, r_c, is defined as the radius at which v_ϕ is maximum, then the circulation in the core, Γ_c, of the vortex can be defined as

$$\Gamma_c = 2\pi r_c (v_\phi)_{max} \tag{4}$$

Squire (Ref. 7) suggested that a turbulent trailing vortex can be described by the same solution as Equation (1) if ν is replaced by ν_t, where ν_t is the kinematic eddy viscosity. Thus,

$$\frac{\Gamma}{\Gamma_0} = 1 - e^{-\eta \frac{\nu}{\nu_t}} \tag{5}$$

with

$$\eta = \frac{V_\infty r^2}{4\nu z}$$

If

$$\frac{\Gamma_c}{\Gamma_0} = k = 1 - e^{-\eta_c \frac{\nu}{\nu_t}} \tag{6}$$

with

$$\eta_c = \frac{V_\infty r_c^2}{4\nu z} \tag{7}$$

then k can be obtained from Equations (4) and (5). Theoretically, $k = 0.716$, although empirically it varies, depending on Γ_0/ν.

Also, from Equations (4) and (5),

$$\frac{\nu_t}{\Gamma_0} = a = \frac{-1}{16\pi^2} \frac{k^2}{\ell n(1-k)} \frac{\Gamma_0 V_\infty}{(V_\phi)^2_{max} z} \tag{8}$$

If the observed value of the maximum tangential velocity at an axial distance z is known, ν_t can be estimated from Equation (8). Also $(V_\phi)^2_{max} z$ is approximately constant far downstream (self-similar solution), where z is measured from a virtual origin chosen so that $(V_\phi)^2_{max} z$ is a constant.

Empirically, according to S. P. Govindaraju and P. G. Saffman (Ref. 8), the value of 'a' is a function of Reynolds number, i.e., Γ_0/ν, and it varies from 10^{-3} to 10^{-5} depending on Γ_0/ν. P. R. Owen (Ref. 9), using k=0.716, obtained

$$(V_\phi)^2_{max} z = \left(\frac{1}{4\pi A}\right)^2 \Gamma_0^{3/2} \nu^{-1/2} V_\infty \tag{9}$$

where A depends on the age of the vortex. For sufficiently far downstream distances, A can be taken as 1.2. Equations (8) and (9) therefore give

$$\nu_t = \frac{-k^2}{\ell n(1-k)} A^2 \Gamma_0^{1/2} \nu^{1/2} \tag{10}$$

Equation (5) can also be used to determine the vortex decay caused by the injection of a turbulent jet into the core by replacing ν_t by ε_m, where ε_m is the kinematic eddy viscosity of the injected jet.

According to the measurements of Van der Hegge Zijne (Ref. 10) and Alexander, Baron, and Comings (Ref. 11) for incompressible jets (turbulent) in still air, and for

$$\varepsilon_m = 0.0137 V_j d_j \tag{11}$$

where V_j is the jet velocity and d_j is the jet diameter, Abramovich (Ref. 12) showed that the compressibility effects were negligible when the maximum velocity of jet mixing flow is subsonic.

Wygnanski's results (Ref. 13) show that ε_m for the jet in a free stream depends on the value of free-stream velocity, jet thrust, mass flow, etc. In the mass injection process, a jet issues in a core of a vortex. If it is assumed that the axial velocity in the core is equal to the free-stream velocity, it can be assumed that

$$\varepsilon_m = 0.0137 \int \delta (V_j - V_\infty) dj \tag{12}$$

where δ is a function of the free-stream velocity V_∞. It is observed that the value of δ reaches an asymptotic value of 1/2 for subsonic jets for $V_\infty > 150$ fps. Thus δ is approximately a constant.

With mass injection,

$$\frac{\Gamma_{mc}}{\Gamma_0} = 1 - e^{-\eta_c \frac{\nu}{\varepsilon_m}} \tag{13}$$

with

$$\eta_c = \frac{V_\infty r_c^2}{4\nu z}$$

where Γ_{mc} is the circulation with mass injection at η_c.

Eliminating Γ_0 from Equations (6) and (13), the following expression is obtained:

$$\frac{\Gamma_{mc}}{\Gamma_c} = \frac{1}{k}\left(1 - e^{-\eta_c \frac{\nu}{\varepsilon_m}}\right)$$

Using Equation (6) this expression can be rewritten as

$$\frac{\Gamma_{mc}}{\Gamma_c} = \frac{1}{k}\left(1 - e^{\ell n(1-k)\frac{\nu t}{\varepsilon_m}}\right) \tag{14}$$

Combining Equations (10) and (11) yields

$$\frac{\nu_t}{\varepsilon_m} = \frac{-k^2}{\ell n(1-k)} \frac{\Lambda^2 \Gamma_0^{1/2} \nu^{1/2}}{0.0137 \delta (V_j - V_\infty) d_j} \tag{15}$$

and, therefore, Equation (14) becomes

$$\frac{\Gamma_{mc}}{\Gamma_c} = \frac{1}{k}\left[1 - e^{\frac{-k^2\Lambda^2}{0.0137} \frac{\nu^{1/2}\Gamma_0^{1/2}}{\delta (V_j - V_\infty) d_j}}\right] \tag{16}$$

Substituting $k = 0.716$, $\Lambda = 1.2$, $\nu = 166 \times 10^{-6}$ ft^2/sec, the following expression is obtained:

$$\frac{\Gamma_{mc}}{\Gamma_c} = 1.4\left[1 - e^{-0.693 \frac{\Gamma_0^{1/2}}{\delta (V_j - V_\infty) d_j}}\right] \tag{17}$$

The verification of the above relation can be obtained empirically by using the vorticity surveys from Reference 4 and those from the tests in the present program. The circulation values were obtained by integrating the vorticity plots taken at 6.5 chord lengths downstream.

Instead of comparing Γ_{mc}/Γ_c, comparisons can be made of the total integrated values of the circulation, that is, Γ_m/Γ_0. It was observed that $\Gamma_{mc}/\Gamma_c \approx \Gamma_m/\Gamma_0$.

$$\frac{\Gamma_m}{\Gamma_0} = 1.4\left[1 - e^{-0.693 \frac{\Gamma_0^{1/2}}{\delta (V_j - V_\infty) d_j}}\right] \tag{18}$$

One of the constraints on Equation (18) is that the expression in the brackets must have a value less than 1.0/1.4, that is, less than 0.716. The expression is invalid for values above

0.716 since the ratio Γ_m/Γ_0 would then be greater than unity. Physically, this means that no dissipative effect can be expected unless the jet velocity, V_j, exceeds the free-stream velocity, V_∞, by some incremental value. It is seen that if $V_j = V_\infty$, the expression in the brackets reduces to unity.

Comparisons of the theoretically-predicted and experimentally-measured flow rate for the conditions tested in Reference 4 and in the present program are shown in Figure 28. For the reasons discussed above, there is a break in the curve where $V_j = V_\infty$.

The break in the curve also occurs at the lower mass flows for the lower free-stream velocities, wherein the effect of mass injection on the basis of the difference, $V_j - V_\infty$, occurs at lower rates of mass flow. For the cases in which the velocity of injection was near sonic, the effect of mass injection occurs as soon as $m_i > 0$ because of the large difference in $V_j - V_\infty$.

In Reference 4, it was also shown that the variation of the circulation strength could be correlated in terms of the thrust rather than the mass flow, and that the effects of mass injection were most pronounced over a narrow range of thrust. The data from Reference 4 and the additional data that were obtained in this program are shown in Figure 29 with the corresponding theoretical variation of the circulation strength. The efficiency of maximizing the velocity of injection is also evident in these data. Because of the wide range of test conditions for which the experimental data correlates well with the predicted results, it is felt that the effects of vortex dissipation can be confidently extended to larger scales for vortices having the same age. Using the theoretical expression presented in Equation (18), a sonic nozzle having a diameter of 1.1 inches would dissipate the strength of a vortex having an initial value of 400 ft^2/sec to 40% of its strength at 6.5 chord lengths. The thrust developed by this nozzle is approximately 20 lb, which is the same as the value determined from extrapolating the experimental data. On the basis of the qualitative evaluation made in this program with tuft grids regarding the continuing dissipation of injected vortices with increasing downstream position, and on the basis of the quantitative measurements of injected vortices by NASA/Ames, it could be expected that an injected vortex that is trailed off a helicopter blade would also continue to dissipate with time. Because of the difficulty in obtaining quantitative measurements at positions farther downstream in the wake in this program, it is difficult to predict the variation in strength of an injected vortex with increasing time. The minimal benefits

that could be expected, however, on the basis of the dissipative effect shown at 6.5 chord lengths, are sufficiently encouraging to warrant serious consideration of the technique for adaptation to flight hardware.

The application of vortex injection has been discussed most frequently with regard to two-bladed rotor systems because of the inherent higher blade loadings associated with these rotor systems, which have, in part, helped to exaggerate the effects of blade-vortex interactions. For this rotor system, the effects of mass injection can be implemented with some confidence of success, because the most troublesome blade-vortex interactions that occur for the system are those in which a blade intersects its own vortex at the time that the age of the trailed vortex is approximately 1-1/2 revolutions. At a rotational speed of Ω = 324 rpm, blade-vortex interaction would occur approximately 0.28 second following the time that the vortex was trailed off the blade. In the wind tunnel measurements, the vortex, say, for V = 230 fps, α_T = 13.5°, was reduced to less than one-half of its uninjected strength in approximately 0.05 second. Allowing for wake contraction and advance ratio, a time interval of approximately 0.15 second would still be available before blade-vortex interaction would occur. It is expected that this time increment would be sufficient to reduce the injected vortex strength and thus minimize the effects of the interactions.

V. CONCLUSIONS

The research conducted under this contract has shown that mass injection holds viable promise for the rapid dissipation of a trailed tip vortex. It has also shown that a vortex can be diffused by suitable variation in the tip geometry of a lifting surface.

The following specific conclusions were made on the basis of the results of this research program.

Quantitative measurements demonstrated that:

1. A two-stage nozzle is slightly more effective in dissipating a tip vortex at low mass flows than a single-stage nozzle of comparable area, but it effects vortex spreading at a much lower mass-flow rate than the single-stage nozzle and thus is not a satisfactory system.

2. In terms of thrust, the most efficient method to dissipate a vortex by mass injection is by maximizing the velocity of injection.

3. At a position 6.5 chord lengths downstream of the model, the modified circulation strength of the injected vortex when plotted versus thrust reaches a minimum value. Little additional dissipative effect is obtained for thrust rates above this value.

4. The maximum degree of vortex dissipation is achieved for mass-flow or thrust rates that do not effect vortex spreading.

5. On the basis of the data obtained at a distance of 6.5 chord lengths downstream of the model, the optimum dissipative thrust is approximately 0.05 lb/unit of original circulation strength for all the configurations that were tested.

6. The performance characteristics of the blade sections tested are unaffected by the injection process.

7. Higher peak lift-to-drag ratios and higher lift-curve slopes are achieved by a model having an Ogee-tip geometry than a model having standard blade tips.

8. Beyond the peak lift-to-drag ratios, the L/D of a model having Ogee blade tips drops more sharply with increasing angle of attack than the standard blade tip.

9. On the basis of experimental data and theory, the requirements of the vortex injection system to dissipate a concentrated vortex scale linearly with the initial circulation strength of the vortex.

Qualitative observations demonstrated that:

1. The swirl motions of the vortex as visualized by a tuft-grid pattern are reduced with increasing downstream distance for a mass-injected vortex.

2. Neither the mass-injected vortex nor one diffused by the Ogee tip reforms at least for a downstream distance equivalent to 20 chord lengths of the model.

3. Based on helium-bubble flow visualization studies, the flow patterns across the lifting surfaces are basically the same whether or not the tip vortices are injected.

VI. RECOMMENDATIONS

On the basis of the results of this research program, it is recommended that:

1. Theoretical analyses of the benefits of mass injection and the Ogee-tip configurations be conducted in regard to the changes in dynamic loads, acoustic signatures, and performance characteristics for various flight conditions of various helicopter rotor configurations, particularly for those in which blade-vortex proximity or interaction is encountered.

2. The effects of high subsonic and transonic tip speeds on the effectiveness of the mass-injection technique be investigated.

3. The effects of the "effective" sweep angle which a rotor blade experiences as it traverses the azimuth in forward flight on the effectiveness of the mass-injection technique be investigated.

4. The effects of mass injection on the dynamic, acoustic, and performance characteristics of full-scale rotor blades be investigated under controlled conditions for flight conditions that can be simulated in a wind tunnel.

5. The effects of the "effective" sweep angle which a rotor blade experiences as it traverses the azimuth in forward flight on the Ogee configuration be investigated.

6. A theoretical analysis of the stability and dissipative characteristics of noninjected and injected vortices be developed so that applications to flight systems can be enhanced and expedited without resorting to detailed testing.

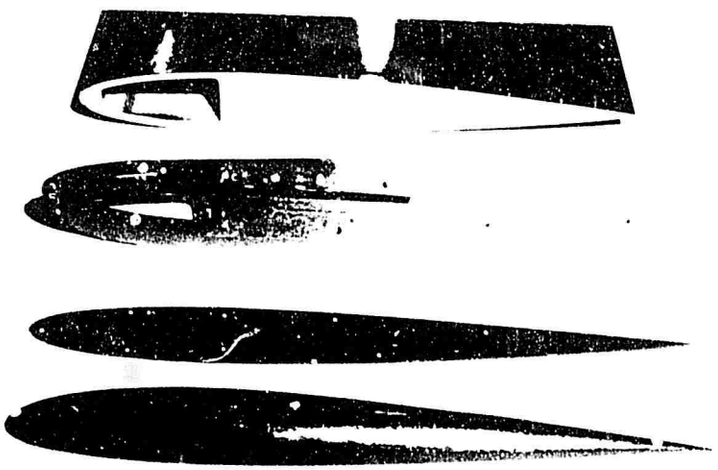

Figure 1. Typical Nozzle Assembly.

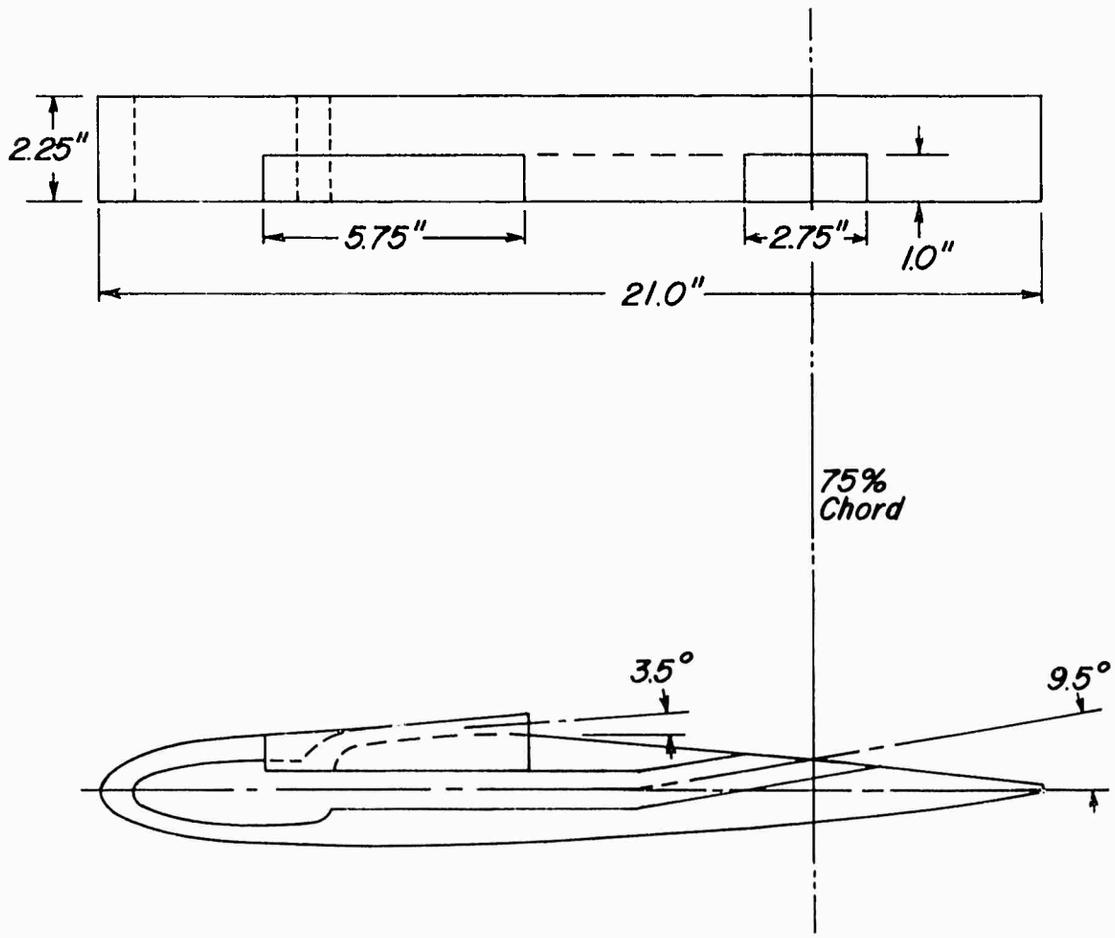

Figure 2 . Schematic Diagram of the Two-Section Nozzle.

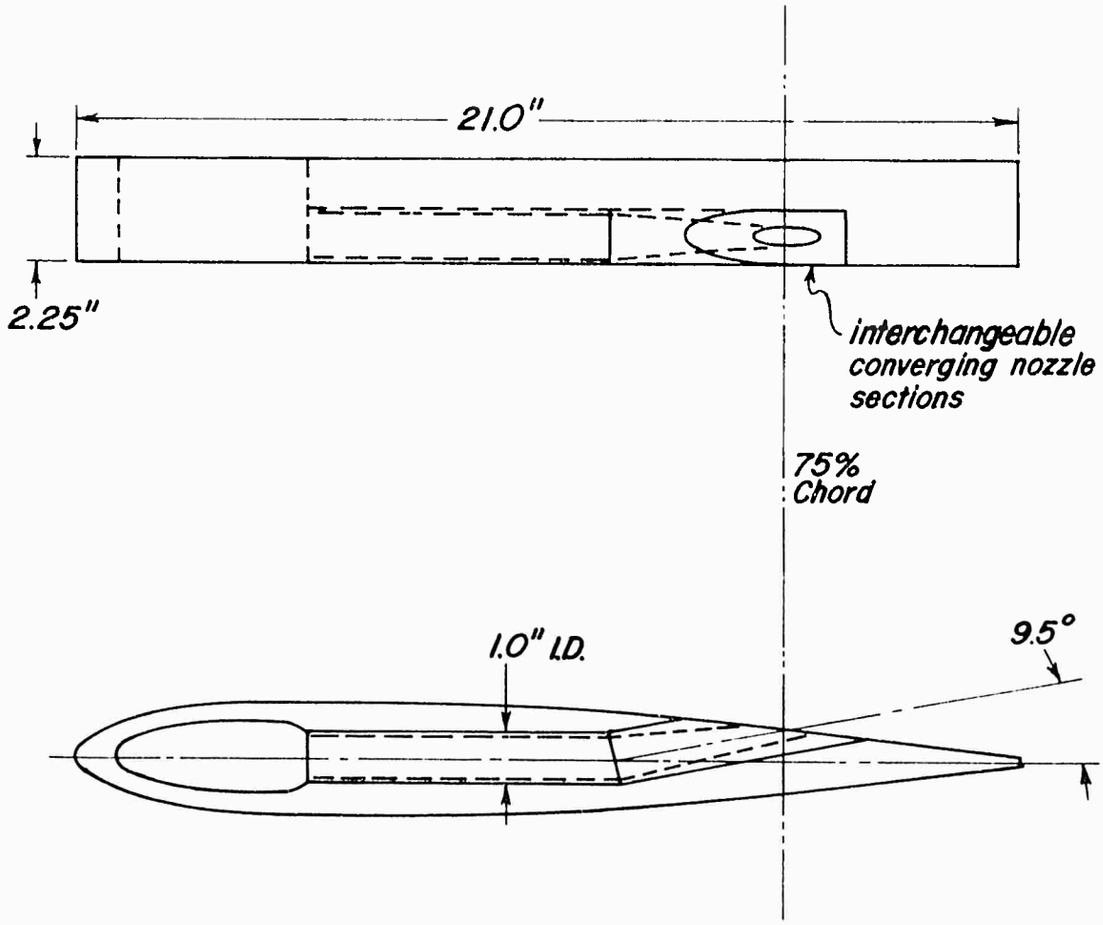

Figure 3. Schematic Diagram of the High-Velocity Nozzle Section.

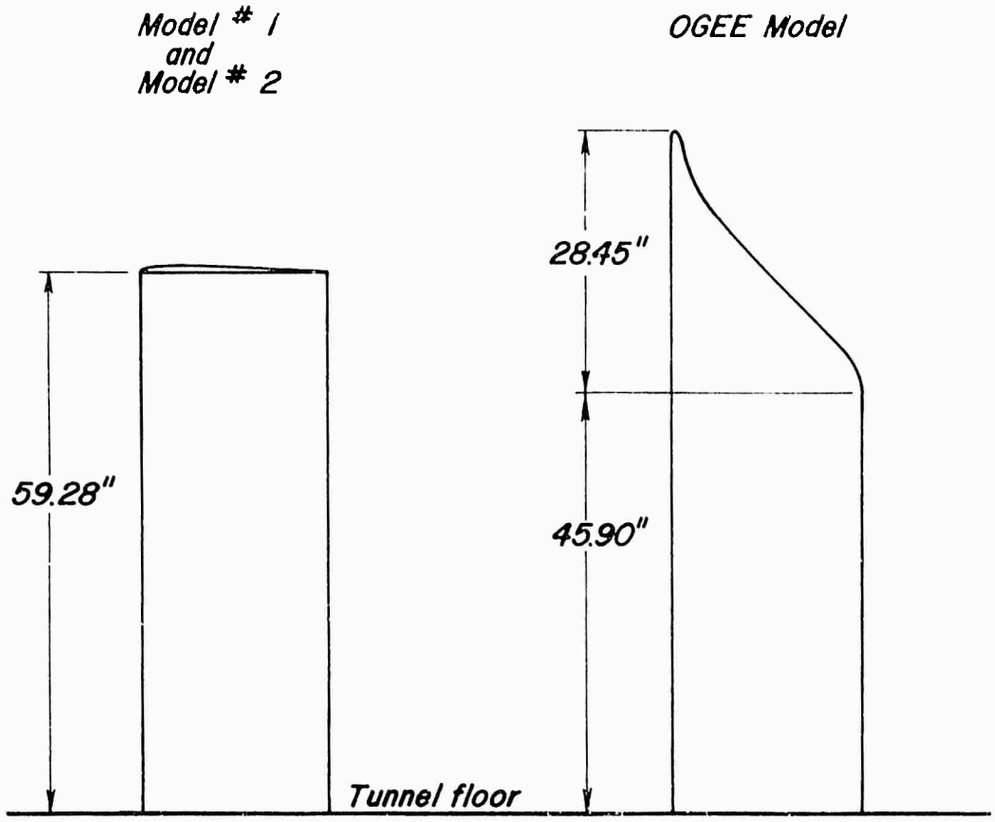

Figure 4. Schematic Diagram of the Model Installations in the Wind Tunnel.

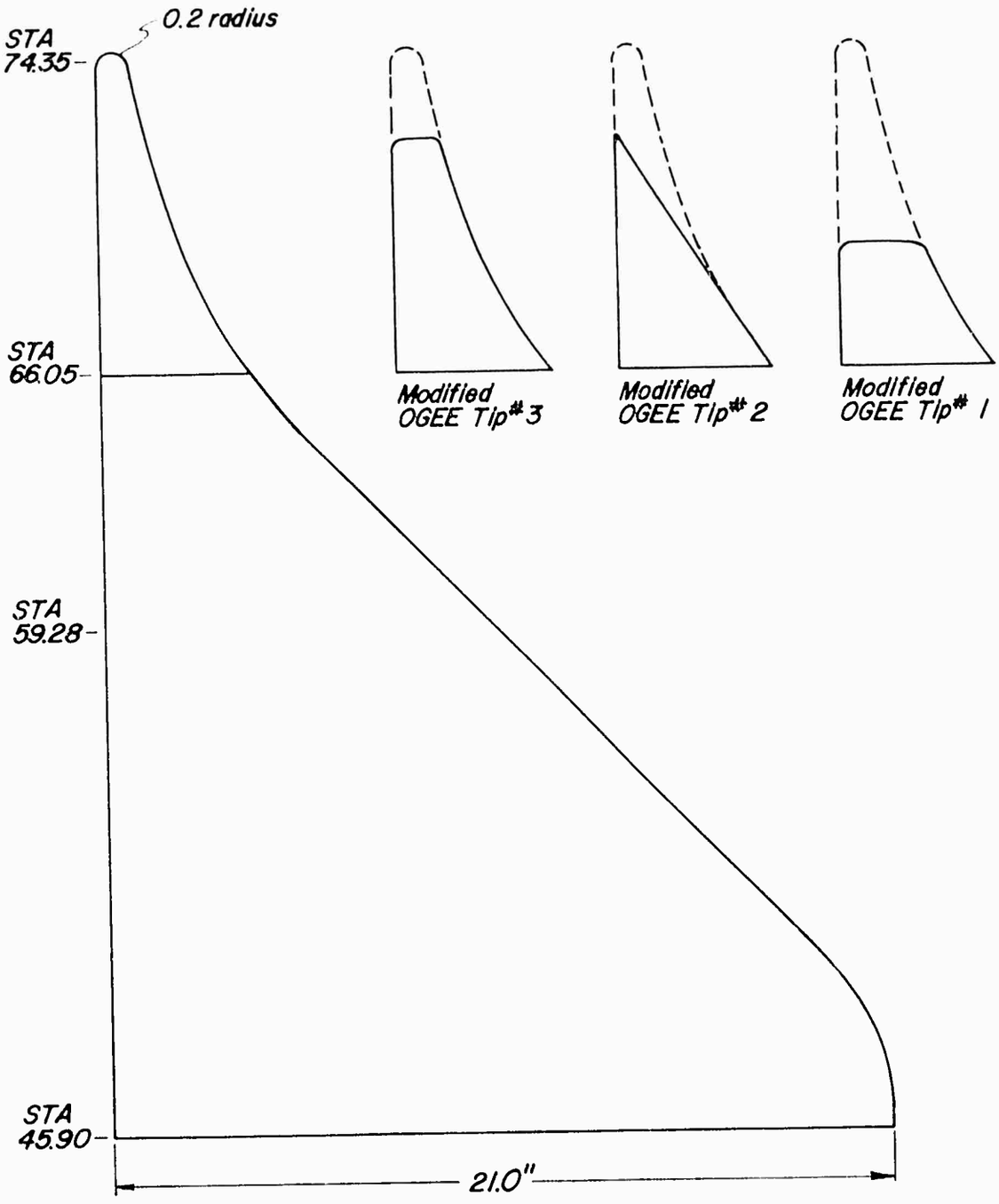

Figure 5. Ogee Tip Configurations.

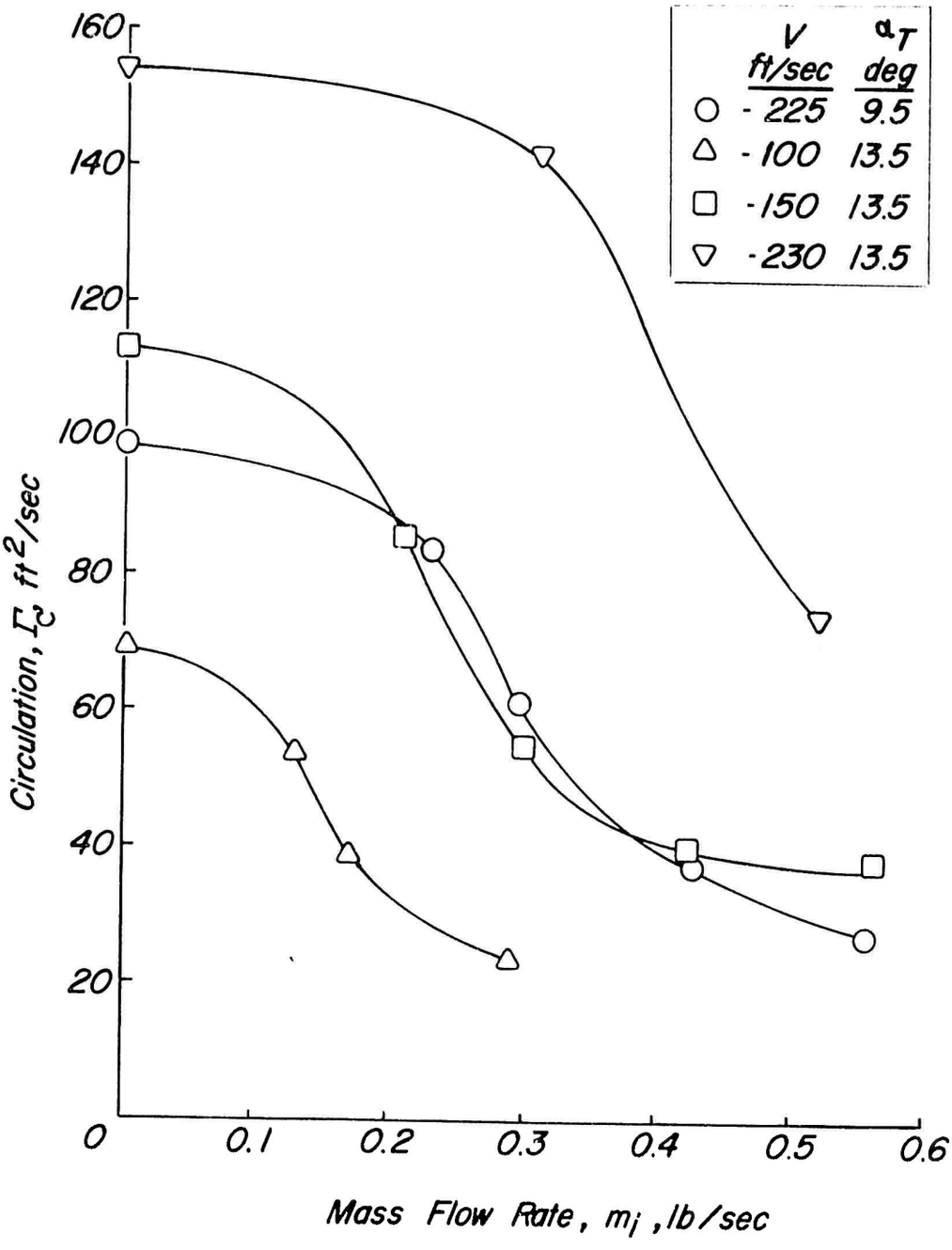

Figure 6. Circulation Vs. Mass Flow Rate at Low-Velocity Injection.

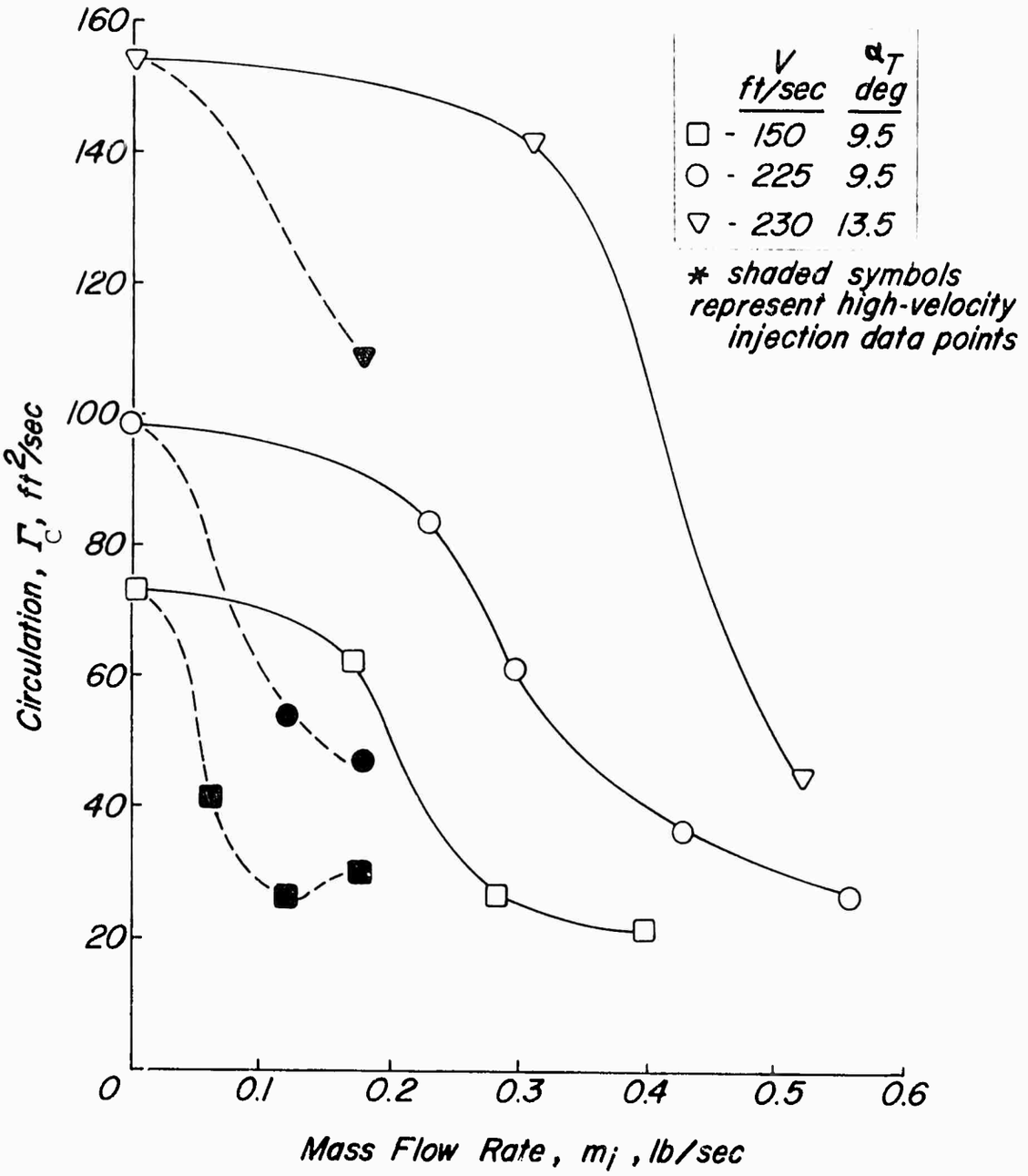

Figure 7. Circulation Vs. Mass Flow Rate at High-Velocity Injection.

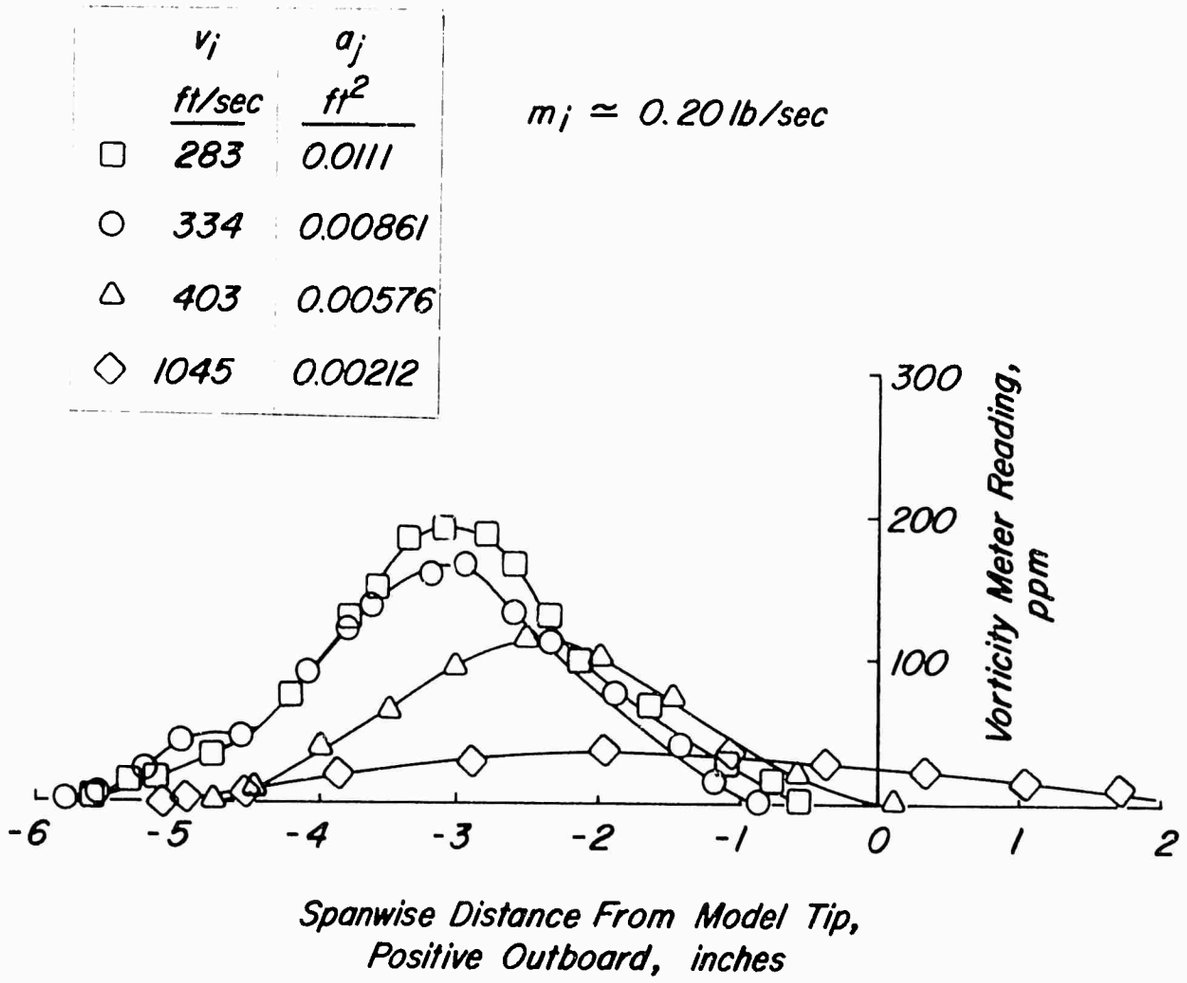

Figure 8. Comparison of Vorticity Distributions; V = 150 ft/sec and α_T = 9.5°.

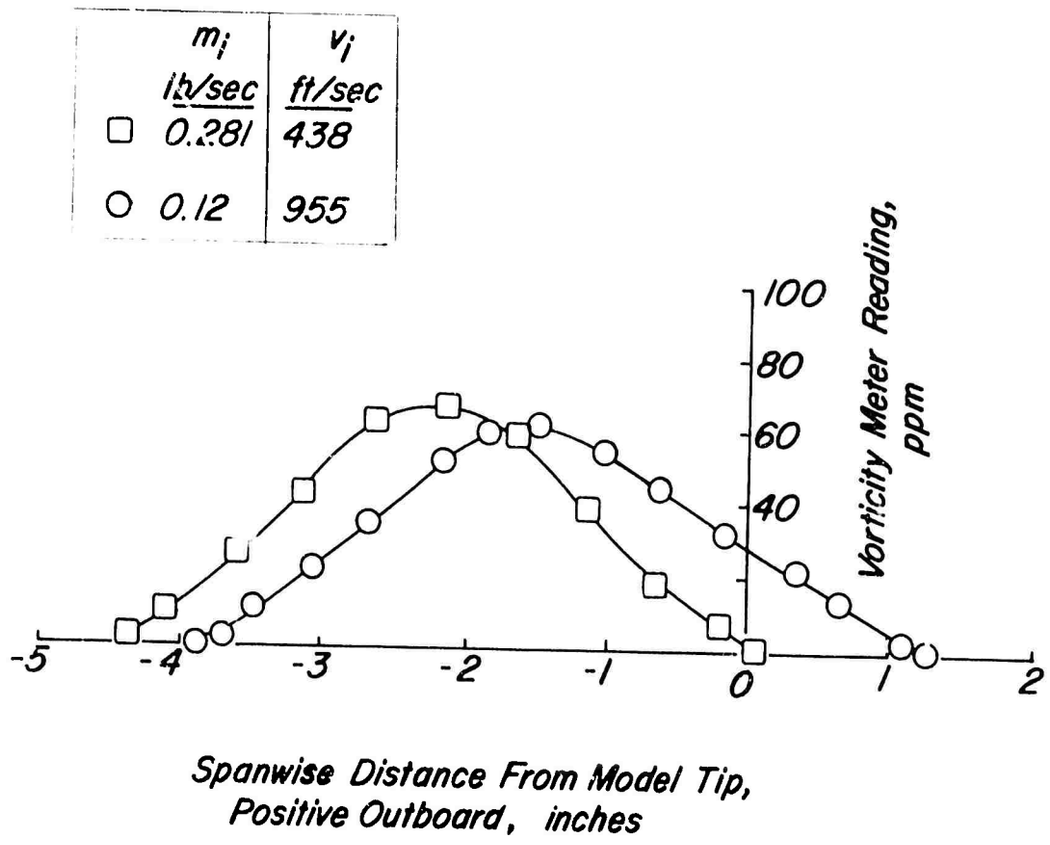

Figure 9. Comparison of Vorticity Distributions; V = 150 ft/sec and α_T = 9.5°.

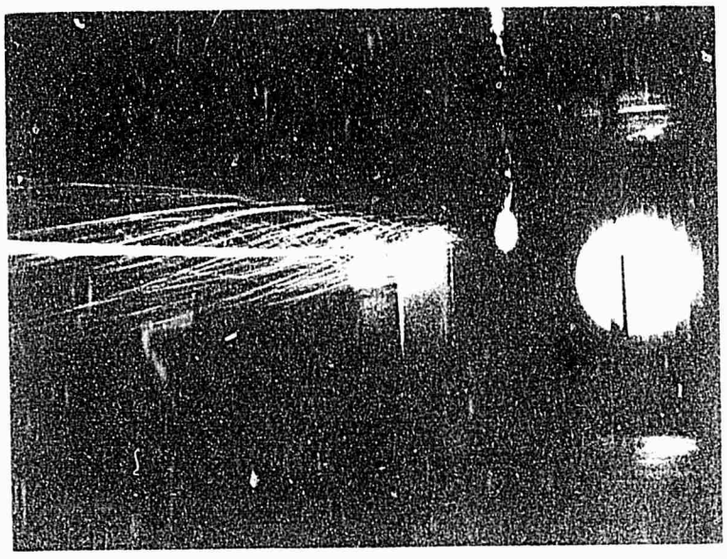

Without Mass Injection

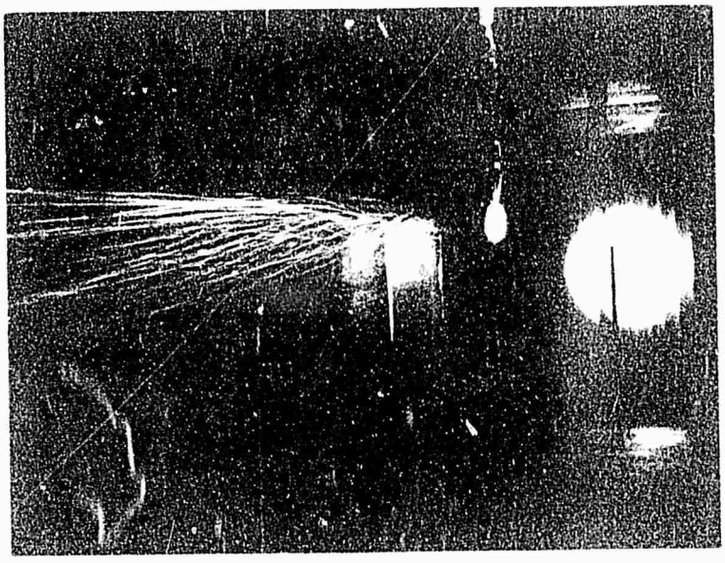

With Mass Injection

Figure 10. Influence of Mass Injection on the Flow Field With a 1/2-Inch-Diameter High-Velocity Nozzle.

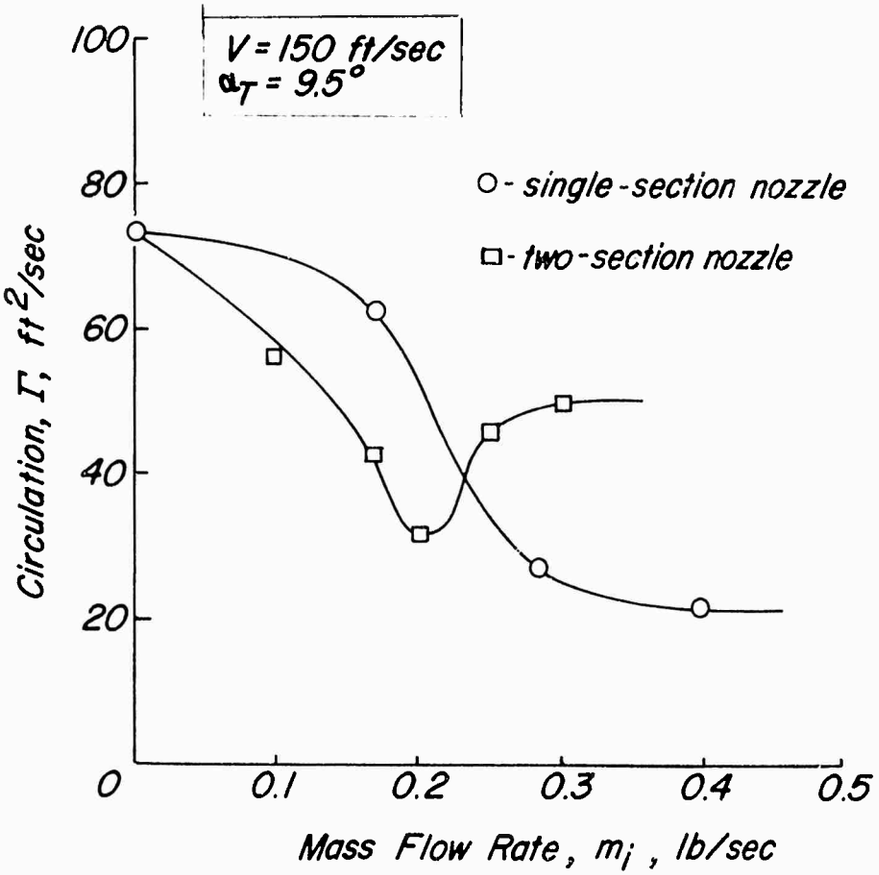

Figure 11. Comparison of Circulation Vs. Mass Flow Rate of the Two-Section and Single-Section Nozzle.

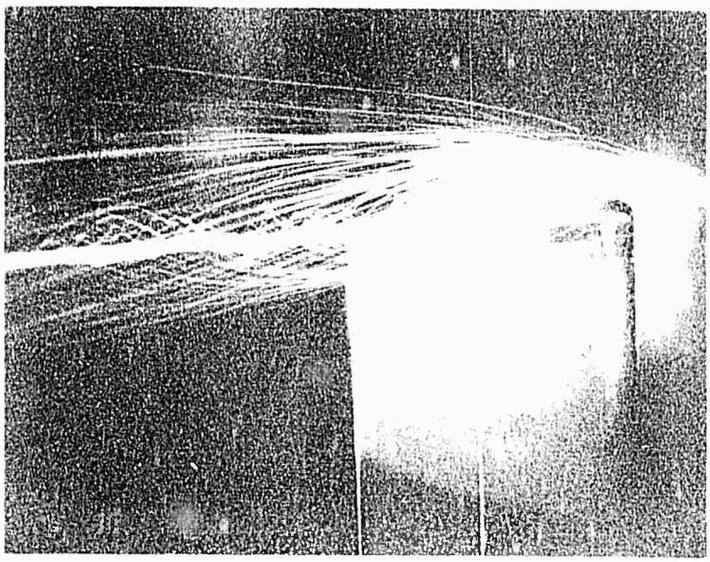

Without Mass Injection

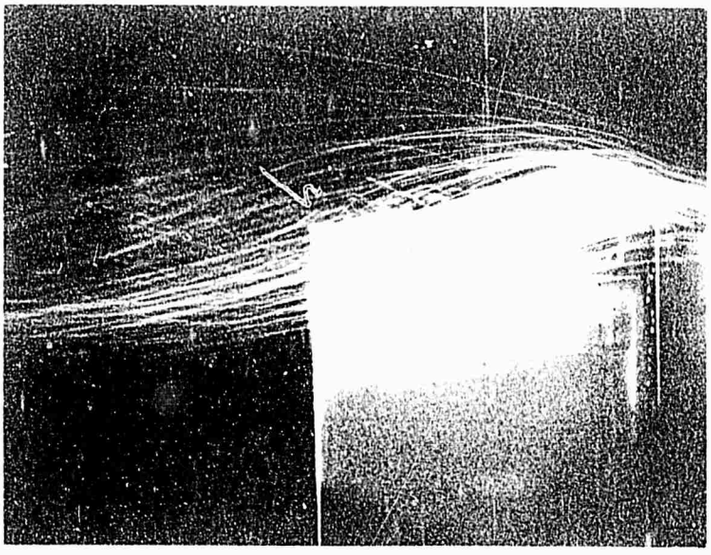

With Mass Injection

Figure 12. Influence of Mass Injection With a Two-Section Nozzle on the Flow Field in the Proximity of the Model.

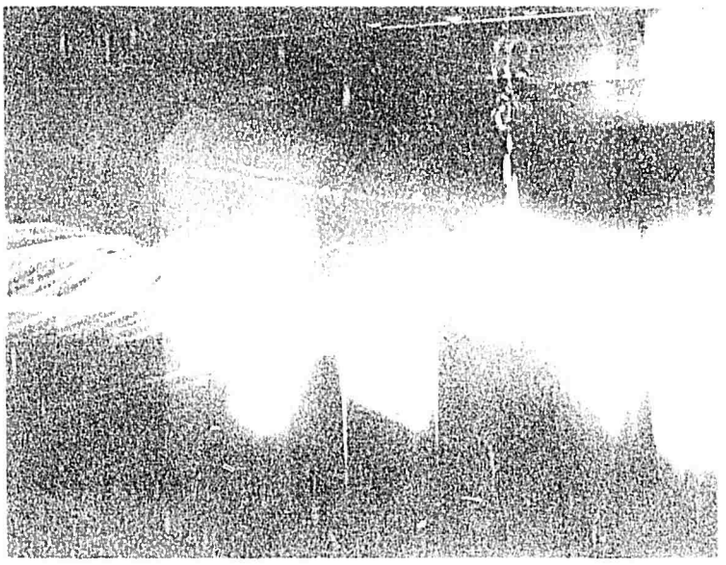

Without Mass Injection

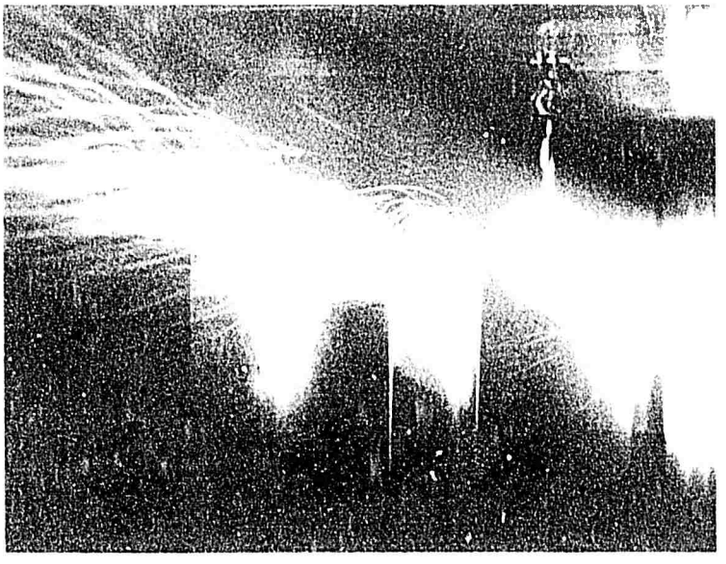

With Mass Injection

Figure 13. Influence of Mass Injection With a Two-Section Nozzle on the Flow Field in the Wake of the Model.

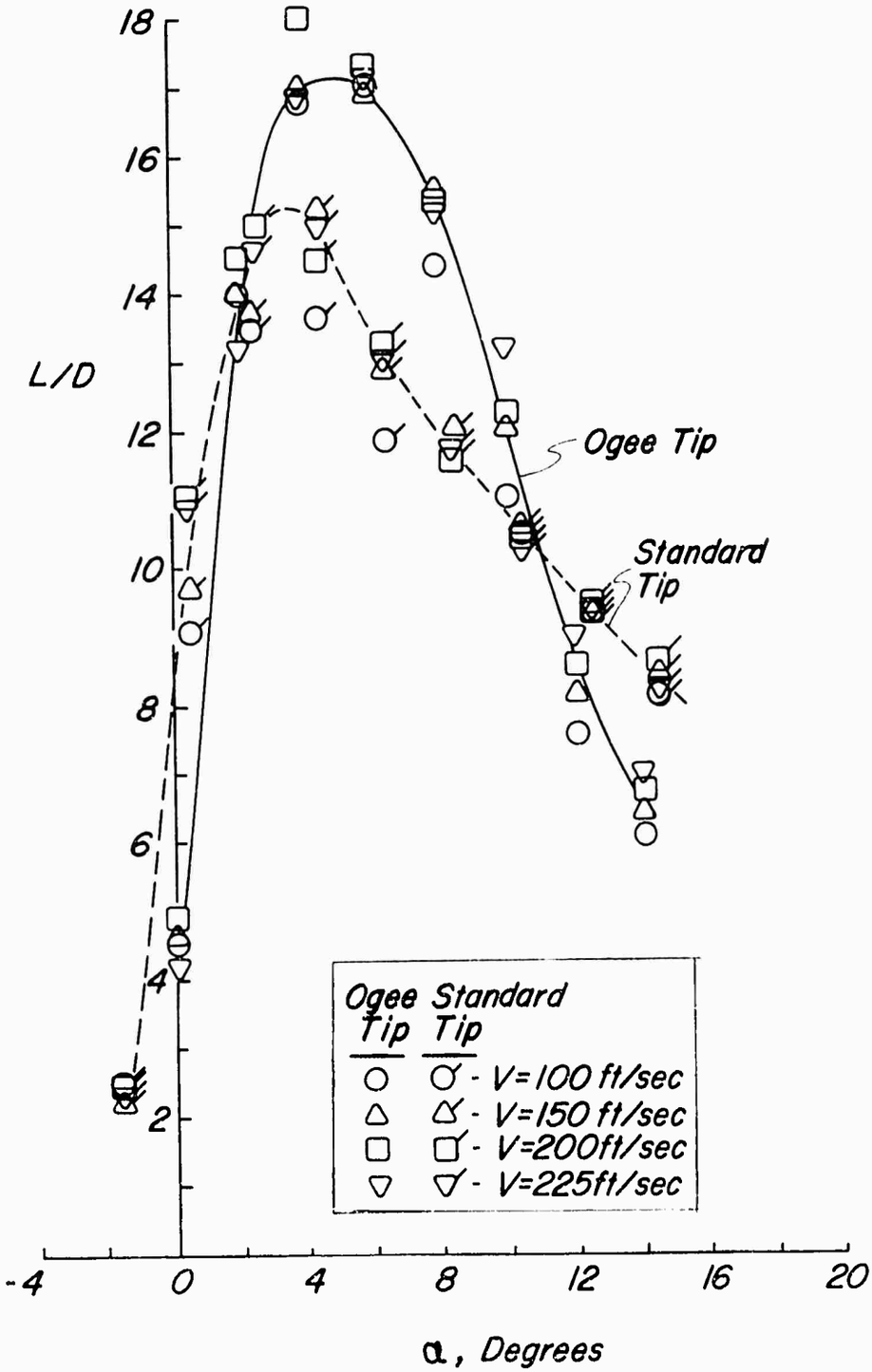

Figure 14. Comparison of Lift-To-Drag Ratio Vs. Angle of Attack for the Standard-Tip and Ogee-Tip Configurations.

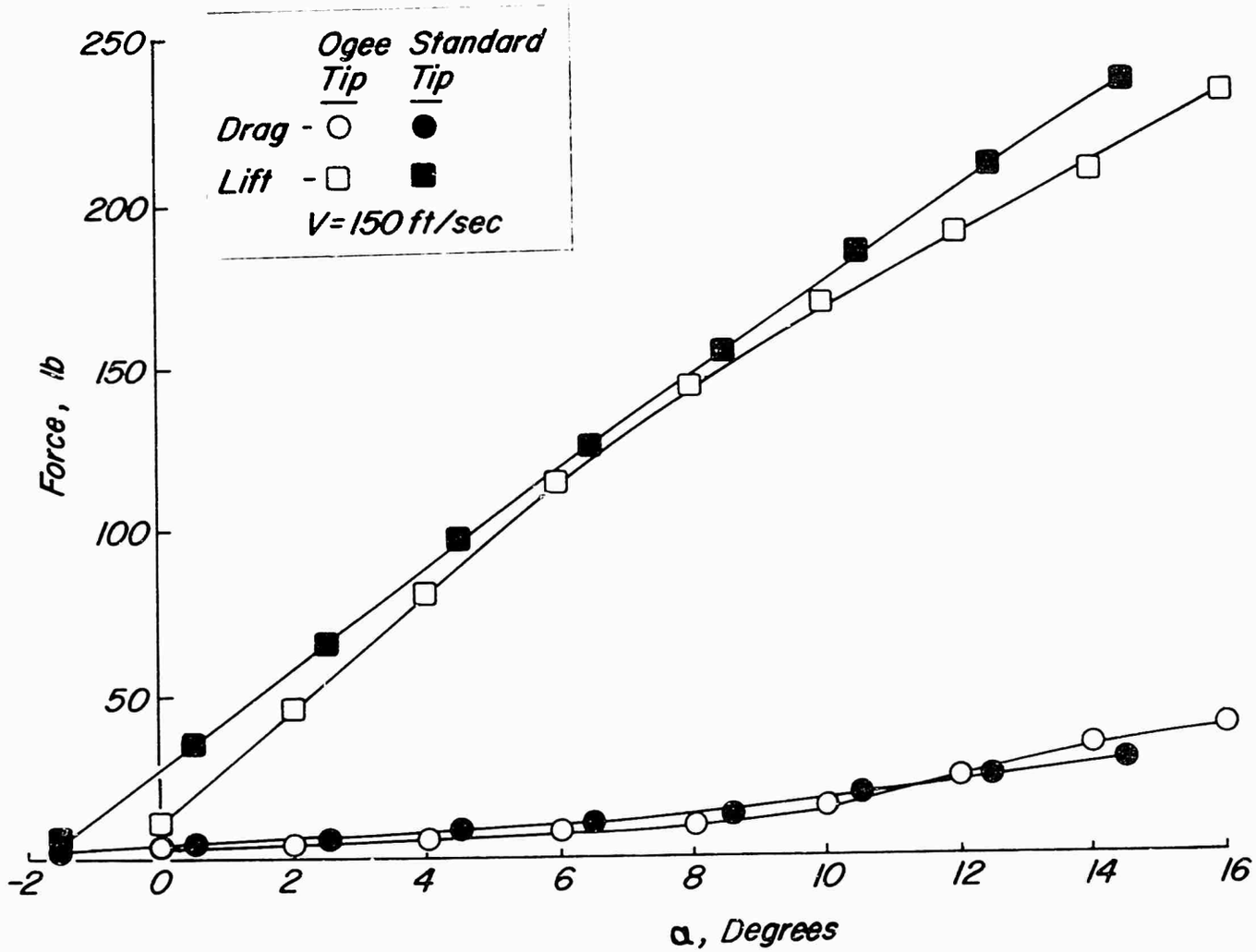

Figure 15. Comparison of Lift and Drag Vs. Angle of Attack for the Standard-Tip and Ogee-Tip Configurations.

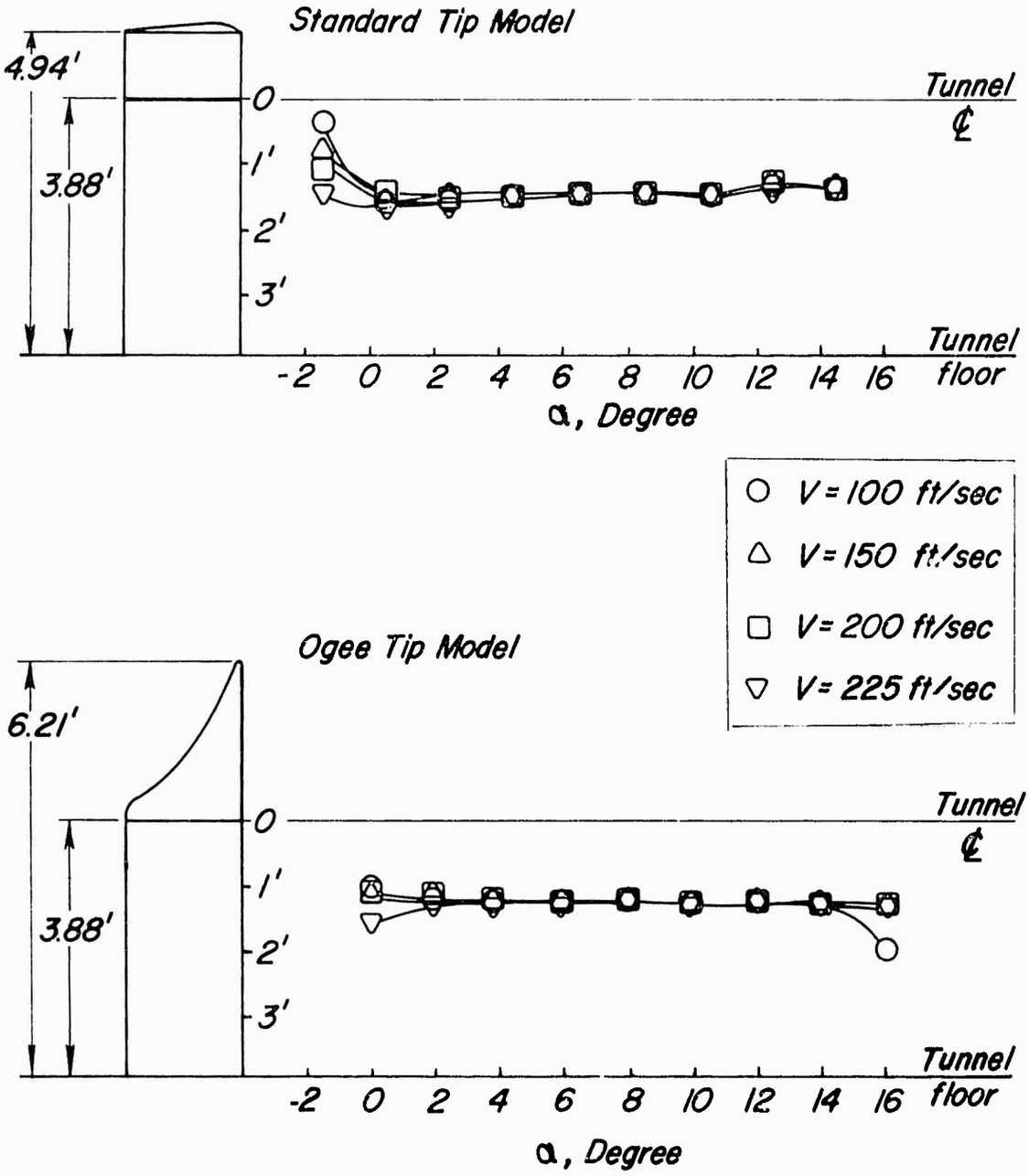

Figure 16. Variation of the Spanwise Lift Center Vs. Angle of Attack for the Standard-Tip and Ogee-Tip Configurations.

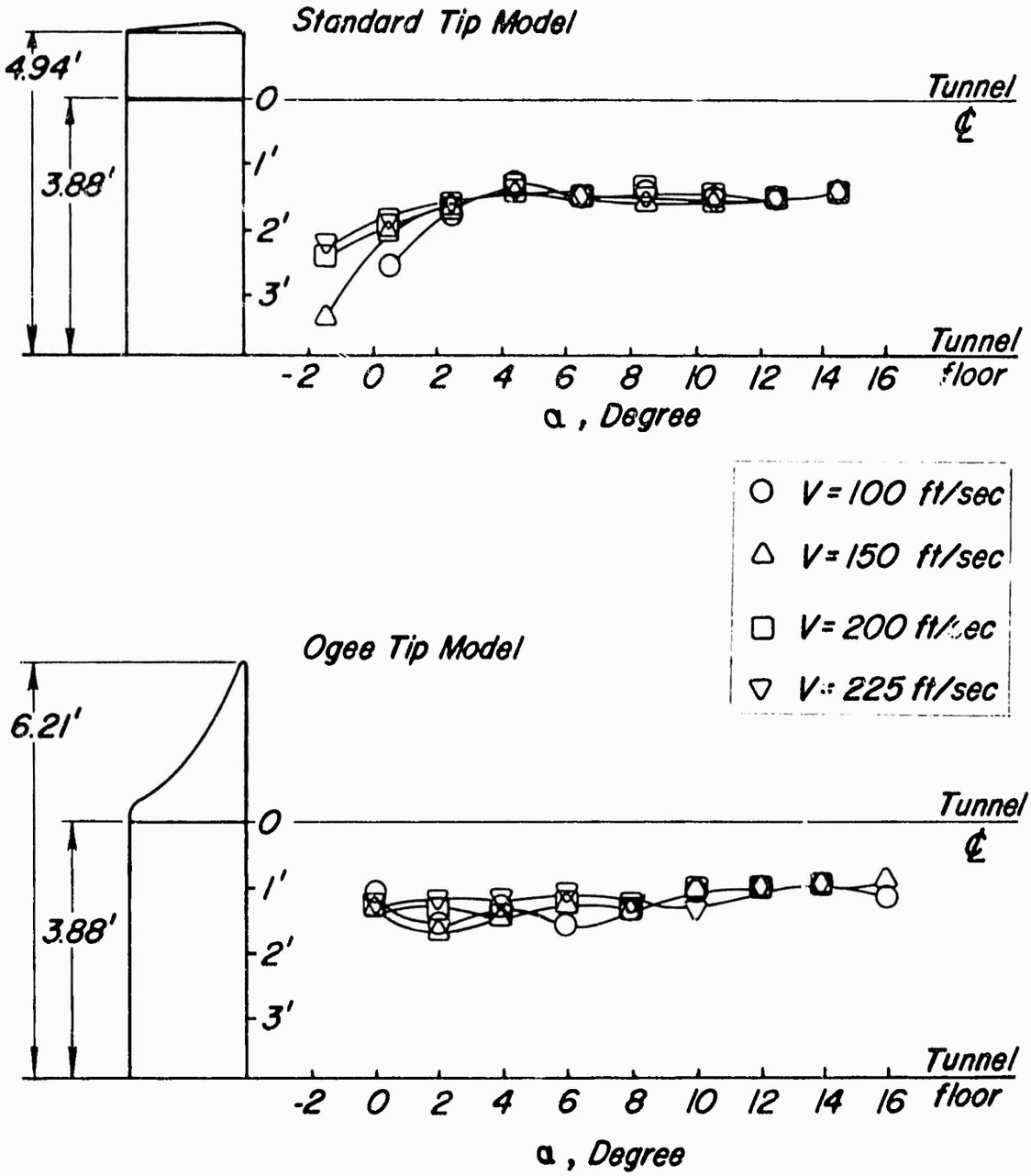

Figure 17. Variation of the Spanwise Drag Center Vs. Angle of Attack for the Standard-Tip and Ogee-Tip Configurations.

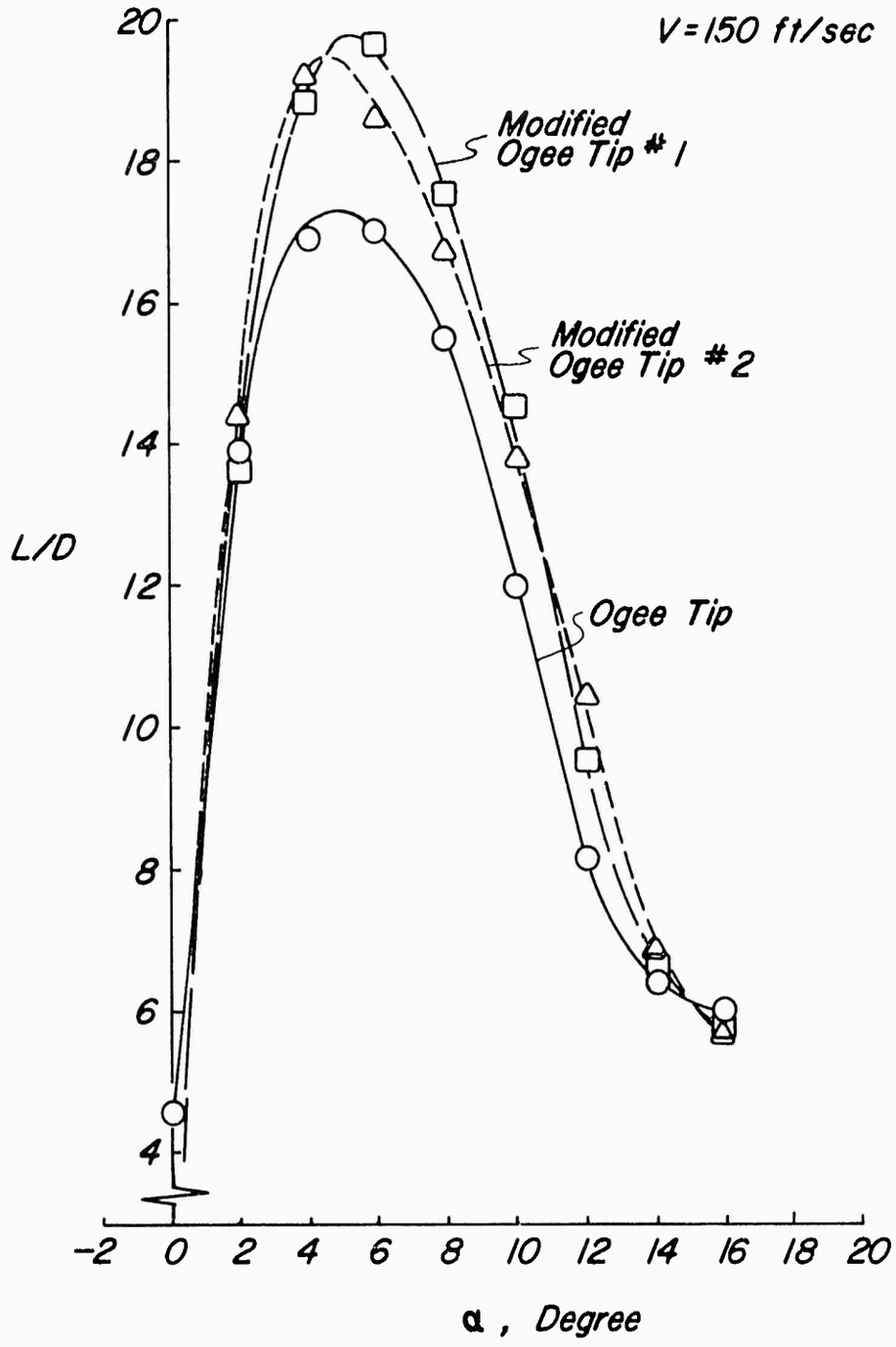

Figure 18. Comparison of Lift-to-Drag Ratios Vs. Angle of Attack for Various Ogee-Tip Configurations.

Unmodified
Ogee

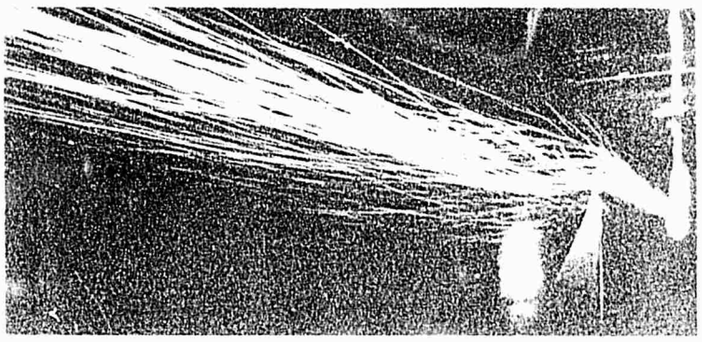

Modification
No. 2

Modification
No. 1

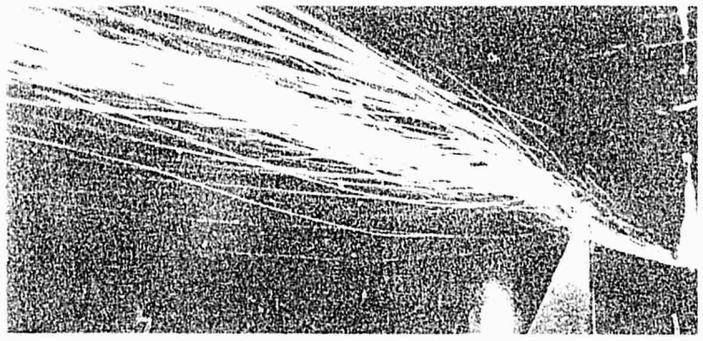

Modification
No. 1

Figure 19. Flow Field on the Test Side for Various Downstream Configurations.

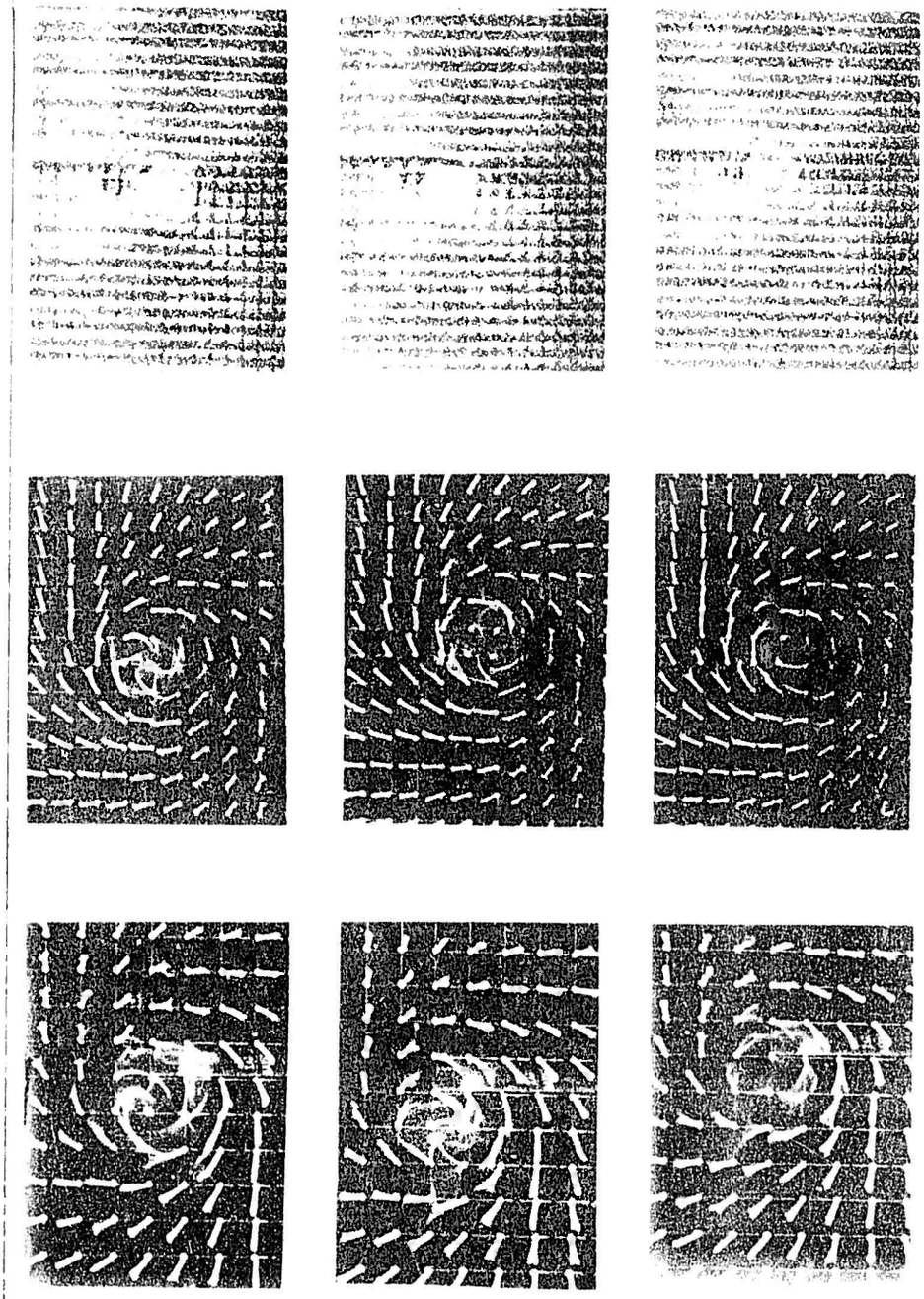

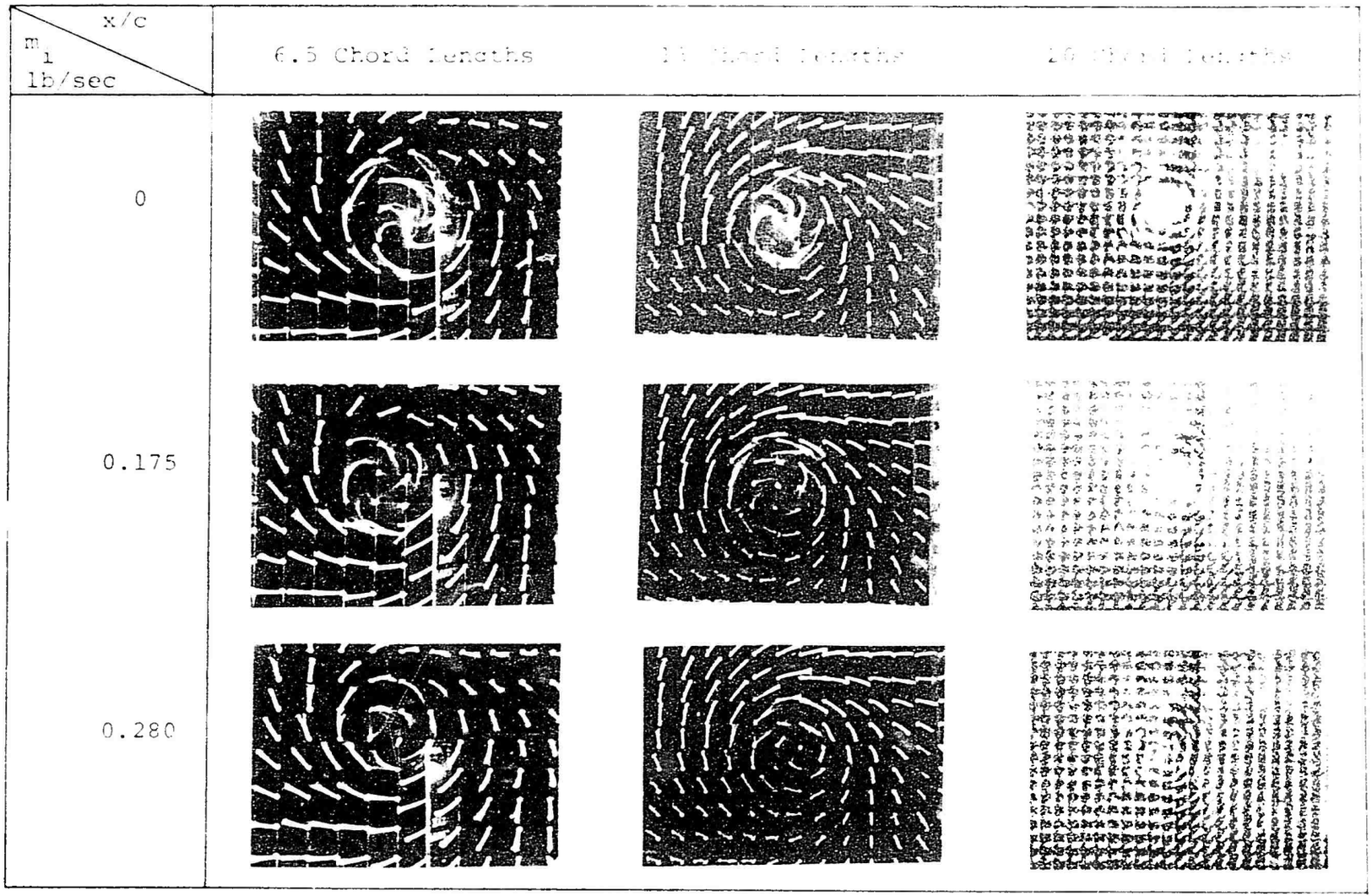

Figure 21. Tuft-Grid Visualization for Model No. 1; V = 100 ft/sec, α_g = 13.5°.

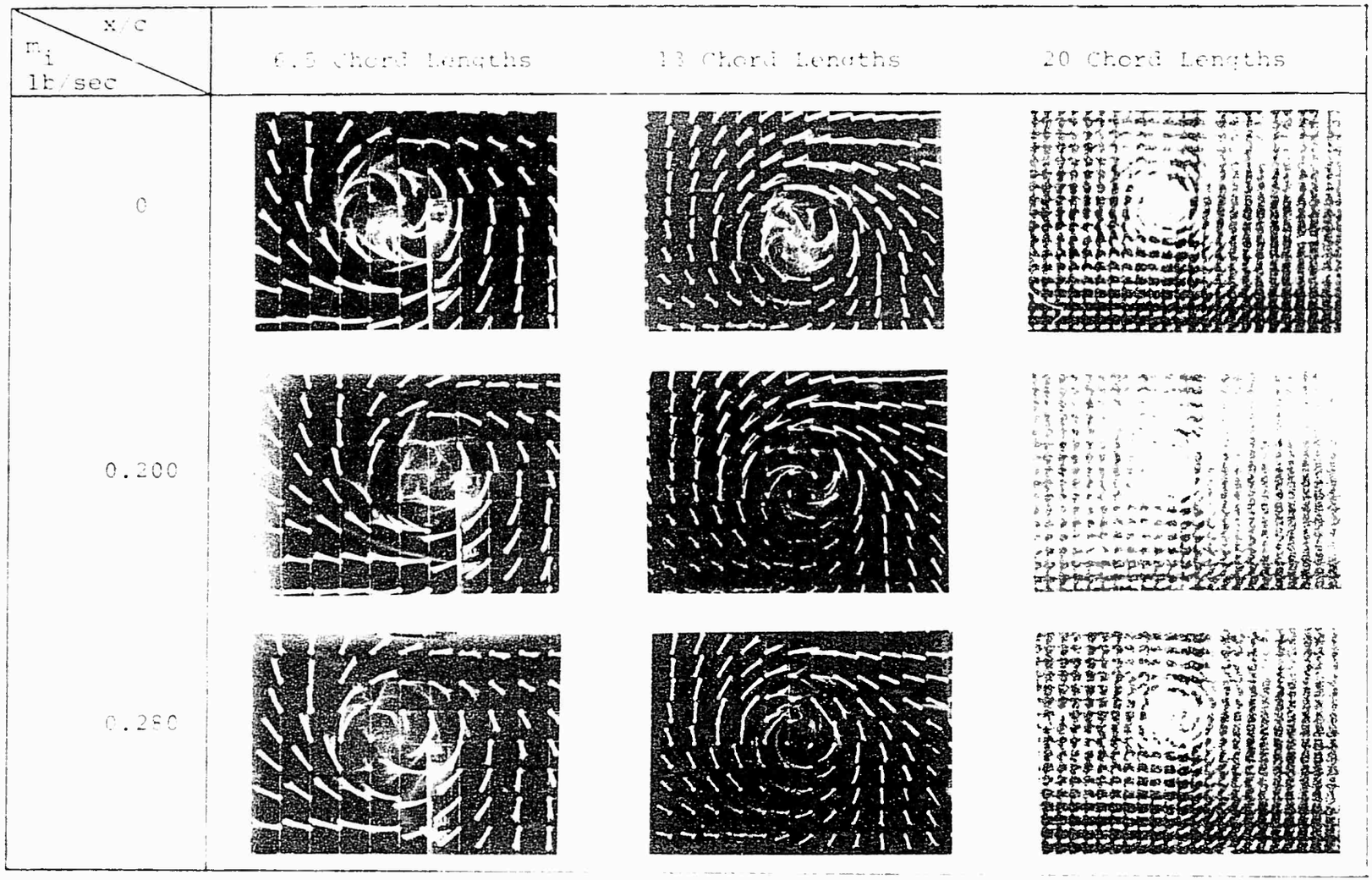

Figure 21. Tuft-Grid Visualization for Model No. 1; V = 150 ft/sec, α_∞ = 13.5°.

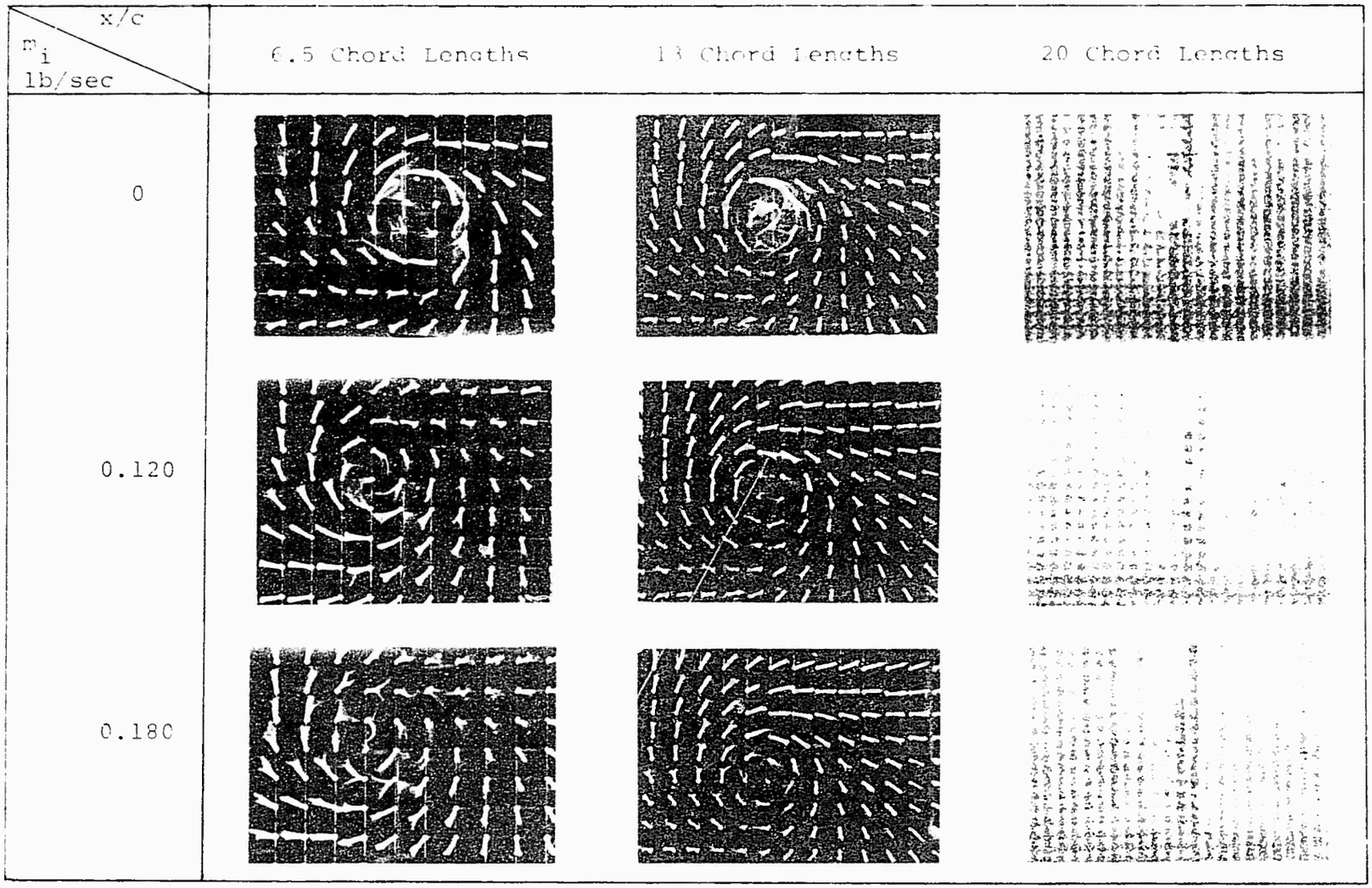

Figure 23. Tuft-Grid Visualization for Model No. 2; V = 150 ft/sec, α_T = 9.5°.

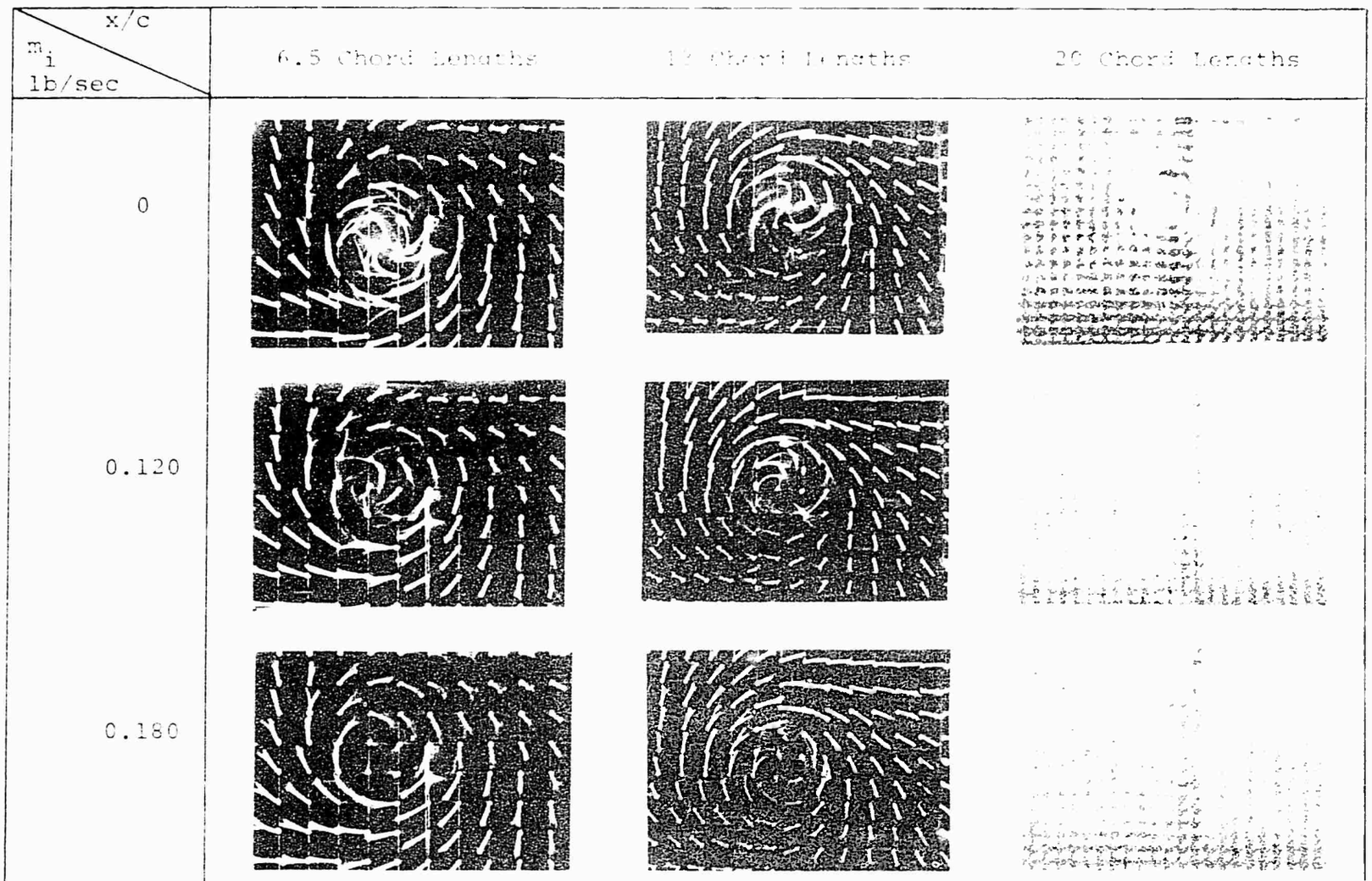

Figure 24. Tuft-Grid Visualization for Model No. 2; V = 100 ft/sec, α_w = 13.5°.

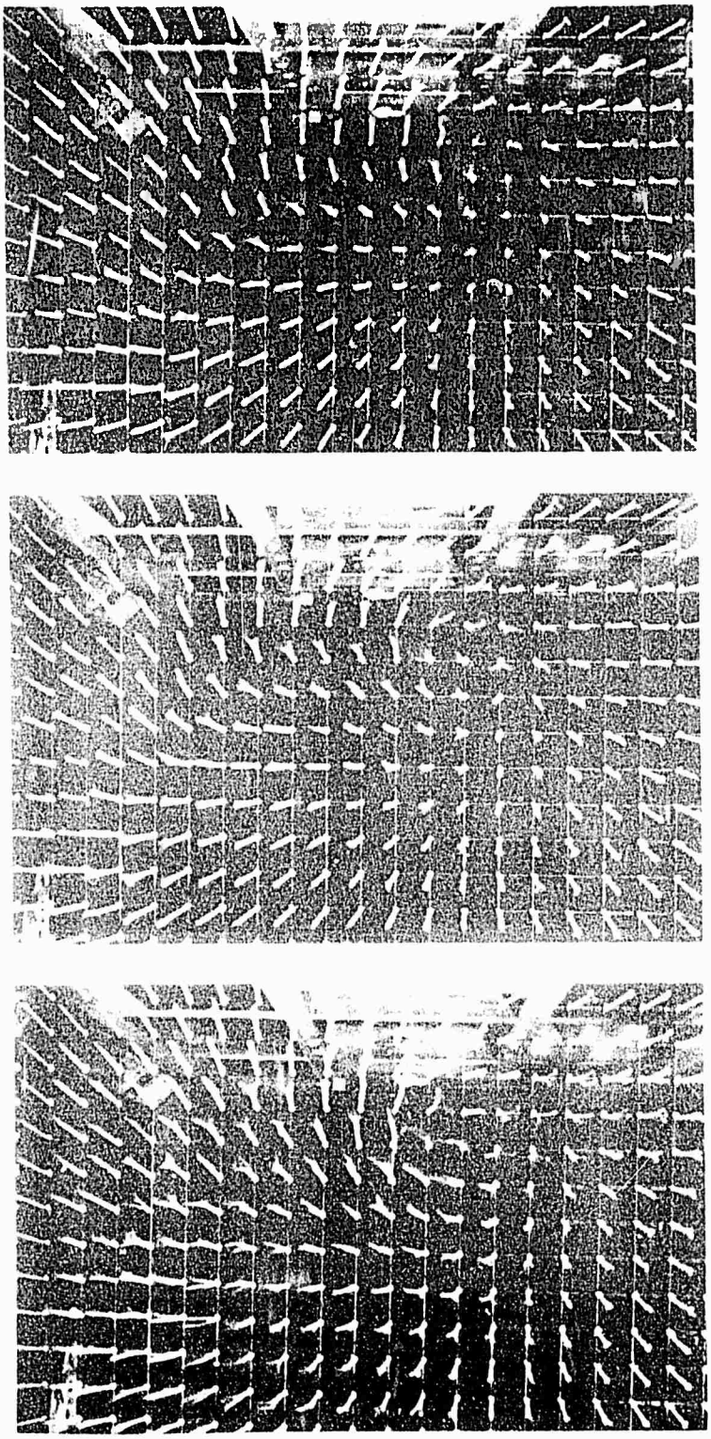

Figure 25. Tuft-Grid Patterns for the Ogee-Tip Configuration; 6.5 Chord Lengths Downstream, V = 150 ft/sec.

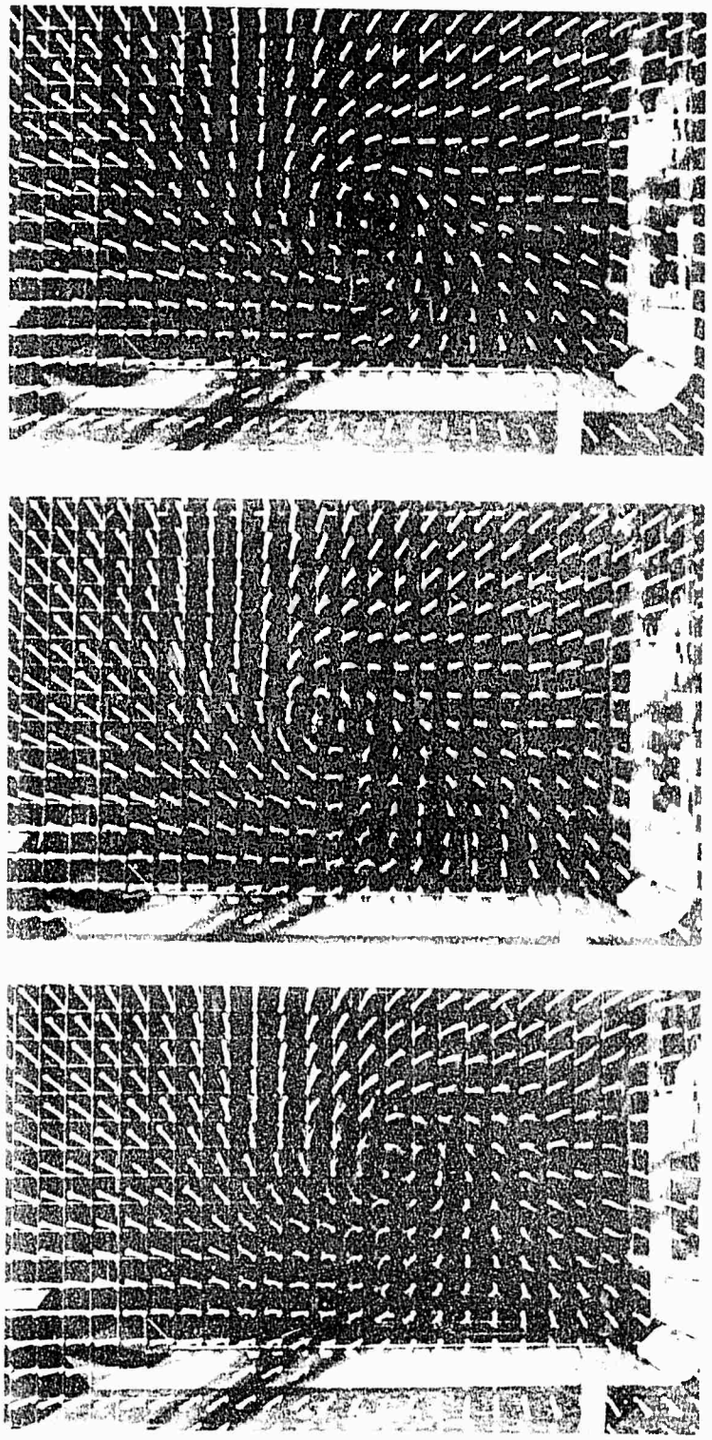

Figure 26. Tuft-Grid Patterns for the Ogee-Tip Configuration; 13 Chord Lengths Downstream, V = 150 ft/sec.

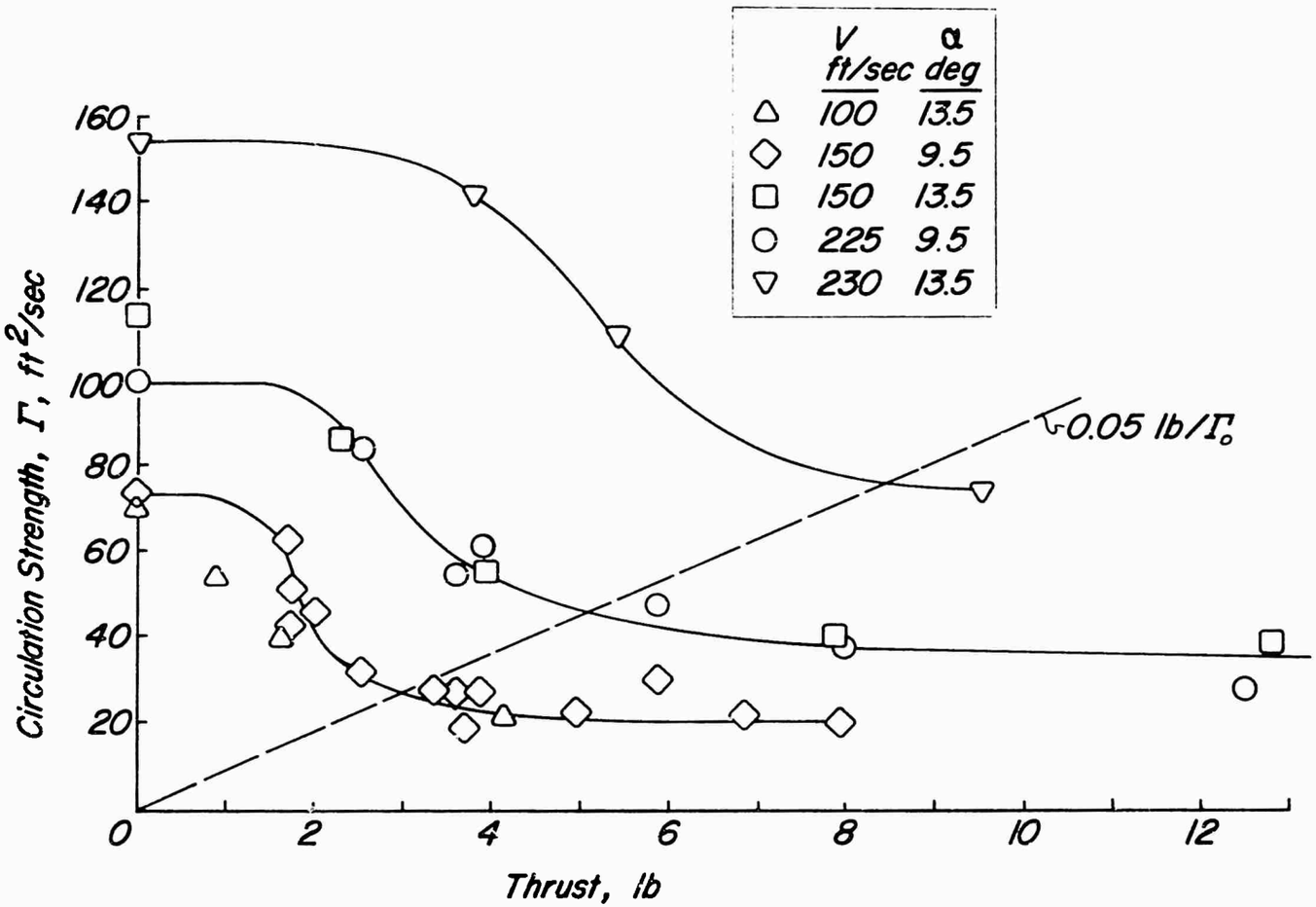

Figure 27. Circulation Strength Vs. Thrust.

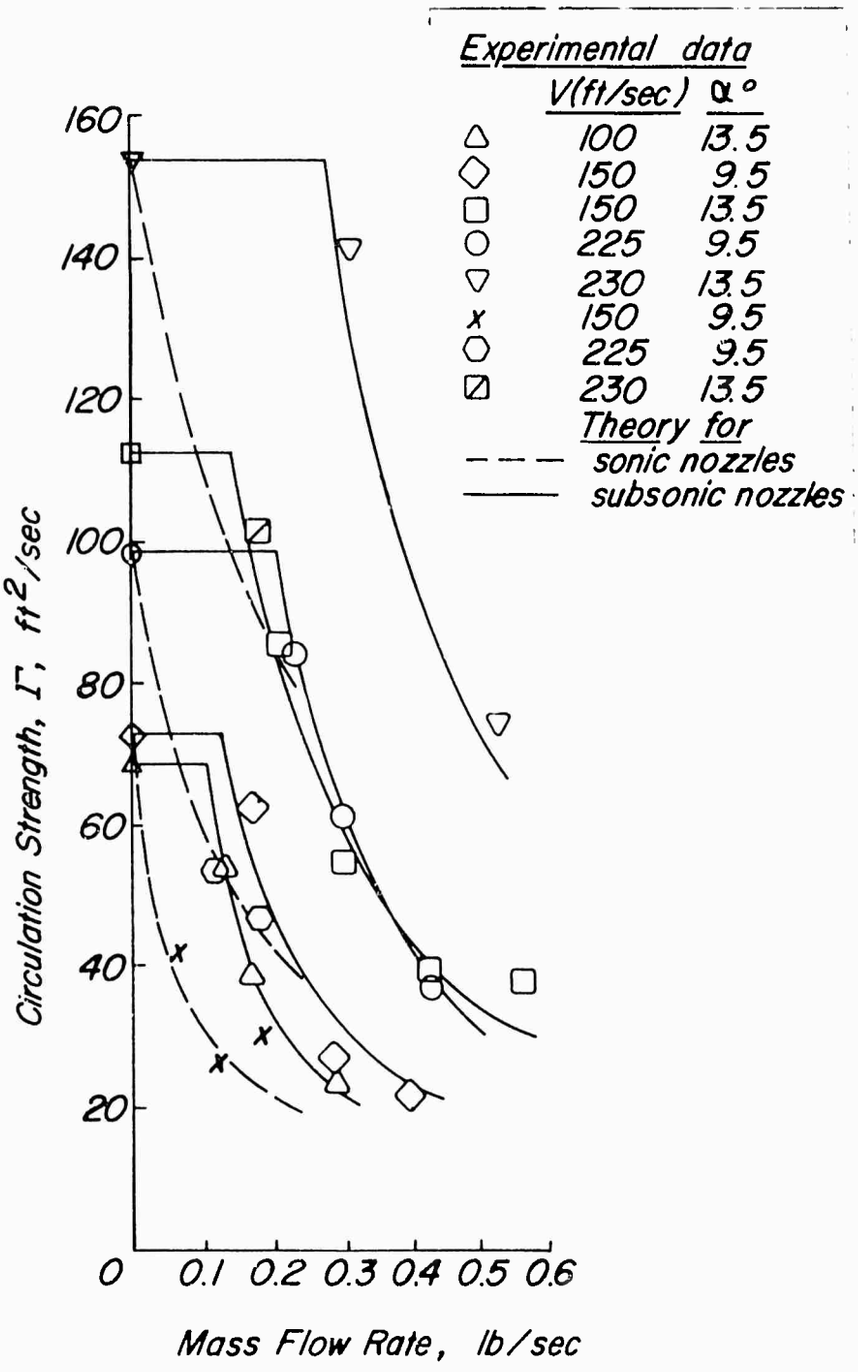

Figure 28. Circulation Strength Vs. Mass Flow Rate.

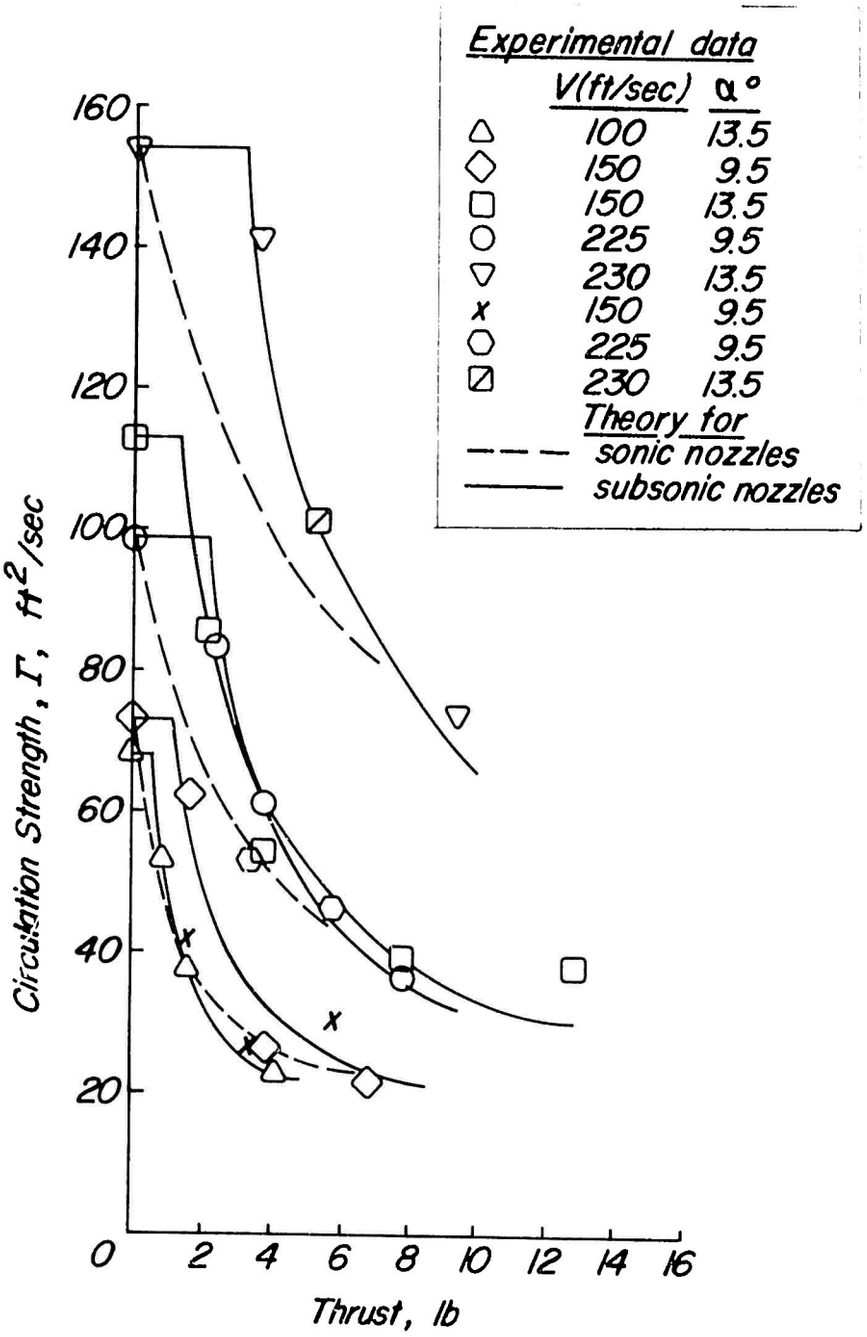

Figure 29. Circulation Strength Vs. Thrust.

VII. LITERATURE CITED

1. Rinehart, Stephen, STUDY OF MODIFICATION OF ROTOR TIP VORTEX BY AERODYNAMIC MEANS, ONR Contract N00014-69-C-0169, Rochester Applied Science Associates, Inc., RASA Report No. 70-02, AD 704804, 1970.

2. Rinehart, S.A., Balcerak, J.C., White, R.P., Jr., AN EXPERIMENTAL STUDY OF TIP VORTEX MODIFICATION BY MASS FLOW INJECTION, ONR Contract N00014-69-C-0169, Rochester Applied Science Associates, Inc., RASA Report No. 71-01, AD 726736, 1971.

3. White, R. P., Jr., and Balcerak, J.C., AN INVESTIGATION OF THE MIXING OF LINEAR AND SWIRLING FLOWS, ONR Contract N00014-71-C-0226, Rochester Applied Science Associates, Inc., RASA Report 72-04, February 1972.

4. White, R.P., Jr., and Balcerak, J.C., INVESTIGATION OF THE DISSIPATION OF THE TIP VORTEX OF A ROTOR BLADE BY MASS INJECTION, Rochester Applied Science Associates, Inc.; USAAMRDL TR 72-43, Eustis Directorate, U. S. Army Air Mobility Research and Development Laboratory, August 1972, AD 750634.

5. Rorke, J.B., Moffitt, R.C., and Ward, J.F., WIND TUNNEL SIMULATION OF FULL-SCALE VORTICES, Presented at the 28th Annual National Forum of the American Helicopter Society, Washington, D.C., May 1972.

6. Lamb, H., HYDRODYNAMICS, Cambridge University Press, 6th Edition, p. 591, 1932.

7. Squire, H.B., THE GROWTH OF A VORTEX IN TURBULENT FLOW, ARC 16,666, 1954.

8. Govindaraju, S.P., and Saffman, P.G., FLOW IN A TURBULENT TRAILING VORTEX, The Physics of Fluids, Volume 14, Number 10, October 1971.

9. Owen, P.R., THE DECAY OF A TURBULENT TRAILING VORTEX, Aeronautical Quarterly, Vol. XXI, p. 69, February 1970.

10. Zijne, Van der Hegge, Applied Science Research, 7A, p. 293, 1958.

11. Alexander, Baron, and Comings, University of Illinois Bulletin, No. 413, 1953.

12. Abramovich, G.N., THE THEORY OF A FREE JET OF A COMPRESSIBLE GAS, NACA TM No. 1058, 1944.

13. Wygnanski, I., TWO-DIMENSIONAL TURBULENT JET IN A UNIFORM, PARALLEL STREAM, AIAA Journal, Vol. 7, No. 1, p. 86, January 1969.

APPENDIX I
MASS FLOW RATE VERSUS STATIC PRESSURE

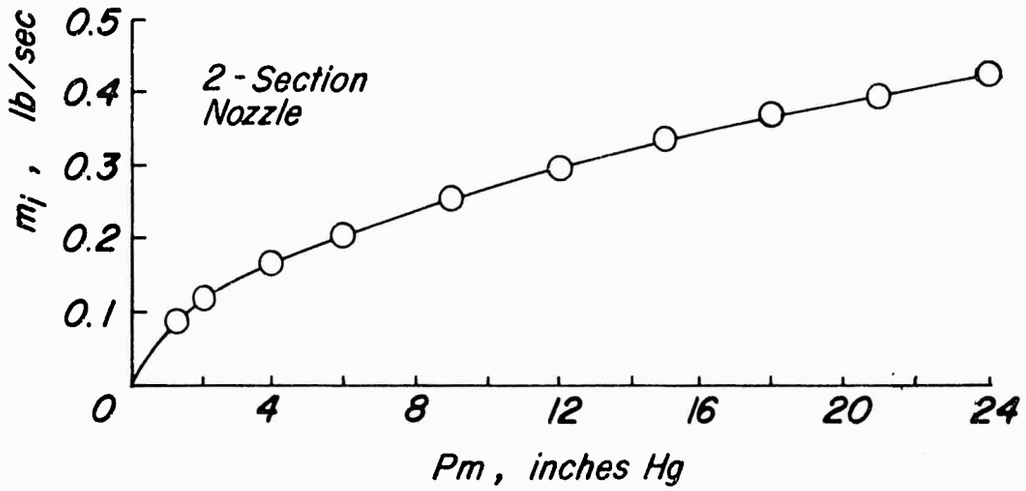

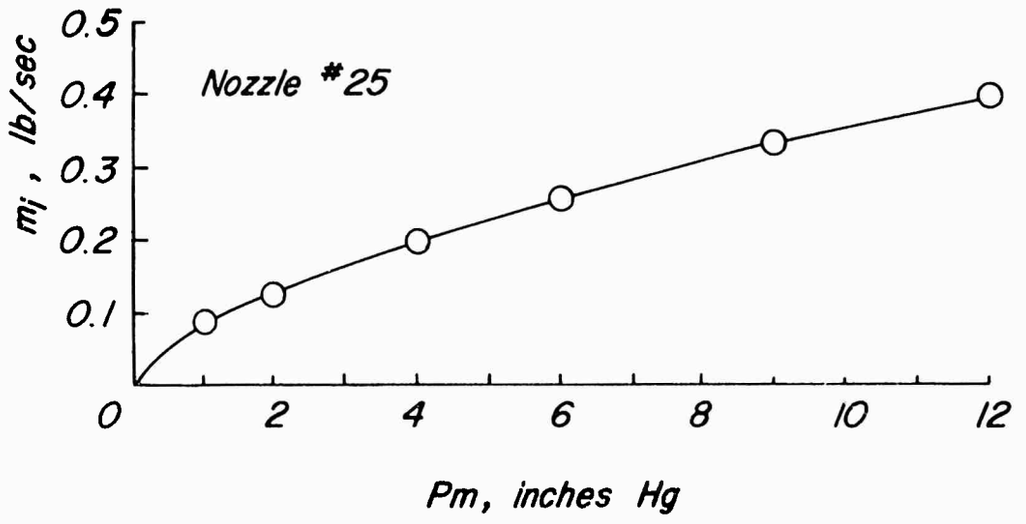

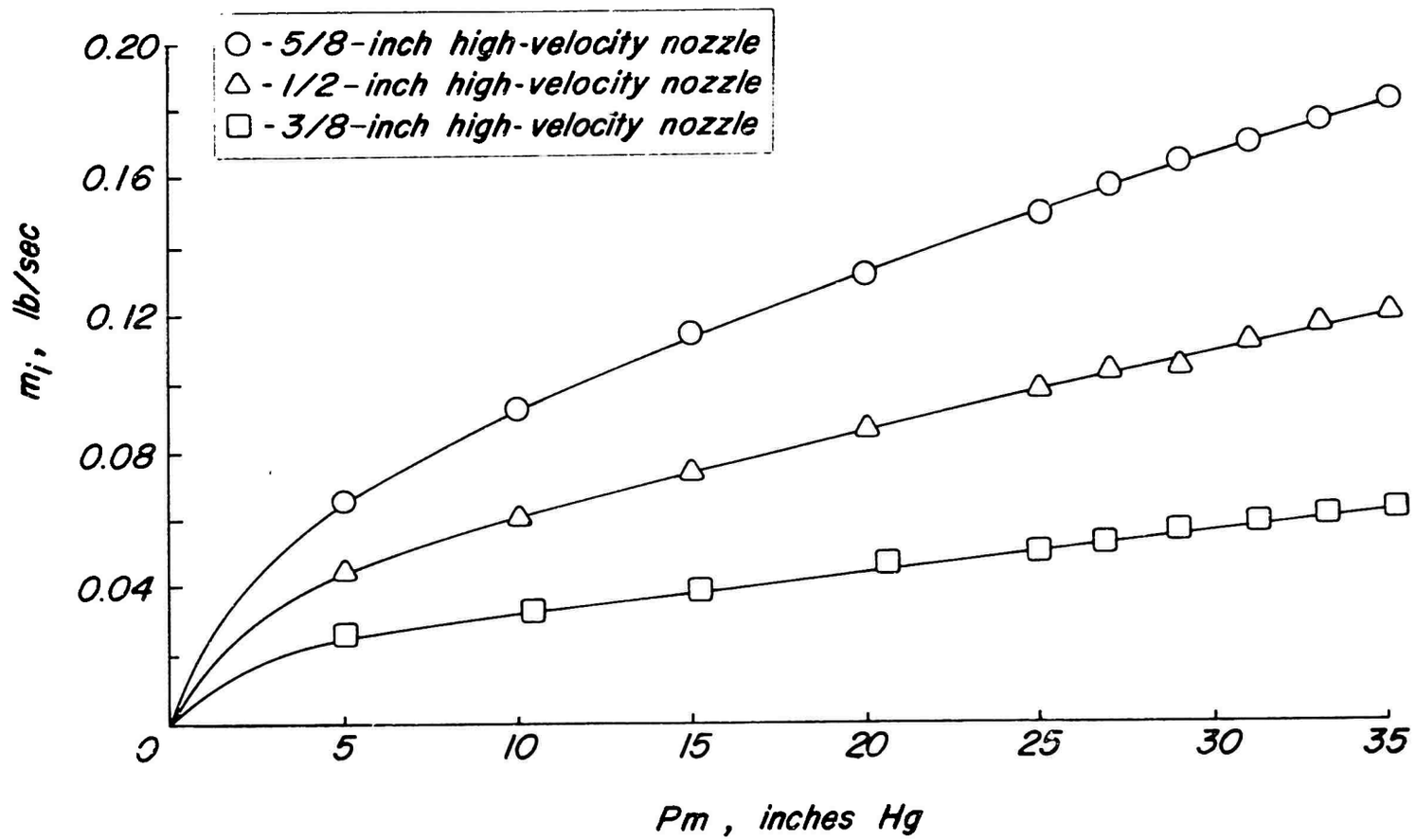
○ - 5/8-inch high-velocity nozzle
△ - 1/2-inch high-velocity nozzle
□ - 3/8-inch high-velocity nozzle
0.20
0.16
0.12
0.08
0.04
0
5
10
15
20
25
30
35
m_j, lb/sec
Pm, inches Hg

APPENDIX II
VORTICITY SURVEYS

Nozzle #18
V = 100 fps
α_T = 13.5°
m_i = 0.13 lb/sec

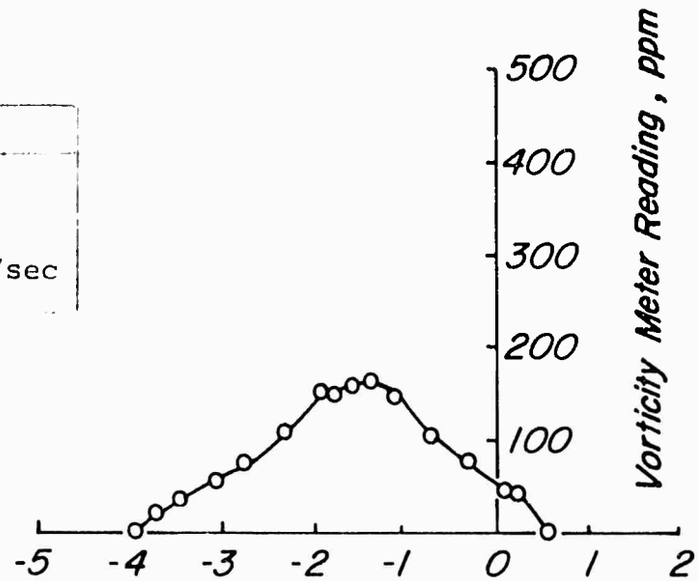

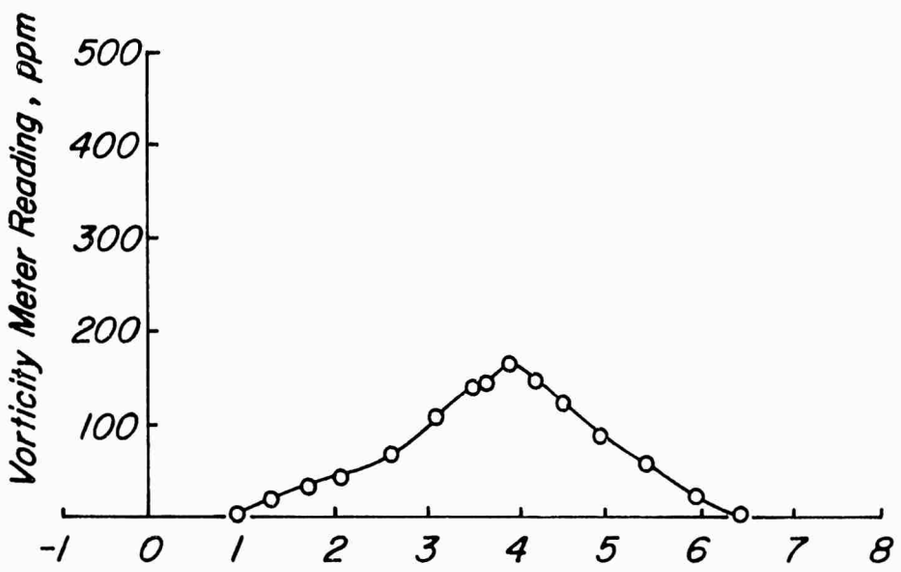

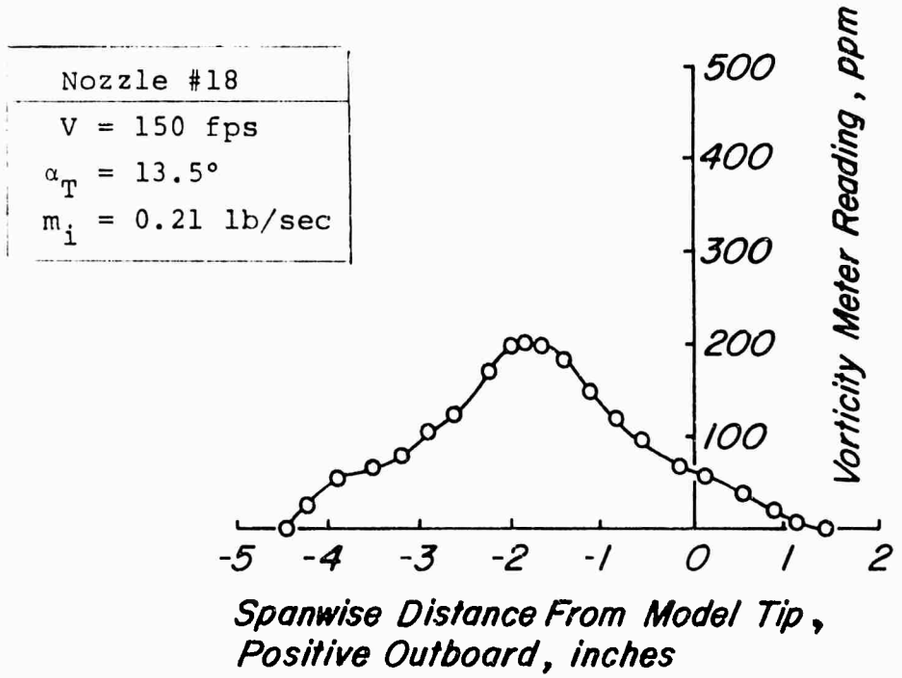
Nozzle #18
V = 150 fps
α_T = 13.5°
m_i = 0.21 lb/sec
500
400
300
200
100
Vorticity Meter Reading, ppm
-5 -4 -3 -2 -1 0 1 2
Spanwise Distance From Model Tip, Positive Outboard, inches

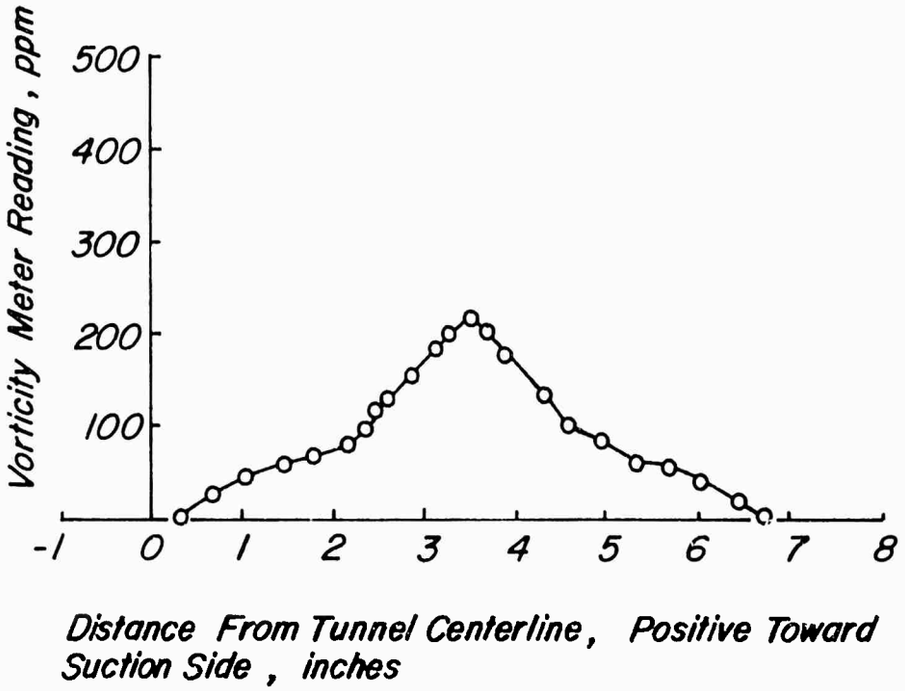
Vorticity Meter Reading, ppm
500
400
300
200
100
-1 0 1 2 3 4 5 6 7 8
Distance From Tunnel Centerline, Positive Toward Suction Side, inches

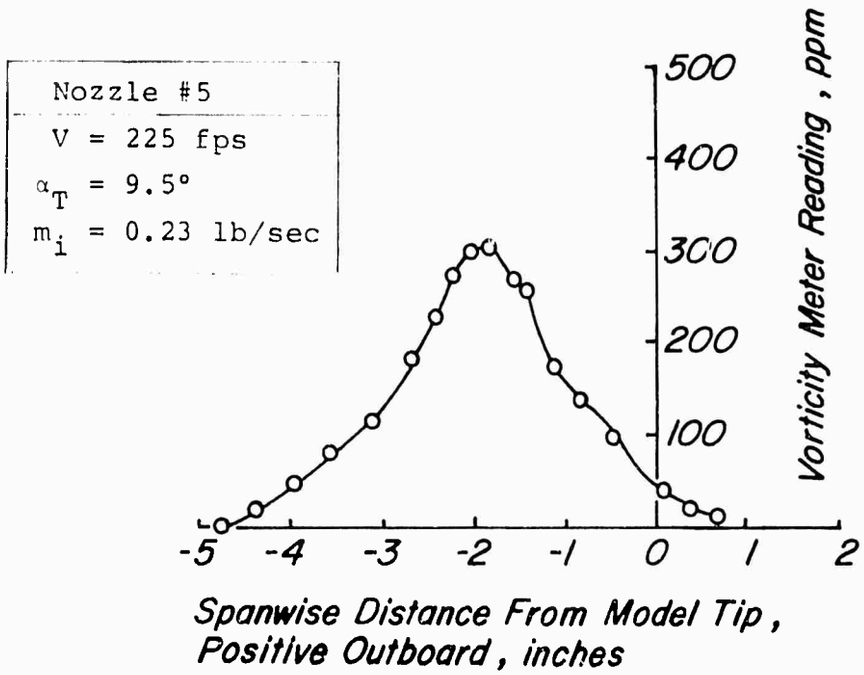
Nozzle #5
V = 225 fps
α_T = 9.5°
m_i = 0.23 lb/sec
500
400
300
200
100
Vorticity Meter Reading , ppm
-5 -4 -3 -2 -1 0 1 2
Spanwise Distance From Model Tip , Positive Outboard , inches

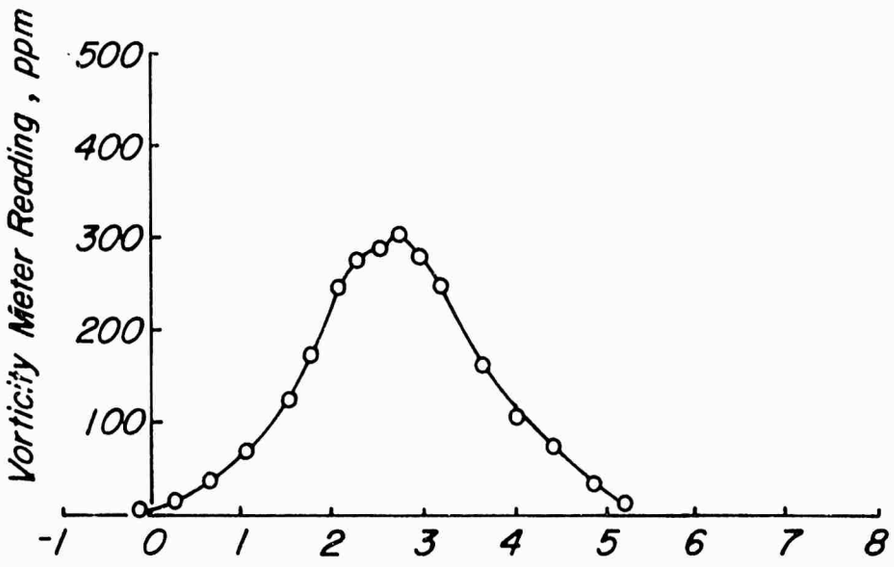
Vorticity Meter Reading , ppm
500
400
300
200
100
-1 0 1 2 3 4 5 6 7 8
Distance From Tunnel Centerline , Positive Toward Suction Side , inches

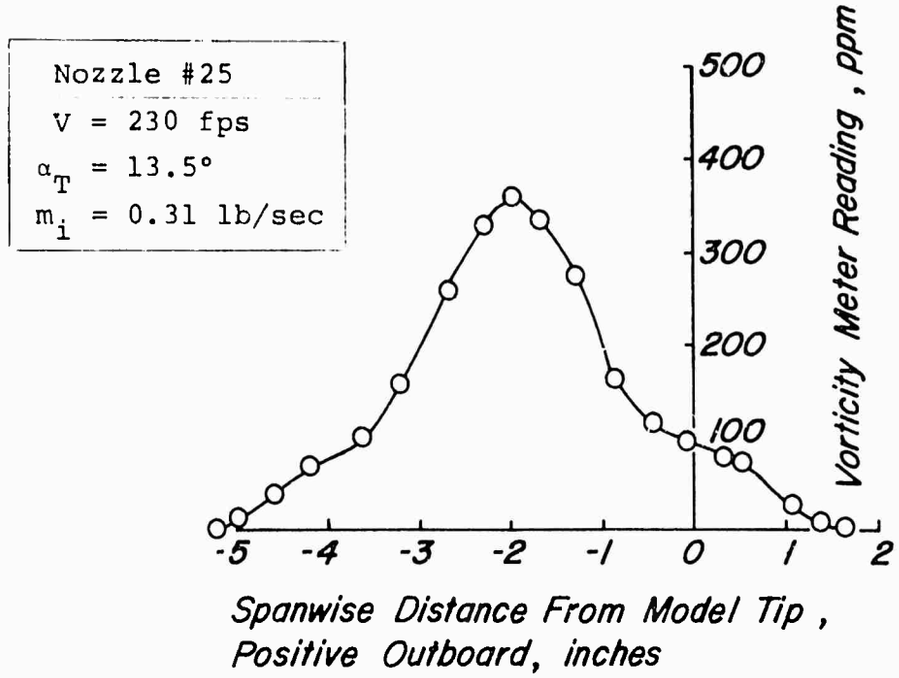
Nozzle #25
V = 230 fps
α_T = 13.5°
m_i = 0.31 lb/sec
500
400
300
200
100
Vorticity Meter Reading , ppm
-5
-4
-3
-2
-1
0
1
2
Spanwise Distance From Model Tip ,
Positive Outboard, inches

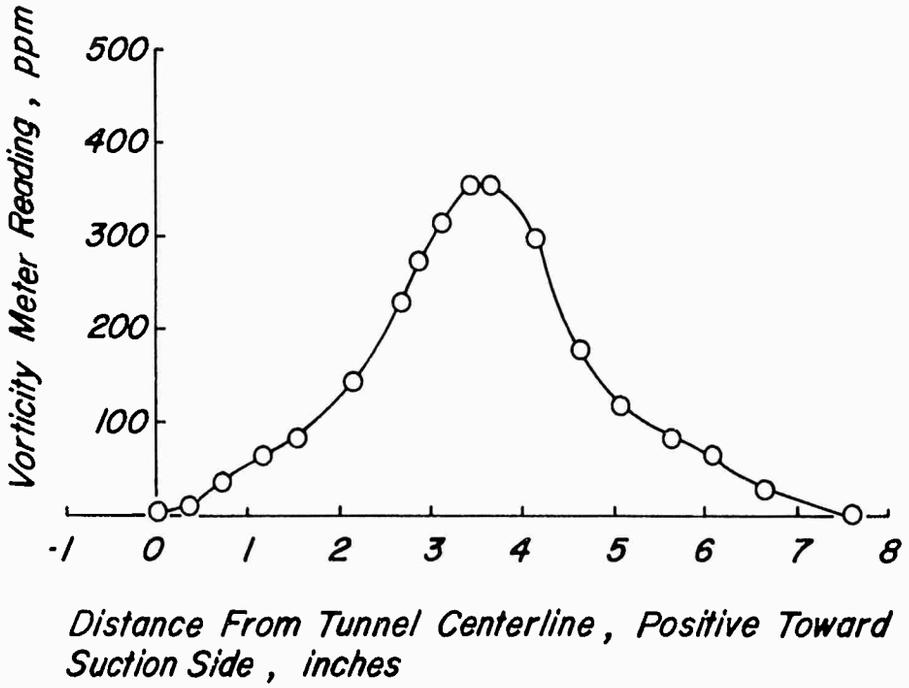
Vorticity Meter Reading , ppm
500
400
300
200
100
-1
0
1
2
3
4
5
6
7
8
Distance From Tunnel Centerline , Positive Toward
Suction Side , inches

3/8-inch high-velocity nozzle
V = 150 fps
α_T = 9.5°
m_i = 0.06 lb/sec

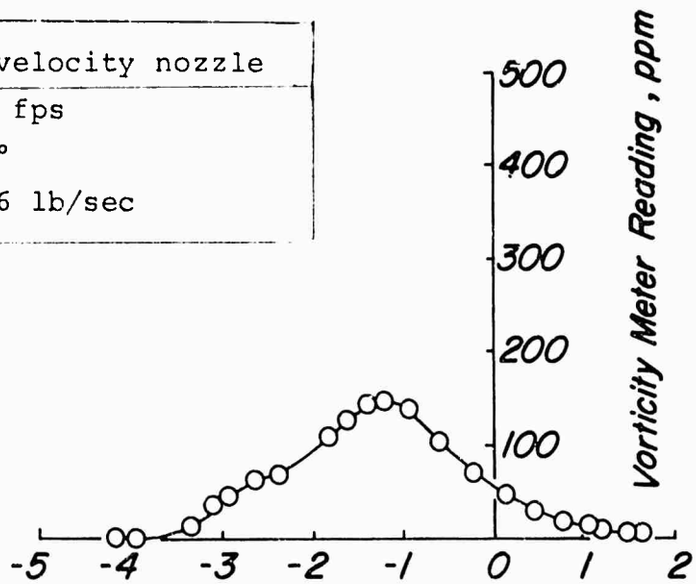

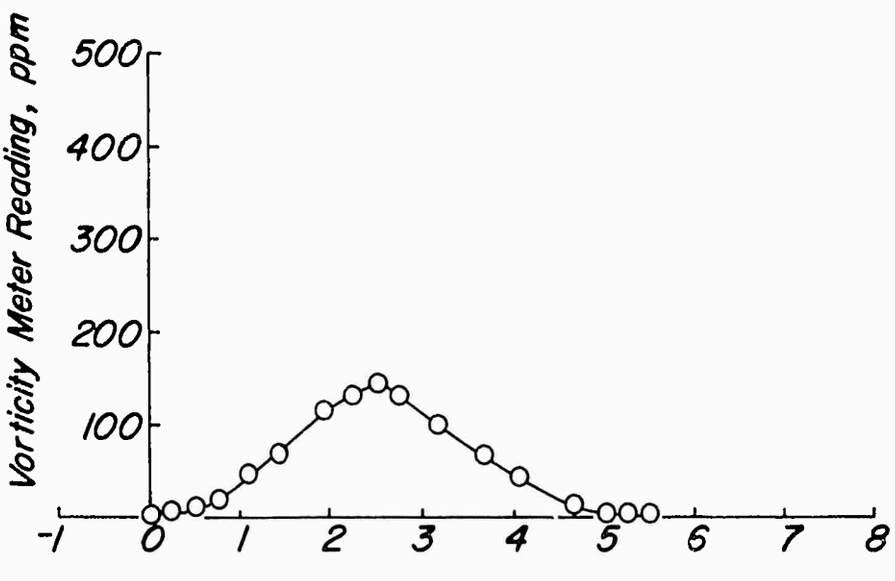

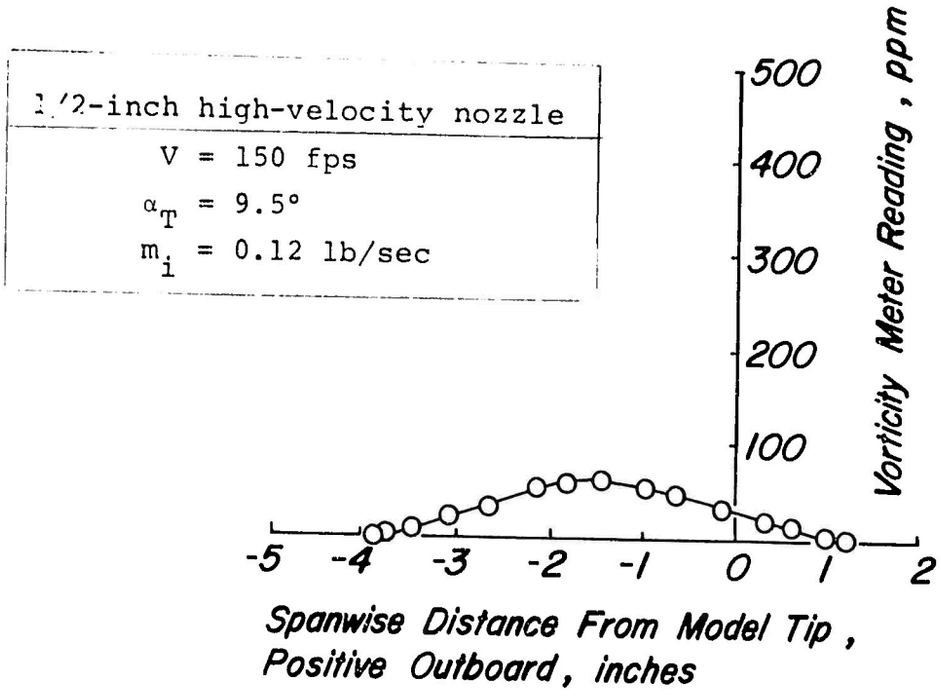
1/2-inch high-velocity nozzle
V = 150 fps
α_T = 9.5°
m_i = 0.12 lb/sec
500
400
300
200
100
Vorticity Meter Reading , ppm
-5 -4 -3 -2 -1 0 1 2
Spanwise Distance From Model Tip ,
Positive Outboard, inches

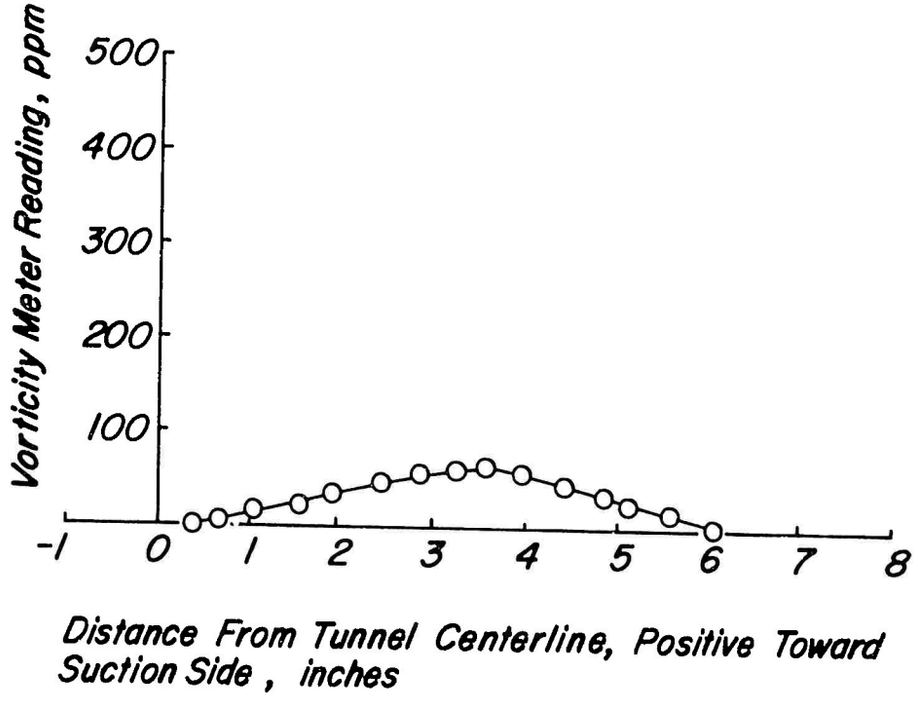
Vorticity Meter Reading, ppm
500
400
300
200
100
-1 0 1 2 3 4 5 6 7 8
Distance From Tunnel Centerline, Positive Toward
Suction Side , inches

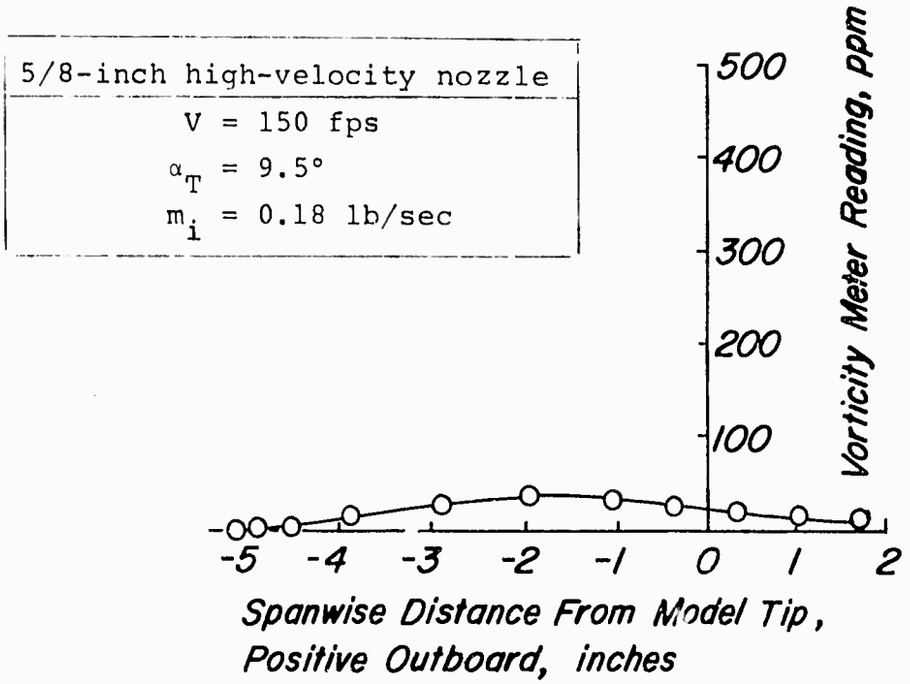
5/8-inch high-velocity nozzle
V = 150 fps
α_T = 9.5°
m_i = 0.18 lb/sec
500
400
300
200
100
Vorticity Meter Reading, ppm
-5 -4 -3 -2 -1 0 1 2
Spanwise Distance From Model Tip, Positive Outboard, inches

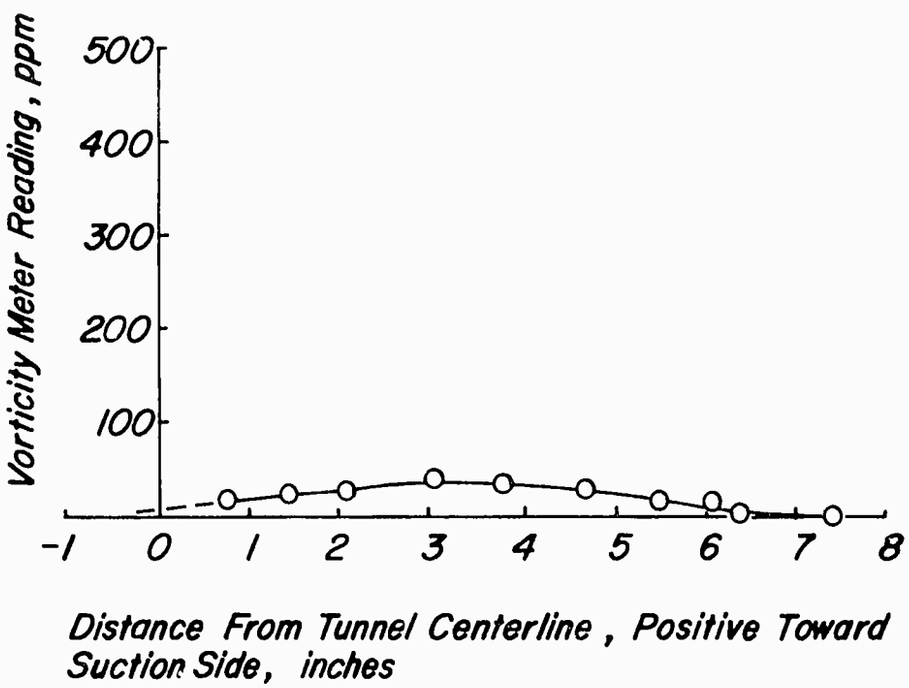
Vorticity Meter Reading, ppm
500
400
300
200
100
-1 0 1 2 3 4 5 6 7 8
Distance From Tunnel Centerline, Positive Toward Suction Side, inches

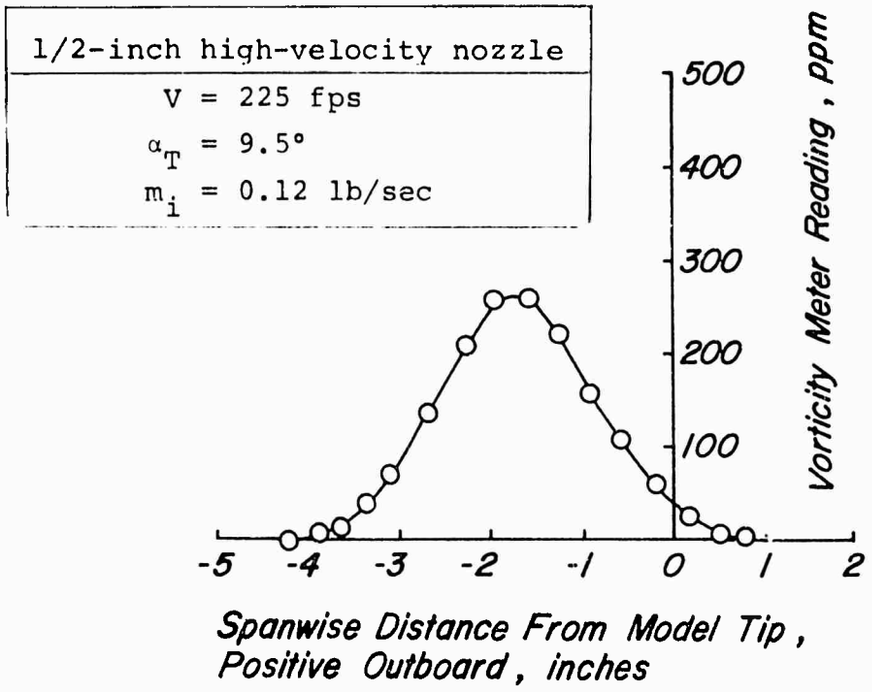
1/2-inch high-velocity nozzle
V = 225 fps
α_T = 9.5°
m_i = 0.12 lb/sec
500
400
300
200
100
Vorticity Meter Reading , ppm
-5 -4 -3 -2 -1 0 1 2
Spanwise Distance From Model Tip , Positive Outboard , inches

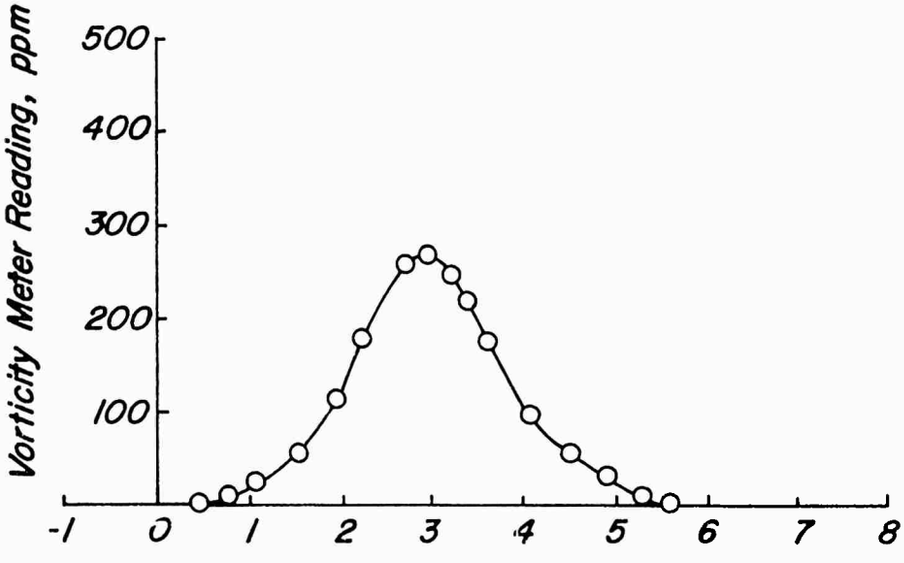
Vorticity Meter Reading, ppm
500
400
300
200
100
-1 0 1 2 3 4 5 6 7 8
Distance From Tunnel Centerline , Positive Toward Suction Side , inches

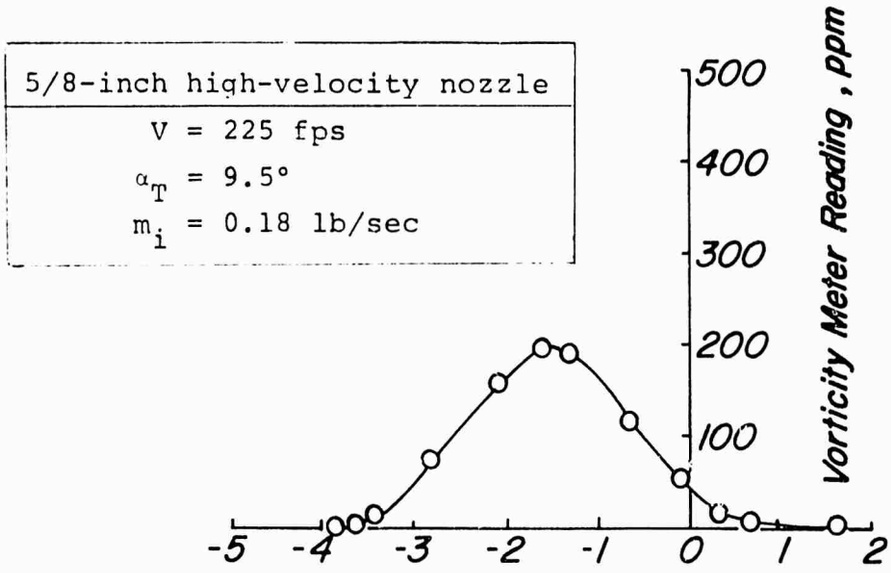
5/8-inch high-velocity nozzle
V = 225 fps
α_T = 9.5°
m_i = 0.18 lb/sec
500
400
300
200
100
Vorticity Meter Reading, ppm
-5
-4
-3
-2
-1
0
1
2
Spanwise Distance From Model Tip, Positive Outboard, inches

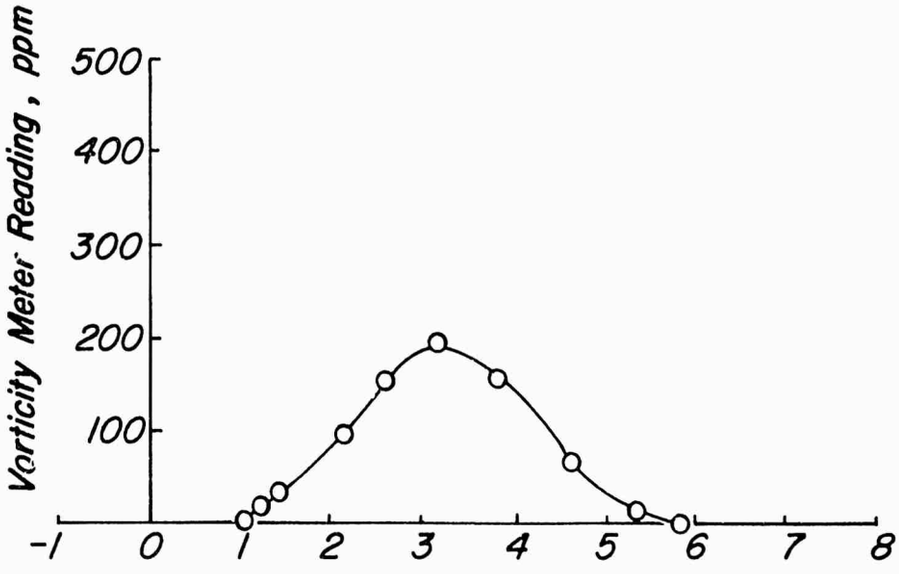
Vorticity Meter Reading, ppm
500
400
300
200
100
-1
0
1
2
3
4
5
6
7
8
Distance From Tunnel Centerline, Positive Toward Suction Side, inches

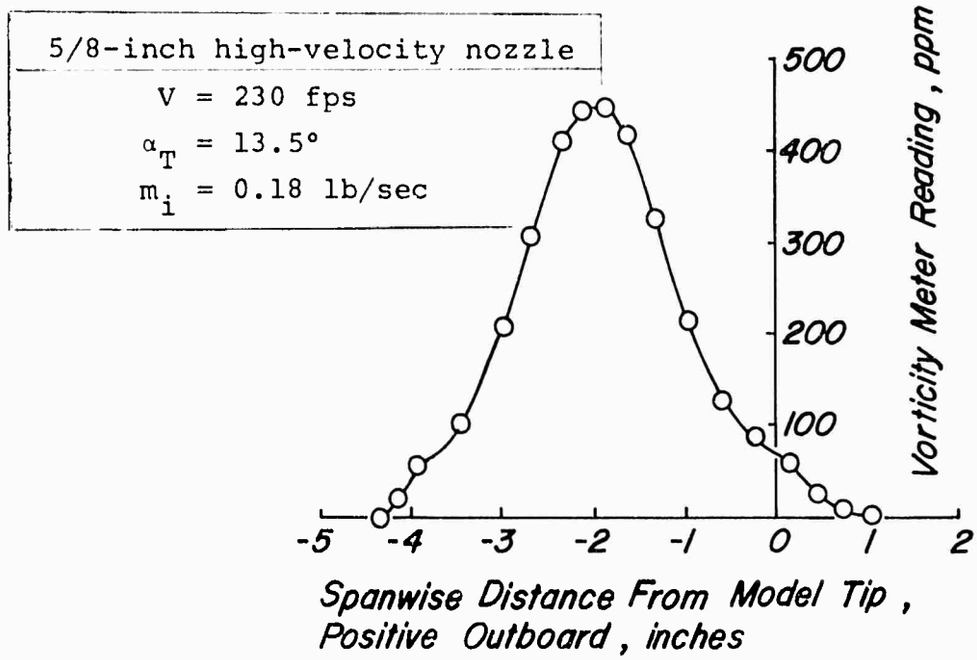
5/8-inch high-velocity nozzle
V = 230 fps
α_T = 13.5°
m_i = 0.18 lb/sec
500
400
300
200
100
Vorticity Meter Reading, ppm
-5
-4
-3
-2
-1
0
1
2
Spanwise Distance From Model Tip, Positive Outboard, inches

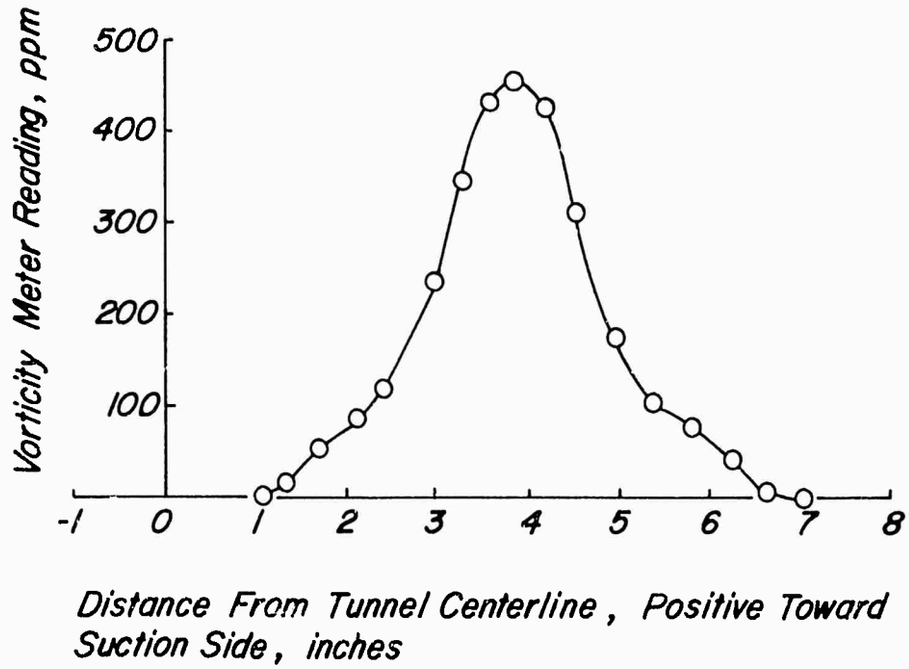
Vorticity Meter Reading, ppm
500
400
300
200
100
-1
0
1
2
3
4
5
6
7
8
Distance From Tunnel Centerline, Positive Toward Suction Side, inches

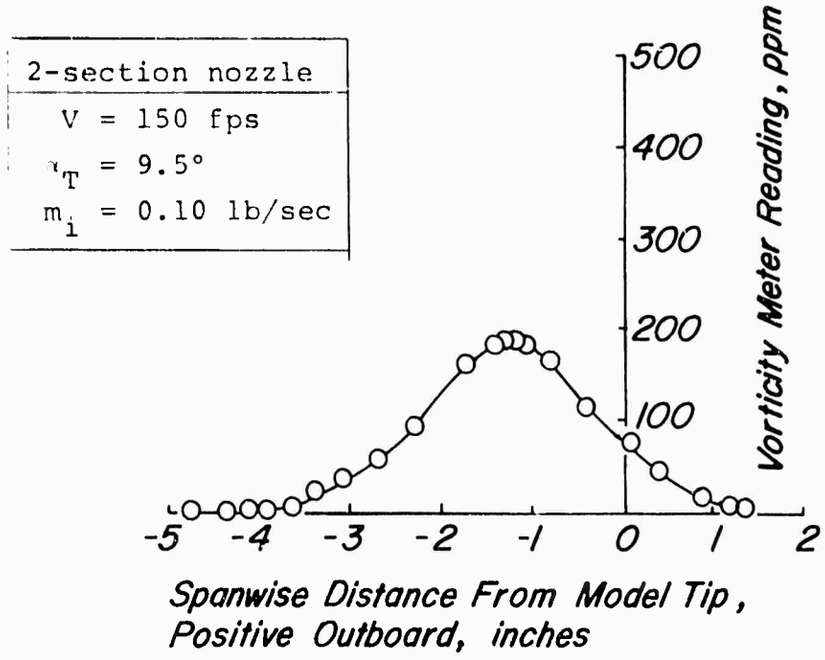
2-section nozzle
V = 150 fps
γ_T = 9.5°
m_i = 0.10 lb/sec
500
400
300
200
100
Vorticity Meter Reading, ppm
-5 -4 -3 -2 -1 0 1 2
Spanwise Distance From Model Tip, Positive Outboard, inches

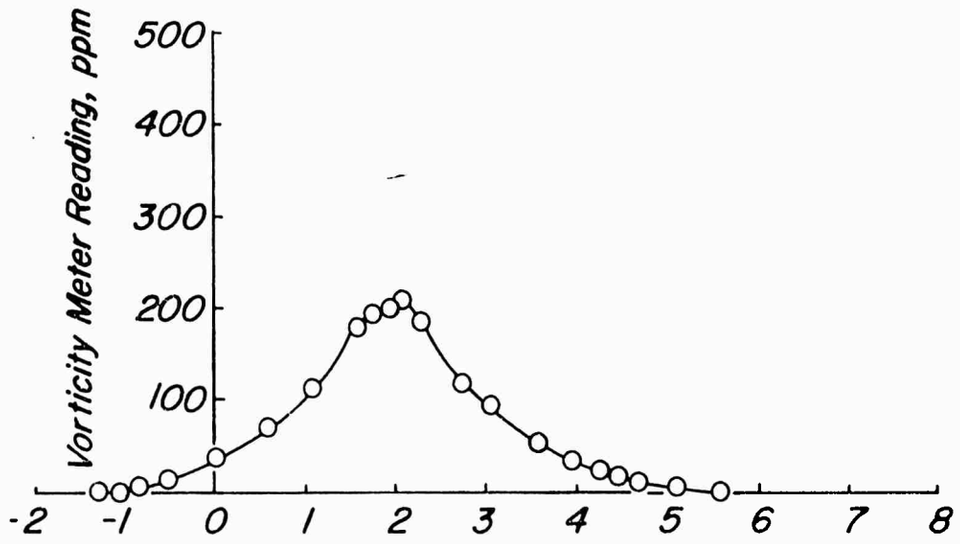
Vorticity Meter Reading, ppm
500
400
300
200
100
-2 -1 0 1 2 3 4 5 6 7 8
Distance From Tunnel Centerline, Positive Toward Suction Side, inches

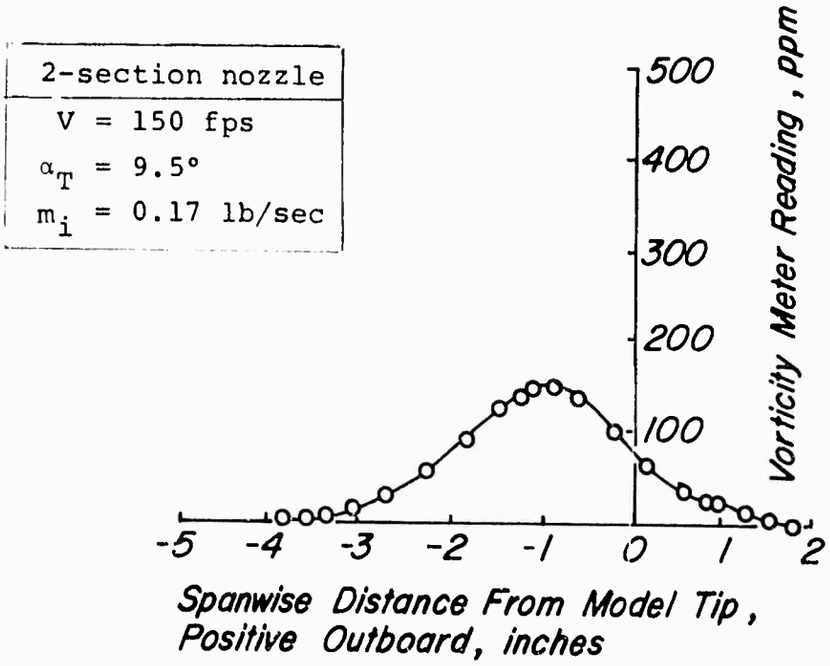
2-section nozzle
V = 150 fps
α_T = 9.5°
m_i = 0.17 lb/sec
500
400
300
200
100
Vorticity Meter Reading , ppm
-5 -4 -3 -2 -1 0 1 2
Spanwise Distance From Model Tip ,
Positive Outboard, inches

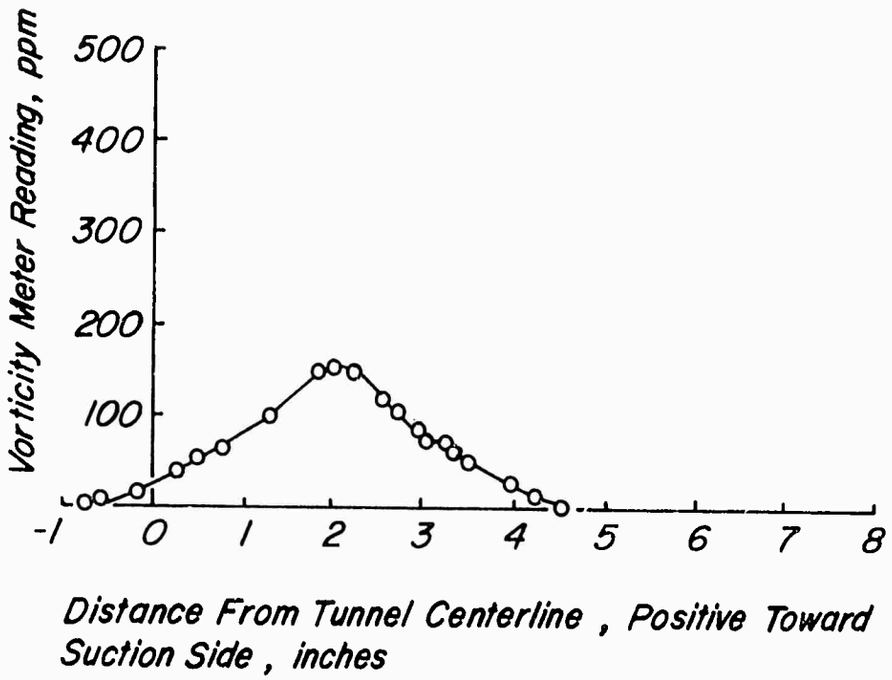
Vorticity Meter Reading, ppm
500
400
300
200
100
-1 0 1 2 3 4 5 6 7 8
Distance From Tunnel Centerline , Positive Toward
Suction Side , inches

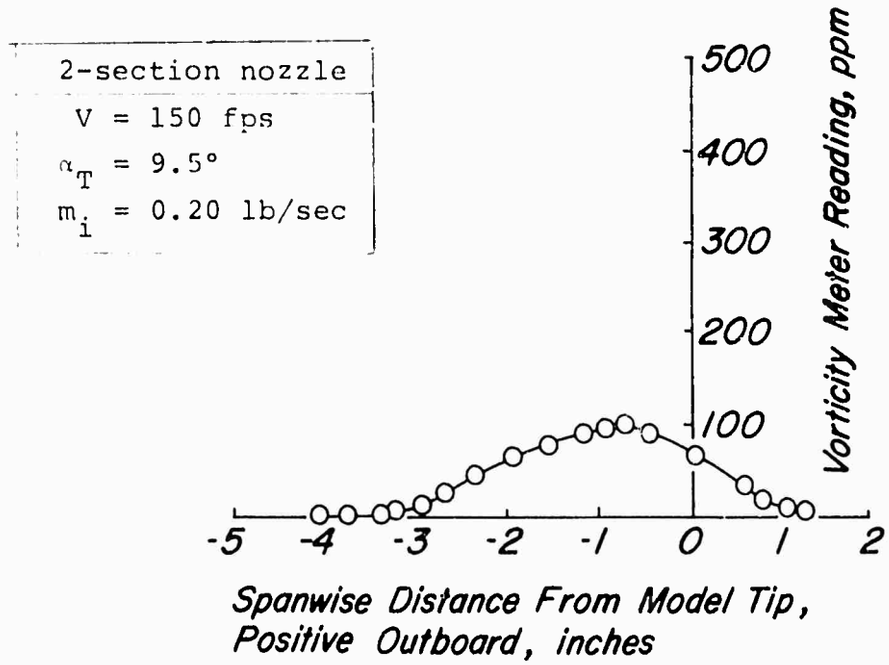
2-section nozzle
V = 150 fps
α_T = 9.5°
m_i = 0.20 lb/sec
500
400
300
200
100
Vorticity Meter Reading, ppm
-5
-4
-3
-2
-1
0
1
2
Spanwise Distance From Model Tip, Positive Outboard, inches

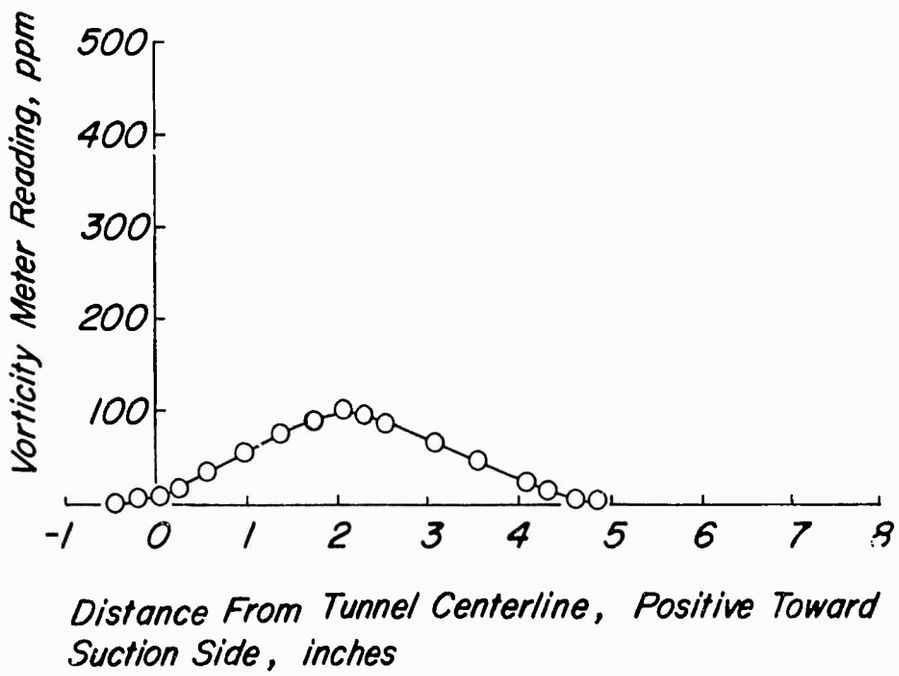
Vorticity Meter Reading, ppm
500
400
300
200
100
-1
0
1
2
3
4
5
6
7
8
Distance From Tunnel Centerline, Positive Toward Suction Side, inches

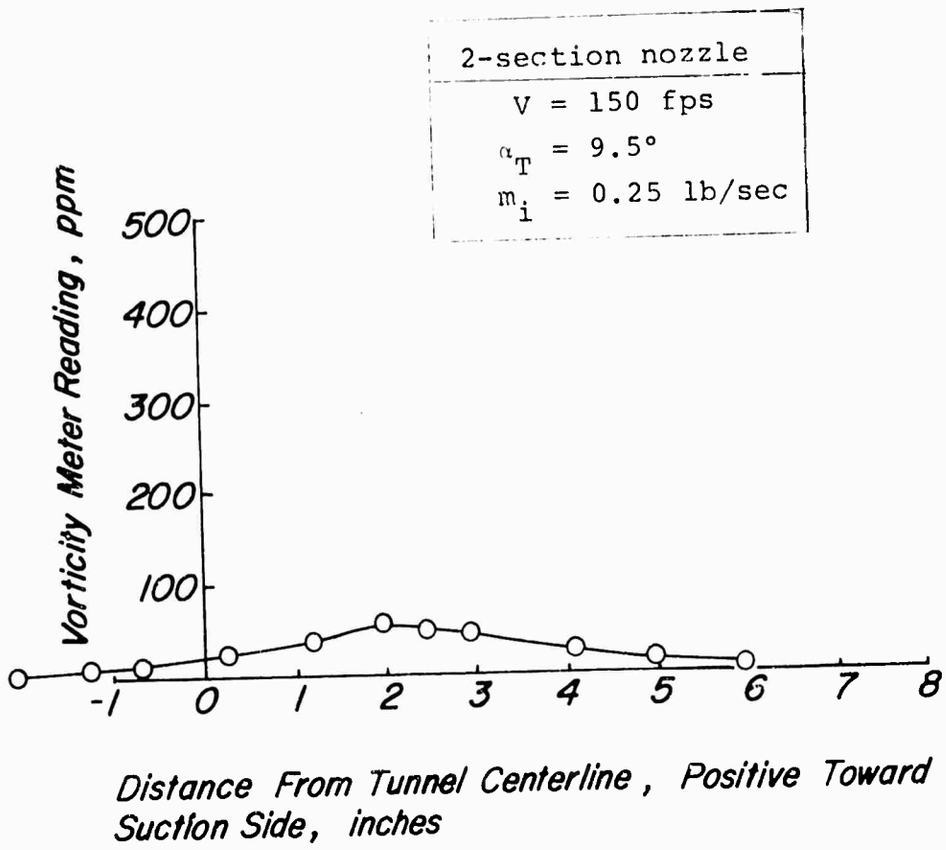
2-section nozzle
V = 150 fps
α_T = 9.5°
m_i = 0.25 lb/sec
Vorticity Meter Reading, ppm
500
400
300
200
100
-1
0
1
2
3
4
5
6
7
8
Distance From Tunnel Centerline, Positive Toward Suction Side, inches

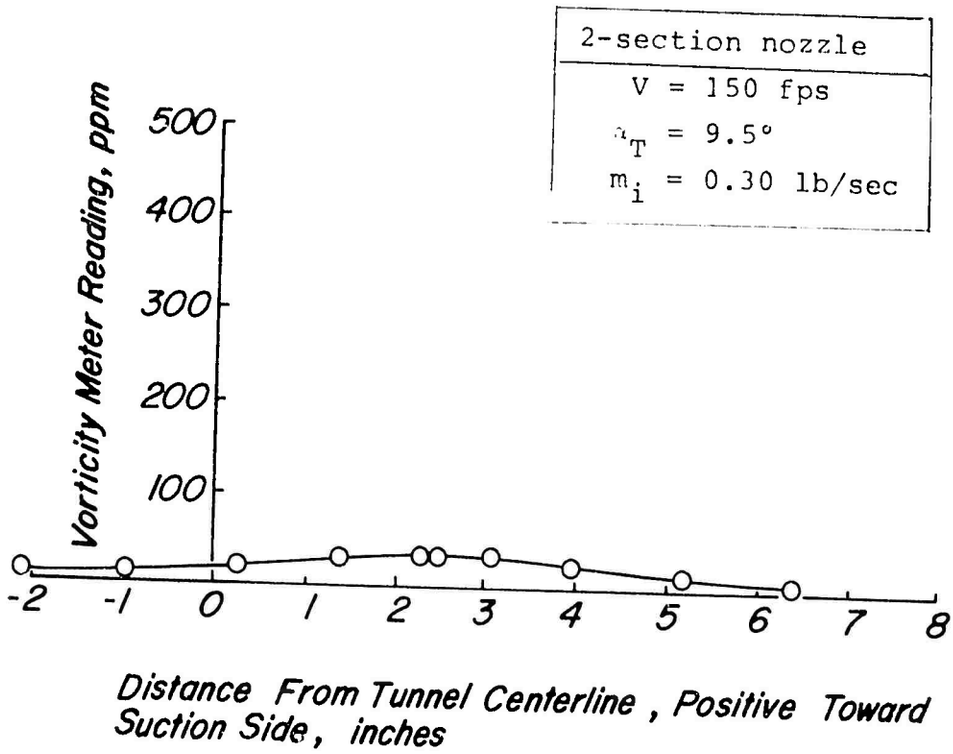
2-section nozzle
V = 150 fps
α_T = 9.5°
m_i = 0.30 lb/sec
Vorticity Meter Reading, ppm
500
400
300
200
100
-2
-1
0
1
2
3
4
5
6
7
8
Distance From Tunnel Centerline, Positive Toward Suction Side, inches

APPENDIX III
BALANCE MEASUREMENTS FOR VARIOUS OGEE-TIP CONFIGURATIONS

TABLE I. PERFORMANCE PARAMETERS FOR OGEE TIP

V (ft/sec)	α_T (deg)	Lift (lb)	Roll Moment* (ft-lb)	Drag (lb)	Drag Moment* (ft-lb)	Pitch Moment* (ft-lb)
100	0.0	5.8	-6.2	1.28	-1.4	-0.6
100	2.0	20.5	-26.8	1.47	-2.3	-1.8
100	4.0	34.6	-46.5	2.06	-2.7	-3.1
100	6.0	48.2	-62.7	2.83	-4.3	-3.9
100	8.0	62.7	-80.4	4.36	-5.9	-5.3
100	10.0	72.9	-95.9	6.64	-7.0	-8.0
100	12.0	80.2	-106.2	10.64	-10.6	-9.0
100	14.0	89.5	-121.0	14.87	-12.8	-13.2
100	16.0	67.7	-137.7	23.94	-26.3	-18.0
150	0.0	12.6	-15.3	2.73	-3.7	-1.2
150	2.0	45.7	-58.1	3.28	-5.4	-4.5
150	4.0	81.2	-104.1	4.79	-6.7	-7.6
150	6.0	113.3	-148.1	6.66	-8.9	-9.8
150	8.0	143.7	-184.5	9.25	-13.1	-12.8
150	10.0	168.0	-226.5	13.97	-15.6	-17.9
150	12.0	189.2	-251.0	23.26	-21.8	-22.2
150	14.0	207.2	-278.2	32.38	-27.7	-29.9
150	16.0	231.3	-312.3	37.98	-34.0	-33.7
200	0.0	22.8	-26.2	4.68	-6.5	-2.9
200	2.0	83.0	-112.0	5.72	-7.8	-8.8
200	4.0	145.1	-190.1	8.05	-10.8	-14.5
200	6.0	207.2	-271.3	11.98	-15.6	-19.7
200	8.0	256.3	-336.5	16.60	-23.7	-26.0
200	10.0	303.6	-398.4	24.98	-29.4	-32.7
200	12.0	342.6	-449.8	40.27	-35.6	-42.7
200	14.0	375.6	-516.3	55.42	-47.7	-51.9
225	0.0	25.9	-40.6	6.16	-7.5	-2.8
225	2.0	101.0	-143.9	7.64	-9.1	-10.2
225	4.0	180.9	-246.5	10.71	-12.5	-17.3
225	6.0	258.9	-346.5	15.18	-17.1	-24.2
225	8.0	325.5	-436.3	21.33	-27.0	-31.8
225	10.0	393.0	-518.6	29.74	-37.9	-40.4
225	12.0	437.5	-561.7	48.75	-44.3	-50.7
225	14.0	479.8	-657.5	68.15	-8.0	-65.0

* Roll and Drag Moments are about the tunnel centerline; Pitch Moment is about the model 15.5% chord

TABLE II. PERFORMANCE PARAMETERS FOR MODIFIED OGEE TIP #1

V (ft/sec)	α_T (deg)	Lift (lb)	Roll Moment* (ft-lb)	Drag (lb)	Drag Moment* (ft-lb)	Pitch Moment* (ft-lb)
100	-2.0	-13.0	17.9	1.24	-2.8	0.3
100	0.0	1.4	0.9	0.40	5.8	-4.7
100	2.0	17.6	-23.2	1.31	-2.0	-2.0
100	4.0	31.8	-42.2	1.83	-2.8	-3.2
100	6.0	47.0	-62.1	2.35	-3.8	-4.5
100	8.0	59.9	-79.5	3.72	-4.8	-6.3
100	10.0	71.8	-94.9	5.15	-6.5	-7.7
100	12.0	81.5	-107.4	8.66	-8.3	-9.4
100	14.0	86.0	-112.2	13.84	-11.3	-13.8
100	16.0	70.6	-84.4	21.75	-22.1	-18.6
100	18.0	64.3	-65.6	25.08	-28.7	-16.9
150	-2.0	-29.3	44.0	2.65	-5.2	0.8
150	0.0	3.4	0.8	1.89	3.8	-6.2
150	2.0	38.6	-48.1	2.80	-4.0	-5.5
150	4.0	72.0	-95.1	3.81	-5.3	-8.2
150	6.0	104.8	-140.8	5.32	-6.5	-10.9
150	8.0	137.5	-180.8	7.84	-10.5	-14.2
150	10.0	163.8	-214.8	11.25	-14.4	-17.1
150	12.0	187.4	-245.3	19.59	-18.2	-21.6
150	14.0	201.5	-268.5	30.44	-24.0	-31.0
150	16.0	216.6	-302.6	37.91	-32.4	-35.2
150	18.0	163.1	-195.8	55.07	-58.9	-41.5
200	-2.0	-51.4	78.5	4.60	-8.8	1.4
200	0.0	7.0	-1.9	3.49	0.7	-8.3
200	2.0	70.2	-94.4	4.74	-7.5	-10.3
200	4.0	130.6	-174.7	6.83	-8.9	-15.6
200	6.0	188.3	-251.6	9.39	-12.0	-20.6
200	8.0	247.2	-325.7	13.95	-19.0	-26.8
200	10.0	299.1	-392.3	20.11	-26.3	-32.8
200	12.0	336.5	-447.5	31.96	-32.3	-39.2
200	14.0	364.2	-490.9	53.81	-43.3	-55.0
200	16.0	388.7	-535.1	67.68	-55.9	-63.8

TABLE II - Continued

V (ft/sec)	α_T (deg)	Lift (lb)	Roll Moment* (ft-lb)	Drag (lb)	Drag Moment* (ft-lb)	Pitch Moment* (ft-lb)
225	-2.0	-65.4	101.3	5.74	-11.4	1.9
225	0.0	7.8	-6.2	4.78	-1.6	-9.4
225	2.0	89.0	-121.8	6.02	-9.7	-13.5
225	4.0	164.1	-223.8	8.19	-12.4	-20.2
225	6.0	240.8	-322.5	12.10	-15.8	-26.7
225	8.0	314.4	-418.6	17.97	-24.5	-34.6
225	10.0	382.5	-499.7	26.01	-34.6	-42.6
225	12.0	442.3	-587.7	37.47	-45.6	-49.5
225	14.0	495.0	-662.3	57.17	-54.2	-63.0
225	16.0	540.7	-729.0	71.64	-70.5	-70.9

*Roll and Drag Moments are about the tunnel centerline; Pitch Moment is about the model 15.5% chord.

TABLE III. PERFORMANCE PARAMETERS FOR MODIFIED OGEE TIP #2

V (ft/sec)	α_T (deg)	Lift (lb)	Roll Moment* (ft-lb)	Drag (lb)	Drag Moment* (ft-lb)	Pitch Moment* (ft-lb)
100	-2.0	-13.0	19.2	1.34	-1.7	1.7
100	0.0	1.1	1.9	0.52	8.9	-3.4
100	2.0	17.7	-21.4	1.36	0.3	-1.3
100	4.0	33.1	-39.8	1.85	-0.5	-2.4
100	6.0	47.9	-59.4	2.61	-1.7	-3.5
100	8.0	59.9	-76.7	3.85	-2.1	-4.7
100	10.0	71.2	-91.4	5.77	-4.9	-5.9
100	12.0	77.6	-100.3	10.03	-6.7	-8.7
100	14.0	86.2	-112.7	13.93	-10.1	-11.9
100	16.0	69.3	-82.6	21.63	-19.7	-16.2
100	18.0	62.9	-65.8	24.77	-25.8	-17.2
150	-2.0	-29.3	44.9	2.66	-5.0	2.1
150	0.0	4.0	1.3	1.91	6.3	-5.2
150	2.0	40.2	-49.9	2.78	-1.9	-4.6
150	4.0	74.3	-93.7	3.87	-3.6	-7.3
150	6.0	108.2	-139.6	5.81	-6.0	-10.2
150	8.0	138.3	-179.8	8.25	-8.3	-13.1
150	10.0	164.4	-215.2	11.93	-13.2	-15.9
150	12.0	185.7	-239.6	17.82	-16.8	-19.3
150	14.0	201.8	-263.8	29.95	-21.8	-29.2
150	16.0	219.4	-301.2	38.66	-29.1	-35.3
150	18.0	158.7	-193.1	54.69	-55.7	-39.8
200	-2.0	-52.2	78.6	4.66	-8.7	2.7
200	0.0	6.6	-1.1	3.96	2.9	-6.7
200	2.0	73.4	-93.4	4.87	-5.0	-9.5
200	4.0	133.9	-175.0	6.91	-6.9	-14.5
200	6.0	199.3	-259.2	10.17	-11.4	-20.3
200	8.0	250.8	-324.3	14.58	-16.7	-25.8
200	10.0	295.9	-391.2	20.94	-25.0	-30.3
200	12.0	359.8	-463.5	30.22	-33.8	-36.1
200	14.0	393.3	-517.0	43.27	-41.0	-47.9
200	16.0	436.5	-547.9	68.56	-53.5	-64.3

TABLE III. - Continued

V (ft/sec)	α_T (deg)	Lift (lb)	Roll Moment* (ft-lb)	Drag (lb)	Drag Moment* (ft-lb)	Pitch Moment* (ft-lb)
225	-2.0	-65.2	98.8	5.53	-11.4	2.0
225	0.0	8.4	-4.4	4.59	-0.2	-9.2
225	2.0	90.7	-119.3	5.94	-7.5	-13.3
225	4.0	167.8	-218.7	8.27	-10.1	-20.4
225	6.0	243.9	-317.6	12.24	-15.0	-27.3
225	8.0	317.8	-415.6	17.90	-22.7	-35.1
225	10.0	385.8	-498.9	26.89	-33.0	-43.3
225	12.0	445.8	-581.5	37.00	-45.7	-51.3
225	14.0	497.4	-659.5	55.28	-53.7	-60.2
225	16.0	547.1	-733.3	72.02	-69.0	-70.6

* Roll and Drag Moments are about the tunnel centerline; Pitch Moment is about the model 15.5% chord

TABLE IV. PERFORMANCE PARAMETERS FOR MODEL #1

V (ft/sec)	α_T** (deg)	Lift (lb)	Roll Moment* (ft-lb)	Drag (lb)	Drag Moment* (ft-lb)	Pitch Moment* (ft-lb)
100	-1.5	2.2	-0.9	0.89	-4.2	0.2
100	0.5	15.3	-24.6	1.69	-4.3	-0.1
100	2.5	29.1	-44.5	2.15	-3.8	-2.3
100	4.5	41.4	-63.6	3.04	-3.9	-3.8
100	6.5	55.4	-80.7	4.66	-7.0	-5.2
100	8.5	67.4	-93.0	5.74	-8.4	-8.4
100	10.5	79.4	-112.5	7.61	-11.8	-10.5
100	12.5	91.4	-126.2	9.93	-14.2	-12.3
100	14.5	101.0	-141.6	12.38	-17.6	-14.0
150	-1.5	4.9	-3.8	2.24	-7.5	1.2
150	0.5	35.0	-51.4	3.63	-7.0	-1.4
150	2.5	65.6	-96.3	4.80	-8.1	-5.7
150	4.5	97.2	-145.9	6.38	-9.4	-9.9
150	6.5	124.3	-182.9	9.66	-14.8	-13.6
150	8.5	153.9	-225.7	12.76	-19.3	-19.1
150	10.5	184.3	-266.4	17.51	-26.3	-24.4
150	12.5	209.9	-300.5	22.71	-32.2	-28.8
150	14.5	234.6	-329.7	27.86	-39.9	-33.7
200	-1.5	9.4	-9.5	4.07	-9.9	1.6
200	0.5	62.5	-88.6	5.69	-10.4	-3.6
200	2.5	122.5	-187.9	8.17	-13.4	-11.9
200	4.5	174.1	-268.5	12.00	-17.1	-18.9
200	6.5	225.3	-336.7	17.03	-25.5	-27.2
200	8.5	272.2	-408.2	23.31	-33.4	-36.3
200	10.5	328.1	-461.5	31.53	-45.1	-44.3
200	12.5	373.9	-538.4	40.40	-58.0	-53.0
200	14.5	425.2	-582.9	50.05	-71.7	-62.0
225	-1.5	12.0	-17.7	5.28	-12.3	1.7
225	0.5	78.0	-131.5	7.14	-12.3	-5.7
225	2.5	149.4	-236.1	10.12	-15.9	-14.8
225	4.5	219.2	-337.4	14.62	-20.8	-23.8
225	6.5	282.3	-427.8	21.60	-30.8	-34.0
225	8.5	349.6	-516.9	29.59	-42.7	-45.4
225	10.5	411.6	-611.0	39.76	-62.1	-53.4
225	12.5	472.9	-681.1	50.35	-72.2	-65.1
225	14.5	534.9	-733.5	64.08	-90.9	-75.2

*Roll and Drag Moments are about the tunnel centerline; Pitch Moment is about the model 15.5% chord.

**Angle of Attack includes a -1.5° shift to account for wind tunnel installation and model twist relative to Ogee Model.

APPENDIX IV
NET BALANCE MEASUREMENTS VERSUS MASS FLOW RATE FOR VARIOUS TEST CONDITIONS

TABLE V . PERFORMANCE PARAMETERS FOR DETAILED SURVEYS

V (ft/sec)	α_T (deg)	m_i (lb/sec)	Lift (lb)	Roll Moment* (ft-lb)	Drag (lb)	Drag Moment* (ft-lb)	Pitch Moment* (ft-lb)
100	13.5	0	82.7	-120.6	8.38	-12.2	-11.1
100	13.5	0.13	85.1	-122.8	8.09	-12.0	-12.4
150	9.5	0	131.8	-199.6	10.93	-23.4	-13.3
150	9.5	0.06	135.9	-200.7	11.52	-25.9	-14.3
150	9.5	0.10	131.9	-196.7	9.77	-13.3	-18.1
150	9.5	0.12	131.8	-194.3	9.56	-1.6	-23.9
150	9.5	0.17	132.4	-194.7	9.96	-15.3	-17.0
150	9.5	0.18	132.8	-192.4	10.07	-11.7	-20.0
150	9.5	0.20	131.5	-194.8	9.72	-14.1	-17.5
150	9.5	0.25	131.9	-198.0	10.66	-15.4	-17.6
150	9.5	0.30	133.2	-196.6	8.74	1.0	-25.9
150	13.5	0	194.8	-283.5	18.93	-26.3	-28.6
150	13.5	0.21	193.5	-281.5	18.94	-30.3	-26.7
225	9.5	0	305.4	-469.3	24.03	-32.8	-43.7
225	9.5	0.12	295.1	-445.4	23.52	-43.3	-34.6
225	9.5	0.18	301.0	-449.3	23.23	-34.2	-42.6
225	9.5	0.23	303.5	-459.1	23.89	-33.6	-41.8
230	13.5	0	454.0	-661.3	44.69	-65.5	-62.9
230	13.5	0.18	454.0	-664.7	44.66	-59.6	-68.4
230	13.5	0.31	456.0	-667.9	44.09	-64.8	-66.4

* Roll and Drag Moments are about the tunnel centerline; Pitch Moment is about the model 15.5% chord

TABLE VI. SUMMARY OF DATA FOR WAKE-SURVEY TESTS

V (ft/sec)	α_T (deg)	m_i (lb/sec)	Γ (ft^2/sec)	Thrust (lb)
100	13.5	0	68.9	0
100	13.5	0.130	53.8	0.90
100	13.5	0.170	38.6	1.63
100	13.5	0.289	23.3	4.13
150	9.5	0	73.0	0
150	9.5	0.060	41.7	1.68
150	9.5	0.120	26.3	3.55
150	9.5	0.170	62.1	1.68
150	9.5	0.180	30.0	5.89
150	9.5	0.190	45.3	1.99
150	9.5	0.193	51.5	1.76
150	9.5	0.204	31.8	2.50
150	9.5	0.282	26.7	3.85
150	9.5	0.286	27.7	3.34
150	9.5	0.286	18.3	3.68
150	9.5	0.288	22.0	4.92
150	9.5	0.366	18.9	7.92
150	9.5	0.397	21.4	6.83
150	13.5	0	112.9	0
150	13.5	0.210	85.2	2.30
150	13.5	0.298	54.6	3.93
150	13.5	0.424	39.3	7.84
150	13.5	0.564	37.8	12.77
225	9.5	0	98.7	0
225	9.5	0.120	53.8	3.59
225	9.5	0.180	46.9	5.85
225	9.5	0.230	83.5	2.56
225	9.5	0.296	61.0	3.88
225	9.5	0.429	36.8	7.99
225	9.5	0.557	26.6	12.48
230	13.5	0	154.0	0
230	13.5	0.180	108.6	5.37
230	13.5	0.310	141.6	3.78
230	13.5	0.521	74.0	9.48